2001

Electrocatalytic materials and techniques for the anodic oxidation of various organic compounds

Stephen Everett Treimer
Iowa State University

INFORMATION TO USERS

This manuscript has been reproduced from the microfilm master. UMI films the text directly from the original or copy submitted. Thus, some thesis and dissertation copies are in typewriter face, while others may be from any type of computer printer.

The quality of this reproduction is dependent upon the quality of the copy submitted. Broken or indistinct print, colored or poor quality illustrations and photographs, print bleedthrough, substandard margins, and improper alignment can adversely affect reproduction.

In the unlikely event that the author did not send UMI a complete manuscript and there are missing pages, these will be noted. Also, if unauthorized copyright material had to be removed, a note will indicate the deletion.

Oversize materials (e.g., maps, drawings, charts) are reproduced by sectioning the original, beginning at the upper left-hand corner and continuing from left to right in equal sections with small overlaps.

ProQuest Information and Learning
300 North Zeeb Road, Ann Arbor, MI 48106-1346 USA
800-521-0600

Electrocatalytic materials and techniques for the anodic oxidation of various organic compounds

By

Stephen Everett Treimer

A dissertation submitted to the graduate faculty

in partial fulfillment of the requirements for the degree of

DOCTOR OF PHILOSOPHY

Major: Analytical Chemistry (Industrial Chemistry)

Major Professor: Dennis C. Johnson

Iowa State University

Ames, Iowa

2001

Graduate College

Iowa State University

This is to certify that the Doctoral dissertation of

Stephen Everett Treimer

has met the dissertation requirements of Iowa State University

Signature was redacted for privacy.

Major Professor

Signature was redacted for privacy.

For the Major Program

Signature was redacted for privacy.

For the Graduate College

TABLE OF CONTENTS

I. GENERAL INTRODUCTION

Introduction

Research in this group has been devoted to two primary areas – the development of techniques and materials for use as sensors/detectors and the development of techniques and materials for use in catalyzing anodic oxygen-transfer (O-transfer) reactions, a field now referred to as *electrocatalysis* [1-16]. The following reaction is a generic example of O-transfer reactions:

$$R + H_2O \rightarrow RO + 2H^+ + 2e- \quad (1)$$

In Equation 1 "R" is a generic organic molecule in an either basic or acidic aqueous solution. The species "RO" is the product of a single transfer of oxygen from water to "R". This reaction can be used for organic synthesis, detecting an organic species eluting off an HPLC column, or for converting toxic waste into less toxic compounds. Certainly, the heterogeneous kinetic rate constants that govern Equation 1 vary widely depending on the electrode material used. Additionally, preceding or subsequent reactions can make the overall O-transfer mechanism much more complicated than that shown by Equation 1.

On inert electrodes (Au, Pt, glassy carbon) where electron-transfer reactions are facile, often O-transfer reactions occur very slowly or do not at all. To utilize anodic O-transfer reactions effectively in practical applications (electrolytic remediation, electrosynthesis, amperometric sensors/detectors, etc.), it is necessary to develop new electrode materials or techniques with selective catalytic activity for the transfer of oxygen. The research described within this thesis will focus on these issues. Some recent

developments in the electrocatalysis of anodic O-transfer reactions have augmented some of the topics of greatest interest to us.

Lead dioxide films have long been used in the academic and industrial laboratories to support O-transfer reactions in various organic processes [17-22]. Our group has focused on the use of lead dioxide film anodes doped with variety of metallic and non-metallic dopants incorporated within the non-stoichiometric lattice structure of both the α- and β- forms of lead dioxide. Current trends of metal oxide film electrocatalysis have been toward the use of antimony-doped tin dioxide films, boron-doped diamond films, and a quaternary metal oxide film referred as the *dimensionally stable electrode* [23-29]. The latter of these films holds great promise for the future, however due to the technical difficulties and sophisticated instrumentation required for the preparation of these anodes, we elected to focus on the use of doped-PbO_2 anodes.

The highly doped Bi(V)-doped β-PbO_2 electrode (0.33 at/at) has been well characterized in literature [1,7,12-13]. The Bi(V)-doped β-PbO_2 film supports a wide variety of O-transfer reactions, has good signal-to-noise ratio (S/N), and relatively high mechanical stability. Of greatest benefit is that this film can be deposited with very reproducible characteristics. More recently, we have discovered that the doping of both α- and β-PbO_2 films with Fe(III) generates a film with activity similar to that of Bi(V)-doped β-PbO_2, however at much lower doping levels [2-4, 8-11]. Similar results have been observed recently by at least one other research group [30-31]. We speculate that there is room for improvement in the performance of Fe(III)-doped β-PbO_2 films by raising the dopant level to that found in highly active Bi(V)-doped β-PbO_2 films. Since Fe(III) is non-toxic, perhaps

when the most active Fe(III)-doped β-PbO_2 film is identified, the matrix can be modified to a less toxic and more environmentally friendly substrate, such as MnO_2.

There are several techniques currently being developed to enhance the activity of electrode surfaces. Leddy and coworkers are developing magnetic bead impregnated polymer electrodes that exhibit enhanced heterogeneous kinetics in the presence of magnetic fields [32-33]. Cooper and Coury have investigated the catalytic effects of ultrasonic irradiation of an electrode surface, a technique now referred to as *sonovoltammatry* [34]. Further, Madigan *et al.* used 20 kHz ultrasonic irradiation of an electrode to significantly increase heterogeneous rate constants at a rotated disk electrode [35]. Saterlay *et al.* have used sonoelectrochemistry on boron-doped diamond films to enhance the deposition of lead dioxide and silver films [36-37]. Certainly the more studied auxiliary excitation source in electrochemistry is the irradiation of electrode/solution interfaces with UV light. Bockris, Fox, and Tributsch were some of the first researchers to develop significant fundamental understanding of the role photocatalysis plays in the electrochemical activation of semi-conducting metal oxide films [38-43]. In more recent work, Fox and Rodriguez *et al.* have extended the use of photoelectrocatalytic oxidations for use in environmental remediation [44-45].

The focus of this thesis was first to characterize and improve the applicability of Fe(III) and Bi(V) doped PbO_2 film electrodes for use in anodic O-transfer reactions of toxic and waste organic compounds, e.g. phenol, aniline, benzene, and naphthalene. Further, we investigated the use of alternative solution/electrode interfacial excitation techniques to enhance the performance of these electrodes for remediation and electrosynthetic applications. Finally, we have attempted to identify a less toxic metal oxide film that may

hold promise for future studies in the electrocatalysis and photoelectrocatalysis of O-transfer reactions using metal oxide film electrodes.

Dissertation Organization

The research described in this dissertation was performed under the direction of Professor Dennis C. Johnson beginning in August 1997. This thesis contains six main chapters, preceded by this general introduction and followed by a general conclusion. Five of these chapters are papers that were published, submitted for publication, or undergoing the patent review process prior to submission to peer-reviewed electrochemical or environmental journals. The papers are each written according to the format requirements of the journals to which they were submitted or are intended to be submitted.

Chapter II presents a paper containing a collection of mathematical equations pertaining to the use of Koutecky-Levich plots for the determination of various electron-transfer mechanisms encountered during electrochemical experiments using a rotated disk working electrode. The initial literature survey was performed by Andrew Tang and subsequently updated by this author. There is significant mathematical theory in the literature which supports the use of Koutecky-Levich plots to aid in determining electron-transfer, *EE*, and various *CE* (*C*$_r$*E*$_r$, *C*$_r$*E*$_i$), *EC* (*E*$_r$*C*$_r$, *E*$_r$*C*$_i$, *EC*$_i$'), *ECE* and blocked electrode mechanisms. We offer diagnostic criteria for use in aiding future researchers elucidate electrochemical mechanisms when performing electrochemical measurements at a rotated disk electrode.

Chapter III presents a mathematical model that attempts to describe the current-potential relationships of anodic O-transfer reactions at rotated disk electrodes. We focus on two specific phenomena encountered in electrochemical measurements: the anodic transfer of

oxygen from water to an organic reactant in the absence of reactant adsorption to the electrode, and the anodic transfer of oxygen from water to an organic reactant when the reactant adsorbs weakly to the electrode. The theoretical implications of the model fit very well with experimental results and offer, for the first time, a mathematical explanation to the complex voltammetry observed in anodic O-transfer reactions.

Chapter IV offers a paper that began to apply some of the basic knowledge we have gained in the development of a mathematical model for O-transfer reactions. We attempted to demonstrate the electrocatalytic oxidation of the aromatic molecules toluene and *m*-xylene. We compared the voltammetry of these organic O-transfer reactions at various metal oxide electrodes: undoped lead dioxide, Bi-doped lead dioxide, and Fe-doped lead dioxide. We showed the enhanced rate of oxidation of toluene at very mildly Fe-doped PbO_2 films compared to that of a much more heavily Bi-doped PbO_2 film. We found that toluene is oxidized in a stepwise fashion first to benzyl alcohol, then to benzaldehyde, and finally to benzoic acid. Also, we offered evidence of the stepwise functional group oxidation of *m*-xylene at the Fe-doped PbO_2 film.

Chapter V is a paper that examines a practical application of anodic O-transfer reactions. We have developed an electrochemical cell in which dilute organic solvents are anodically oxidized in a single pass through the cell. We envision such an electrochemical cell to be utilized in liquid chromatographic applications for which organic containing effluent can be oxidized in quantities greater than 90% in a single pass, online configuration. We found that the addition of Mn^{2-} to the dilute solvent solutions allowed anodic oxidation and degradation of various solvents with 99% efficiency in some cases. Solvents that were

examined were: acetonitrile, methanol, methyl *tert*-butyl ether (MTBE), methylene chloride, 1,4 dioxane, and others.

Chapter 6 is a paper that presents the practical application of anodic O-transfer reactions in the remediation of various industrial and groundwater type wastes. The electrochemical incineration of phenol, aniline, and various additional compounds is observed. To measure the efficiency of the incineration process we employed an NDIR CO_2 detector and a closed loop electrochemical reactor in addition to COD measurements.

Our initial experiments demonstrated fairly low activities for the electrochemical incineration of various compounds even at known highly active electrodes. We explored the hypothesis that irradiation of aromatic molecules with ultraviolet (UV) light in a thin sheath around an active anode would increase the rate of incineration compared to no use of UV irradiation. Our first assumption was that irradiation of the chromophore would cause the excited molecule to have a lower energy barrier for oxidation. We found that certainly the use of UV irradiation caused increased anodic oxidation of our target molecules, but evidence points to the conclusion that the UV radiation serves to increase the activity of the semi-conductor metal oxide anode rather than an excitation of the organic molecule.

Finally, chapter VII is an extension of the work that was begun in chapter six, however focusing on one uniquely active anode. We have found that a mixed metal oxide of Fe, Mn, and Pb showed significantly higher activity for the electrochemical incineration of phenol solutions compared to the Fe-doped PbO_2 anode. The constant-current incineration CO_2-time curves exhibit a very distinct appearance and proved to be reproducible. In addition, it was found that though this electrode possesses very high initial activity for the oxidation of phenol, the reaction reproducibly terminates at 67-70% completion. The

resulting product solution is believed to be a near quantitative conversion of the phenol aliquot to acetic acid.

Through this research, we have studied anodic O-transfer reactions. Our goal is to improve the practical application of various techniques and materials for the anodic oxidation of organic compounds in aqueous solutions. We foresee industry, government, and academia utilizing some of the methods we've developed for such purposes ranging from environmental remediation of pollution to the conversion of industrial waste to saleable starting materials for use in other product development.

References

[1] I.-H. Yeo, D.C. Johnson, *J. Electrochem. Soc.*, **1987**, *134*, 1973.

[2] J. Feng, D.C. Johnson, *J. Appl. Electrochem.*, **1990**, *20*, 116.

[3] J. Feng, D.C. Johnson, *J. Electrochem. Soc.*, **1990**, *137*, 507.

[4] J. Feng, D.C. Johnson, *J. Electrochem. Soc.*, **1991**, *138*, 3328.

[5] D.C. Johnson, H. Chang, J. Feng, W. Wang, in *Electrochemical Technology for a Cleaner Environment*, D. Genders and N. Weinberg, Editors, p. 331, Electrosynthesis Co., Inc., East Amherst, **1992**.

[6] J.E. Vitt, D.C. Johnson, *J. Electrochem. Soc.*, **1992**, *139*, 774.

[7] K.T. Kawagoe, D.C. Johnson, *J. Electrochem. Soc.*, **1994**, *141*, 3404.

[8] J. Feng, D.C. Johnson, S.N. Lowery, J.J. Carey, *J. Electrochem. Soc.*, **1994**, *141*, 2708.

[9] J. Feng, L.L. Houk, D.C. Johnson, *J. Electrochem. Soc.*, **1995**, *142*, 3626.

[10] J. Feng, L.L. Houk, D.C. Johnson, S.N. Lowery, J.J. Carey, *J. Electrochem. Soc.*, **1995**, *142*, 3626.

[11] D.C. Johnson, N.Đ. Popović, J. Feng, L.L. Houk, K.T. Kawagoe, *Proc. Electrochem. Soc.*, **1996**, *95-26*, 176.

[12] N.Đ. Popović, D.C. Johnson, *Anal. Chem.*, **1998**, *70*, 468.

[13] N.Đ. Popović, J.A. Cox, D.C. Johnson, *J. Electroanal. Chem.*, **1998**, *456(1-2)*, 203.

[14] L.L. Houk, S.K. Johnson, J. Feng, R.S. Houk, D.C. Johnson, *J. Appl. Electrochem.*, **1998**, *28*, 1167.

[15] S.K. Johnson, L.L. Houk, J. Feng, R.S. Houk, D.C. Johnson, *Environ. Sci. Technol.* **1999**, *33*, 2638.

[16] D.C. Johnson, J. Feng and L.L. Houk, *Electrochim. Acta*, **2000**, *46*, 323.

[17] A.T. Kuhn, *The Electrochemistry of Lead*, Academic Press, London, **1979**.

[18] B.E. Conway, in *Electrodes of Conductive Metal Oxides*, S. Trasatti, Ed., Elsevier, New York, **1981**.

[19] D. Pletcher, F. Walsh, *Industrial Electrochemistry*, 2nd ed., Chapman and Hall, New York **1990**.

[20] H. Lund, D. E. Danly, C. J. H. King, in *Organic Electrochemistry*, 3rd ed., H. Lund and M. Baizer, Editors, p. 276, 1288, Marcel Dekkar Inc., New York **1991**.

[21] D. Kyriacou, D. Jannakoudakis, *Electrocatalysis for Organic Synthesis*, p. 47, John Wiley & Sons, New York **1991**.

[22] K. Scott, in *Electrochemical Processes for Clean Technology*, p. 233, The Royal Society of Chemistry, Cambridge, **1995**.

[23] C. Comninellis, C. Pulgarin, *J. Appl. Electrochem.*, **1993**, *23(2)*, 108.

[24] B. Correa-Lozano, C. Comninellis, A. De Battisti, *J. Appl. Electrochem.*, **1997**, *27(8)*, 970.

[25] G. Foti, D. Gandini, C. Comninellis, *Curr. Top. Electrochem.*, **1997**, *5*, 71.

[26] J. Xu, M.C. Granger, Q. Chen, J.W. Strojek, T.E. Lister, G.M. Swain, *Anal. Chem.*, **1997**, *69(19)*, 591A.

[27] M.D. Koppang, M. Witek, J. Blau, G.M. Swain, *Anal. Chem.*, **1999**, *71(6)*, 1188.

[28] M. Fryda, A. Dietz, D. Herrmann, A. Hampel, L. Schafer, C.-P. Klages, A. Perret, W. Haenni, C. Comninellis, D. Gandini, *Proc. – Electrochem. Soc.*, **2000**, *99-32*, 473.

[29] S. Trassati, *Electrochim. Acta*, **2000**, *45(15-16)*, 2377.

[30] A.B. Velichenko, D.V. Girenko, S.V. Kovalyov, A.N. Gnatenko, R. Amadelli, F. I. Danilov, *J. Electroanal. Chem.*, **1998**, *454*, 203.

[31] R. Amadelli, L. Armelao, A.B. Velichenko, N.V. Nikolenko, D.V. Girenko, L.V. Kovalyov, and F.I. Danilov, *Electrochim. Acta*, **1999**, *45*, 713.

[32] J. Leddy, S. Amarasinghe, L.A. Zook, F. Tinoco, *Proc. Power Sources Conf.*, **1996**, *37*, 93.

[33] J. Leddy, L.A. Zook, S. Amarasinghe, U.S. Patent 5,981,095: "Magnetic Composites and Methods for Improved Electrolysis," filed 28 January 1999, granted 9 November 1999.

[34] E.L. Cooper, L.A. Coury, Jr., *J. Electrochem. Soc.*, **1998**, *145(6)*, 1994.

[35] N.A. Madigan, L.A. Coury, Jr., *Anal. Chem.*, **1997**, *69(1)*, 5.

[36] A.J. Saterlay, S.J. Wilkins, D.B. Holt, J.S. Foord, R.G. Compton, F. Marken, *J. Electrochem. Soc.*, **2001**, *148(2)*, E66.

[37] A.J. Saterlay, S.J. Wilkins, C.H. Goeting, J.S. Foord, R.G. Compton, F. Marken, *J. Solid State Electrochem.*, **2000**, *4(7)*, 383.

[38] M.A. Fox, in *Topics in Organic Electrochemistry*, A.J. Fry, W.E. Britton, Ed., Plenum Press, New York, 1986.

[39] M.A. Fox, *New J. Chem.*, **1987**, *11(2)*, 129.

[40] M.A. Fox, R. Cardona, E. Gaillard, *J. Am. Chem. Soc.*, **1987**, *109(21)*, 6347.

[41] A.Q. Contractor, J.O'M. Bockris, *Electrochim. Acta*, **1987**, *32(1)*, 121.

[41] M.A. Fox, *NATO ASI Ser., Ser. C*, **1988**, *237*, 445-67.

[42] H. Tributsch, *Catal. Today*, **1997**, *39(3)*, 177.

[43] M.A. Fox, *Chemtech*, **1992**, *22(11)*, 680.

[44] M.A. Fox, M.T. Dulay, *Chem. Rev.*, **1993**, *93(1)*, 341.

[45] J. Rodriquez, M. Gomez, S.-E. Lindquist, C.G. Granqvist, *Thin Solid Films*, **2000**, *360(1,2)*, 250.

II. A CONSIDERATION OF THE APPLICATION OF KOUTEĆKY-LEVICH PLOTS IN THE DIAGNOSES OF CHARGE-TRANSFER MECHANISMS AT ROTATED DISK ELECTRODES

A paper accepted for publication in Electroanalysis

Stephen Treimer, Andrew Tang[1] and Dennis C. Johnson[2]

Abstract

It has become common practice to estimate the numbers of electrons (n, eq mol^{-1}) transferred in faradaic reactions at rotated disc electrodes (RDEs) from the slope of plots of reciprocal current ($1/I$) vs. reciprocal square root of rotational velocity ($1/\omega^{1/2}$). This practice is based on the Koutecky-Levich equation derived for a one-step electron-transfer mechanism. Furthermore, the intercept of the Koutecky-Levich plot is assumed to be a reciprocal function of the heterogeneous rate constant (k_h, cm s^{-1}) for the electron-transfer process. In this review, we examine the validity of the practice of estimating values of n and k_h for various multi-step mechanisms at RDEs.

I. Introduction

I.1. Rotated disc electrodes (RDEs) [1-7]

Applications of rotated disc electrodes (RDEs) to studies of electrode kinetics and mechanisms are documented [1-7]. Advantages of RDEs include: (i) The rate of mass

---

[1] Present Address: PC- Computers, 108-5th St., Ames, IA 50011-3111
[2] Corresponding author.

transport of reactants to a RDE surface is controlled precisely by fixing the rotational velocity (ω) of the electrode. (ii) Electrode currents (I) quickly achieve steady-state values $(\partial I / \partial t = 0)$ following establishment of applied electrode potential (E_{app}) for moderate-to-high rates of rotational velocity (ω > ca. 10 rad s^{-1}). As a consequence, voltammetric response ($I\text{-}E_{app}$) for a species transported from the bulk solution to the RDE surface is independent of potential scan rate for low rates of scan (ϕ < ca. 0.1 V s^{-1}). (iii) Current response at RDEs is insensitive to incidental vibrations of the apparatus.

1.2. The Levich response [1-7]

Consider the simple cathodic mechanism:

$$A + ne^- \rightleftharpoons B; \quad E^{o'} \tag{1}$$

At steady-state, the rates of diffusional and convective transport of A are equal at the electrode surface and expressed:

$$D_A\left(\frac{\partial^2 C_A}{\partial x^2}\right)_{x=0} = v_x\left(\frac{\partial C_A}{\partial x}\right)_{x=0} \tag{2}$$

In Equation 2, v_x is the axial velocity of the solution at the electrode surface ($x \approx 0$) given approximately by the first two terms of a power series:

$$v_x = -0.510\omega^{3/2}\nu^{-1/2}x^2 + 0.333\omega^2\nu^{-1}x^3 \tag{3}$$

where ν is the kinematic viscosity of the solution ($cm^2\ s^{-1}$). The second term in Equation 3 is frequently ignored for solutions of electroactive species having low diffusivity [1-7].

The cathodic electrode current (I_c) for the reduction of the oxidized species (A) to its reduced form (B) is written:

$$I_c = nF\pi r^2 D_A \left(\frac{\partial C_A}{\partial x}\right)_{x=0} = nF\pi r^2 D_A \left(\frac{C_A^b - C_A^s}{\delta}\right) \quad (4)$$

where n is the number of electrons transferred (eq mol^{-1}), F is the Faraday constant (96.487 C eq^{-1}), πr^2 is the geometric disc area (cm^2) and C_A^s is the concentration of A at the electrode surface (x = 0). Also, in Equation 4, δ represents the thickness of the diffusion layer at the electrode surface and is defined by Equation 5 for species having low diffusivity.

$$\delta = [0.620]^{-1} D_A^{1/3} \nu^{1/6} \omega^{-1/2} \quad (5)$$

For large negative applied overpotential ($\eta = E_{app} - E^{o'} << 0$), $C_A^s \rightarrow 0$ and the cathodic response corresponds to that value limited by the maximum rate of convective-diffusional mass transport, as predicted by the so-called *Levich equation* for reactant species having low diffusivity [1].

$$I_{lim,c} = 0.620nF\pi r^2 D_A^{2/3} \nu^{-1/6} \omega^{1/2} C_A^b \quad (6)$$

For species having high diffusivity, the form of the *Levich equation* recommended by Gregory and Riddiford [6] is given by Equation 7: see especially p. 365 of [7].

$$I_{lim,c} = \left[\frac{0.554}{0.893 + 0.316(D/\nu)^{0.36}}\right] nF\pi r^2 D_A^{2/3} \nu^{-1/6} \omega^{1/2} C_A^b \quad (7)$$

Accordingly, for reactant species having high diffusivity, the thickness of the diffusion layer is given by:

$$\delta = \left[\frac{0.554}{0.893 + 0.316(D/\nu)^{0.36}}\right]^{-1} D_A^{1/3} \nu^{1/6} \omega^{-1/2} \quad (8)$$

Evidence that an electrode response corresponds to Equations 6 and/or 7 is the observation of a linear dependence of $I_{lim,c}$ on the product $\omega^{1/2}C_A^b$.

In the remainder of this review, reactant species will be considered to have low diffusivity, i.e., Equations 5 and 6 are assumed to define δ and $I_{lim,c}$.

1.3. Voltammetric principles

For small values of η in a solution of A, having fast electron transfer, C_A^s is defined:

$$C_A^s = C_A^b \exp\{\theta\} \tag{9}$$

where $\theta = nF\eta/RT$. The electrode current can then expressed:

$$I_c = \frac{nF\pi r^2 D_A C_A^b}{\delta[1 - \exp\{\theta\}]} \tag{10}$$

Plots of I_c vs. $\omega^{1/2}$ are predicted to be linear at all η with slopes proportional to n. At $\eta = 0$, i.e., $E_{app} = E^{o'}$, $\exp\{\theta\} = 1$ and $I_c = 0.5I_{lim,c}$. For $\theta << 0$, $\exp\{\theta\} \approx 0$ and $I_c = I_{lim,c}$.

1.4. The Koutecký-Levich response [9]

Equation 6 is the ideal response of fast electron-transfer processes. For systems with slow electron transfer, the electrode current is defined:

$$I_c = nF\pi r^2 k_h C_A^s \tag{11}$$

where k_h (cm s^{-1}) is the heterogeneous rate constant for electron transfer.

$$k_h = k_0 \exp\left[\frac{-\alpha F\eta}{RT}\right] \tag{12}$$

In Equation 12, α is referred to as the electrochemical transfer coefficient. As predicted by Equation 11, $C_A^s \rightarrow C_A^b$ for $k_h \rightarrow 0$ and $C_A^s \rightarrow 0$ for $k_h \rightarrow \infty$.

Of greatest importance for this review are examples of reactions for which the rates of mass transport and electron transfer are comparable and $0 < C_A^s < C_A^b$. These cases are described as having *mixed transport-kinetic control.* The electrode current for such cases is then described by both Equations 4 and 11. Combining these equations to eliminate C_A^s and solving for I_c produces the so-called *Koutecký-Levich equation* [8].

$$I_c = \frac{nF\pi r^2 D_A C_A^b}{\delta + D_A / k_h} \tag{13}$$

The functionally useful form of Equation 13 is the reciprocal of I_c, given by:

$$\frac{1}{I_c} = \frac{\delta}{nF\pi r^2 D_A C_A^b} + \frac{1}{nF\pi r^2 k_h C_A^b} \tag{14}$$

Substituting Equation 5 into Equation 14 yields:

$$\frac{1}{I_c} = \frac{1}{0.62nF\pi r^2 D_A^{2/3} \nu^{-1/6} \omega^{1/2} C_A^b} + \frac{1}{nF\pi r^2 k_h C_A^b} \tag{15}$$

Hence, for cathodic reactions governed by mixed transport-kinetic control, plots of $1/I_c$ vs. $1/\omega^{1/2}$ for constant values of k_h, i.e., fixed η, are predicted to generate straight lines having slopes proportional to $1/n$ and intercepts proportional to $1/k_h$. It is important to observe that the slopes of these plots are independent of applied overpotential.

It is tempting to apply Equation 16 for the analyses of all amperometric and voltammetric data to determine values for n and k_h. Indeed, this action appears viable when

experimental plots of $1/I_c$ vs. $1/\omega^{1/2}$ exhibit linearity. This review examines the nature of $1/I_c$ vs. $1/\omega^{1/2}$ plots predicted for various mechanisms at RDEs.

1.5 Multi-Step Mechanisms

In the discussion below, electron-transfer and chemical steps are represented by symbols ***E*** and ***C***, respectively. Furthermore, subscripts ***r*** and ***i*** qualify the steps as being *reversible* (kinetically fast) or *irreversible* (kinetically slow), respectively. Hence, a C_iE_i designation implies an irreversible chemical step followed by an irreversible electron-transfer step.

It also is assumed that all steps in the mechanism proceed at comparable rates or that one step is slow, i.e., the rate determining step (rds). For example, in an ***EC*** mechanism, the ***E*** step is assumed to be fast, else the ***C*** step does not proceed significantly and the mechanism exhibits the characteristics of a single ***E*** step. It is also assumed that all species in solution have equal values of diffusion coefficient (D).

2.1. *EE* Mechanisms [9,10]

Consider a cathodic mechanism involving two consecutive one-electron steps, i.e., an ***EE*** mechanism, as represented by:

$$A + e = B: \quad E_1^{o'} \tag{16}$$

$$B + e = C: \quad E_2^{o'} \tag{17}$$

In deriving equations for the net cathodic electrode current, it is assumed that the first step is at equilibrium, $E_1^{o'} > E_2^{o'}$, and the diffusion coefficients for all species are identical [9]. Furthermore, in this mechanism, any reaction between the reactant and the product, i.e., comproportionation, is assumed negligible. Sakai *et al.* present a nice treatment for the current response at an RRDE due to an ***EE*** mechanism [10].

2.1.a. Special Case of E_rE_r.

The current for the E_rE_r mechanism is given by:

$$I_c = \frac{F\pi r^2 D_A C_A^b}{\delta}\left[2 - \frac{\exp\{\theta_2\} + 2\exp\{\theta_1 + \theta_2\}}{1 + \exp\{\theta_2\} + \exp\{\theta_1 + \theta_2\}}\right] \tag{18}$$

where $\theta_1 = F\eta_1 / RT$ and $\theta_2 = F\eta_2 / RT$. Taking the reciprocal, Equation 18 becomes:

$$\frac{1}{I_c} = \frac{\delta}{F\pi r^2 D_A C_A^b}\left[\frac{1 + \exp\{\theta_2\} + \exp\{\theta_1 + \theta_2\}}{2 + \exp\{\theta_2\}}\right] \tag{19}$$

Accordingly, plots of $1/I_c$ vs. $1/\omega^{1/2}$ are expected to be linear with zero intercepts and slopes that vary as a function of applied overpotential. At very negative potentials ($E_2^{o'} >> \eta$), the exponential terms in Equation 19 are negligible, and the current is limited by convective-diffusional transport, as described by:

$$\frac{1}{I_c} = \frac{1}{I_{lim,c}} = \frac{1}{0.62nF\pi r^2 D_A^{2/3} \nu^{-1/6} \omega^{1/2} C_A^b} \tag{20}$$

Only in the case where $E_2^{o'} >> \eta$ is the slope of the reciprocal plot a reliable measure of the total value of n for the sequential processes.

2.1.b. Special Case of E_rE_i

The second step in the E_rE_i mechanism is denoted:

$$B + e^- \xrightarrow{k_h} C; \quad E_2^{0'} \tag{21}$$

The electrode current for an E_rE_i mechanism is defined:

$$I_c = \frac{F\pi r^2 D_A C_A^b}{\delta}\left[2 - \frac{D_A[2\exp\{\theta_1\}+1]}{\delta k_h + D_A[\exp\{\theta_1\}+1]}\right]$$

$$= \frac{F\pi r^2 D_A C_A^b}{\delta}\left[\frac{D_A + 2\delta k_h}{\delta k_h + D_A[\exp\{\theta_1\}+1]}\right] \tag{22}$$

According to Equation 22, the apparent value of n approaches 2 eq mol^{-1} for $\delta k_h \rightarrow 0$, i.e., large negative overpotential. This is equivalent to a convective-diffusional transport-limited reaction with n = 2 eq mol^{-1}. Written in reciprocal form, Equation 22 becomes:

$$\frac{1}{I_c} = \frac{\delta}{F\pi r^2 D_A C_A^b}\left[\frac{\delta k_h + D_A[\exp\{\theta_1\}+1]}{D_A + 2\delta k_h}\right] \tag{23}$$

There are two limiting cases for Equation 23: (i) For $E_{app} > E_2$, the second step is slow. This corresponds to $D_A >> 2\delta k_h$, and the current is the same as for E_r and is given by Equation 20. (ii) When $E_{app} < E_2$, the second step is fast. This corresponds to $D_A << 2\delta k_h$, and the reciprocal current is given by:

$$\frac{1}{I_c} = \frac{\delta}{2F\pi r^2 D_A C_A^b} + \frac{\exp\{\theta_1\}}{2F\pi r^2 k_h C_A^b} \tag{24}$$

Hence, for the E_rE_i mechanism , plots of $1/I_c$ vs. $1/\omega^{1/2}$ exhibit a slope inversely proportional to the total number of electrons passed in the step-wise mechanism ($1/n_{tot}$) and an intercept

inversely proportional to the heterogeneous rate constant for the second irreversible step ($1/k_h$). From this, we conclude that, for a multi-stepwise mechanism, the apparent number of electrons (n_{app}) determined from the plot of $1/I_c$ vs. $1/\omega^{1/2}$ corresponds to the sum of the electrons passed for the fast steps plus the rate determining step. Clearly, this value of n_{app} can be equal to or less than the total number of electrons (n_{tot}) determined from the coulometric result of exhaustive electrolysis.

3. Introduction to *EC* and *CE* Mechanisms [11,12]

It is common to have chemical reactions occurring in solution before, after or between electron transfer steps. The mathematical analyses of these mechanisms are simplified by the use of the reaction layer approach [12,13], the principle of which is illustrated by the following example. For an *EC* reaction scheme, we write:

$$A + e \rightleftharpoons B: \quad E^{o'} \tag{25}$$

$$B \xrightarrow{k} C \tag{26}$$

The formation of C from B is assumed to be complete within a reaction layer at the electrode surface having a thickness of μ defined by:

$$\mu = (D_B/k)^{1/2} \tag{27}$$

A small μ corresponds to a very short lifetime of B ($k >> 0$), e.g., for $\mu << \delta$, the contribution from convection can be ignored and the problem is reduced to a diffusion-controlled process modified by a chemical reaction. The reaction layer thickness is also viewed as a parameter that emerges through the solution of the equations describing the electrochemical-chemical system [13], where k is a linear combination of the rate constants of the chemical step.

4. *CE* Mechanisms [13-16]

Initial interpretations of ***CE*** mechanisms were made by Koutecký and Levich [13]. Further contributions were offered by Albery [14], Compton *et al.* [15], and Rebouillat *et al.* [16]. For the electroinactive species A in equilibrium with the electroactive B species, the first step in the ***CE*** mechanism is represented by:

$$A \underset{k_b}{\overset{k_f}{\rightleftharpoons}} B: \quad \text{where} \quad K = k_f/k_b \text{ and } k = k_f + k_b \tag{28}$$

Several unique versions of ***CE*** mechanism exist, and are presented below.

4.1. Case of C_rE_r

The second step is represented by:

$$B - e \rightleftharpoons C: \quad E_1^{o'} \tag{29}$$

For the situation, the electrode current is given by:

$$I_c = \frac{nF\pi r^2 D_B K C^b}{\delta[K - (1-K)\exp\{\theta_1\}] - \mu} \tag{30}$$

where $C^b = C_A^b + C_B^b$. Equation 30 is accurate when $(D_B/v)^{1/3} << k/\omega$. When $K >> 1$, $I_c = I_{lim,c}$. Equation 30 can be rearranged to:

$$\frac{1}{I_c} = \frac{\delta[K + (1 + K)\exp\{\theta_1\}]}{nF\pi r^2 D_B K C^b} + \frac{\mu}{nF\pi r^2 K D_B C^b} \tag{31}$$

According to Equation 31, plots of $1/I_c$ vs. $1/\omega^{1/2}$ are predicted to be linear with intercepts proportional to μ/K. Again, it is important to note that the slopes of reciprocal plots for this mechanism are a function of applied overpotential.

4.2. Case of *C_iE*

The second step is represented by:

$$B + e^- \xrightarrow{k_h} C \tag{32}$$

The current is given by:

$$I_c = \frac{nF\pi r^2 D_B K k_h C^b}{D_B(1 + K) + k_h(\mu + \delta K)} \tag{33}$$

which, in the reciprocal form, is written:

$$\frac{1}{I_c} = \frac{\delta}{nF\pi r^2 D_B C^b} + \frac{D_B(1 + K) + \mu k_h}{nF\pi r^2 D_B K k_h C^b} \tag{34}$$

For this mechanism, the slopes of reciprocal plots are not a function of applied overpotential.

5. *EC* Mechanisms [17–21]

Galus [17] first made observations of the *EC* mechanism represented by:

$$A + e^- \rightleftharpoons B; \quad E_1^{o'} \tag{35}$$

in which species B is converted to an electroinactive species C via a chemical process. Bard and Faulkner have provided a general overview of *EC* processes at RDEs [18].

5.1. Case of E_rC_r

The chemical step is reversible, as represented by:

$$B \underset{k_b}{\overset{k_f}{\rightleftharpoons}} C: \qquad \text{where } K = k_f/k_b \text{ and } k = k_f + k_b \tag{36}$$

The current is given by the expression:

$$I_c = \frac{nF\pi r^2 D_A (1 + K) C_A^b}{\delta[1 + K + \exp\{\theta_1\}] + \mu K \exp\{\theta_1\}} \tag{37}$$

with the reciprocal being written:

$$\frac{1}{I_c} = \frac{\delta[1 + K + \exp\{\theta_1\}]}{nF\pi r^2 D_A (1 + K) C_A^b} + \frac{\mu K \exp\{\theta_1\}}{nF\pi r^2 D_A (1 + K) C_A^b} \tag{38}$$

For this mechanism, slopes of the reciprocal plots are a function of applied overpotential.

5.2. Case of E_rC_i

The second step is irreversible, as represented by:

$$B \overset{k}{\rightarrow} C \tag{39}$$

The current for which is:

$$I_c = \frac{nF\pi r^2 D_A C_A^b}{\delta + \mu \exp\{\theta_1\}} \tag{40}$$

which, in the reciprocal form, is given by:

$$\frac{1}{I_c} = \frac{\delta}{nF\pi r^2 D_A C_A^b} + \frac{\mu \exp\{\theta_1\}}{nF\pi r^2 D_A C_A^b} \tag{41}$$

This expression is reasonably accurate for values of $\delta/\mu > 50$. As noted in Equation 41, slopes of the reciprocal plots are not a function of applied overpotential.

5.3. *EC$_i$'* Mechanisms

McIntyre *et al.* [19] elucidated the *EC$_i$'* mechanism. Compton and co-workers have contributed significant recent interpretations for the *EC$_i$'* mechanism [20,21]. The reactant is regenerated from the product by a chemical step, considered to be *catalytic*, as indicated by:

$$A + e^- \rightleftharpoons B; \quad E_1^{o'} \tag{42}$$

$$B \xrightarrow{k} A \tag{43}$$

The current is given by:

$$I_c = \frac{nF\pi r^2 D_A C_A^b}{\mu[1 + \exp\{\theta_1\}]} \tag{44}$$

For this mechanism, $I_{lim,c} = nF\pi r^2 (D_A/\mu) C_A^b$ at $\theta << 0$.

It is apparent from Equation 44 that the current observed for *EC$_i$'* is a factor of δ/μ times the current due solely to mass transport and is independent of the rotational speed. This conclusion assumes k_f is large compared to D_A/δ and, hence, the effect of mass transport is negligible. When this assumption is no longer valid, the observed current has both mass transport and catalytic components. The observed current approaches the transport-limited current for the A species in the bulk solution as the rotational velocity is increased. In general, for *EC$_i$'* mechanisms, plots of I_c vs. $\omega^{1/2}$ have non-zero intercepts. The *EC$_i$'* mechanism at chemically modified electrodes, though well documented in the literature, will

not be interpreted by this work due to complications arising from the interpretations of Michaelis-Menten style kinetics.

6. *ECE* Mechanism [22-24]

Filinovskii, made some of the early predictions for various ***ECE*** mechanisms [2]. Subsequent work by Amatore and coworkers [22,23] and Compton *et al.* [24] further developed the theoretical model for the ***ECE*** mechanism. In a cathodic ***ECE*** mechanism, the reactant (A) is reduced to the electroinactive species B via electron-transfer. The species B is chemically transformed in solution to an electroactive intermediate (C) which undergoes further reduction to give the final product (D). The three steps in the ***ECE*** mechanism are represented by:

$$A + e^- = B: \qquad E_1^{o'} \tag{45}$$

$$B \underset{k_b}{\overset{k_f}{=}} C: \quad \text{where } K = k_f/k_b \text{ and } k = k_f + k_b \tag{46}$$

$$C + e^- = D: \qquad E_2^{o'}. \tag{47}$$

6.1. Case of *E_rC_rE_r*

The cathodic current for this sequential mechanism is given by:

$$I_c = \frac{2F\pi r^2 D_A K C_A^b}{\delta K - \mu(1-K)\exp\{\theta_1\} + \delta\exp\{\theta_1+\theta_2\}} \tag{48}$$

Rearranging to the reciprocal form, gives:

$$\frac{1}{I_c} = \frac{\delta[K+\exp\{\theta_1+\theta_2\}]}{2F\pi r^2 D_A K C_A^b} + \frac{\mu(1+K)\exp\{\theta_1\}}{2F\pi r^2 D_A K C_A^b} \tag{49}$$

Again, it is important to note that the slopes of reciprocal plots for this mechanism are a function of applied overpotential.

6.2. Case *E,C,E*$_i$

For such a mechanism, the third step corresponds to:

$$C + e^- \xrightarrow{k_h} D: \tag{50}$$

with the current denoted:

$$I_c = \frac{2F\pi r^2 D_A K k_h C_A^b}{\delta K k_h + [D_A + \mu(1+K)k_h]\exp\{\theta_1\}} \tag{51}$$

Rearranging to the reciprocal form, we get:

$$\frac{1}{I_c} = \frac{\delta}{2F\pi r^2 D_A C_A^b} + \frac{[D_A + \mu(1+K)k_h]\exp\{\theta_1\}}{2F\pi r^2 D_A K k_h C_A^b} \tag{52}$$

The slopes of reciprocal plots for this mechanism are not a function of applied potential.

7. Partially Blocked Electrodes [25-33]

The preceding treatments assume that the electrode surfaces are uniformly active and accessible to the reactants. Landsberg, Scheller, and co-workers brought to light significant advances in *blocked* or *inhomogeneous* electrodes: electrodes that are not fully accessible to solution [25-27], possibly the result of the formation of an inert organic film, oxide, adsorbed gas bubbles, or insufficiently clean surface preparation. There are two types of

inhomogeneous electrodes: *macroscopic* [28,29] is when the size of active regions and the distance between them are similar to the thickness of the diffusion layer; and *microscopic* [30,31] is when the size of the active regions and the distance between them are much smaller than the thickness of the diffusion layer.

Useful treatments for the diagnosis of mechanisms at polymer coated rotated disc electrodes using Koutecký-Levich plots have been developed recently, but will not be presented in this brief manuscript.

7.1. Macroscopic Inhomogeneity.

The response of an inhomogeneous electrode is complicated by radial (non-linear) diffusion and convection mass transport. Let f denote the fraction of the surface that is inactive. For an inhomogeneous RDE with $f = 0.5$, Levart [32] compared digital simulations of the effect of the radius of the active sites (r_s) on the ratio (ρ) of the observed currents to the transport-limited currents for a fully active RDE. For these simulations, the diameter of the active sites was set equal to distance between these sites. For $r_s > 10\delta$, ρ was independent of δ. At $r_s > \delta$, ρ increased with increasing δ. Because ρ depends on δ, the I-$\omega^{1/2}$ plot exhibited a reaction under mixed transport-kinetic control. Over the range $0.96 \geq f \geq 0.50$, ρ was greater than $1 - f$; i.e. the current was larger than expected if the total active area behaved as one contiguous surface. The additional current was due to the contribution of radial convection to mass transport.

Radial diffusion is most significant at small electrodes and low rotation speeds. Landsberg and co-workers [25] offered an analytical approach to the current response due to radial convection, further refined by Scheller and co-workers [26,27], and summarized by

Filinovskii and Pleskov [2,3]. According to the model, active sites were circular with radius r_1, uniformly distributed on the electrode surface, and concentric with one end of a larger, imaginary cylinder. Mass transfer between the sites and the solution occurred by diffusion inside the cylinders, each with length δ and radius r_2. Given $\delta >> r_2$, the model predicted linear plots of $1/I$ vs. $1/\omega^{1/2}$, with intercepts as Bessel functions of the quantity r_1/r_2. This case has been experimentally verified [25-27]. For $\delta << r_2$, a plot of I vs. $\omega^{1/2}$ was linear with slope as a different Bessel function of r_1/r_2, less than the Levich slope. The model was not very realistic because each site would have its own diffusion layer [28], but gave the correct functional dependence [26]. Caprani and Frayret [33] developed an equation for a partially blocked surface with independently active sites, for which the current is summed for each microelectrode over the entire surface. The equation is:

$$\rho = 1.1\pi r^{1/3}(1-f)^{5/6}d^{1/6} \tag{53}$$

where r is the radius of the RDE and d is the number of active sites per unit of geometric area.

7.2. Microscopic Inhomogeneity

Amatore *et al.* proposed two sub-cases for diffusion to microscopically inhomogeneous surfaces [30]. First, when $f << 1$, the standard rate constant for electron transfer is $(1 - f)$ times that of the standard rate constant for a fully active electrode. Second, for $f \approx 1$, the amount of reactant electrolyzed is sufficiently low relative to the rate of diffusion, therefore the concentration near the electrode reaches a steady state and the

voltammetric response obtained for a quiescent solution has the appearance of the response obtained in stirred solution. The limiting current is given by:

$$I_{lim} = \frac{F\pi r^2 D_A C_A^b}{2r_0 \Phi(1-f)} \tag{54}$$

where $\Phi(1-f)$ is $0.3(1-f)^{-1/2}$ for disc type sites and $1-(1/\pi)\,\mathrm{Ln}\sin\{(\pi/2)(1-f)\}$ for stripe-type sites and $2r_o$ is the distance between the centers of two adjacent sites.

Although the results of Amatore *et al.* were derived for diffusion to stationary electrodes, they should apply for RDE systems if $\delta >> 2r_o$. Therefore a microscopically inhomogeneous RDE with $f << 1$ is equivalent to a fully active electrode of the same geometry with a slower electron transfer rate at the same applied potential. When $f \rightarrow 1$, the current is not a function of rotational speed and is not necessarily smaller than the diffusion-limited current at a geometrically identical, fully active electrode.

8. Diagnosis of Mechanisms

The primary motivation in many electroanalytical studies of electrode response at hydrodynamic electrodes is the determination of the value for n (eq mol^{-1}) corresponding to the charge-transfer component of the response mechanism. A secondary objective is identification of the simplest mechanism that is consistent with observed variations in electrode response as a function of changes in the rate of convective-diffusional mass transport. And, of course, associated with this mechanistic diagnosis is the evaluation of the rate constant corresponding to the rate-determining step (rds).

Linearity of Levich plots of I vs. $\omega^{1/2}$ over an extended range of ω values, e.g., 5 - 1,000 rad s^{-1} (50 - 10,000 rev min^{-1}), is indicative of a response mechanism that can be

approximated as a single step resulting in the rapid transfer of n electrons characterized by a large heterogeneous rate constant (k_h). For this case, the n value can be reliably estimated from the slope using literature values of ν and D. If these values are not available, the estimation $\nu = 1.0\text{x}10^{-2}$ cm^2 s^{-1} is useful for most aqueous media and D = $1.0\text{x}10^{-5}$ cm^2 s^{-1} is a common approximation for small reactant species in aqueous media. Negative curvature in plots of I vs. $\omega^{1/2}$ can be indicative of slow charge-transfer kinetics, as indicated by Equation 10. Of course, this is the mechanism presumed in the derivation of the Koutecky-Levich equation and, therefore, the plot of $1/I$ vs. $1/\omega^{1/2}$ is recommended. Accordingly, we recommend estimation of n values from both the linear segment of the Levich plot at low ω values (< ca. 100 rad s^{-1}) and from the linear segment of the Koutecky-Levich plot at large ω values (> ca. 100 rad s^{-1}). Equality of these two n values can be interpreted as confirmation of the diagnosis of a one-step mechanism involving the transfer of n electrons with a moderately slow heterogeneous rate constant (k_h). Furthermore, k_h can be evaluated from the non-zero intercept of the Koutecky-Levich plot, as indicated by Equation 15.

Should one observe that the value of n calculated from the Levich plot for low ω values is larger than that estimated from the Koutecky-Levich plot for large ω values can be interpreted as indicative of two or more consecutive charge transfer steps, e.g., E_rE_i and E_rCE_i mechanisms, wherein the second charge-transfer step occurs with a k_h value much smaller than that for the first charge-transfer step. It can be helpful in such cases to determine an overall n value from coulometric results for an exhaustive electrolysis.

Partially blocked electrode surfaces usually are the undesired consequence of the adsorption of organic impurities from the bulk solution and/or the polymerization of free-radical intermediate products of incomplete electrode reactions involving organic reactants. Therefore, electrode response under these situations will demonstrate a steady decay with continued use. Electrode response can be restored by mechanical polishing, sonication, and/or application of positive-negative potential steps to cause anodic or cathodic desorption of the films [34-37].

Finally, apply different electrode geometries and/or chronoamperometry and the corresponding theories to elucidate ambiguous results of the RDE voltammetry to assist in the unambiguous determination of the mechanism [38].

References

[1] V. G. Levich, *Physicochemical Hydrodynamics*, 2nd. ed., Prentice-Hall: Englewood Cliffs, New Jersey, **1962**, pp. 60-72.

[2] Y. V. Pleskov, V. Y. Filinovskii, *The Rotating Disc Electrode* (Ed. H.S. Wroblowa) Consultants Bureau: New York, **1976**, Chapter 2.

[3] V. Y. Filinovskii, Y. V. Pleskov, *Progress in Surface and Membrane Science* (Eds. D. A. Cadenhead, J. F. Danielli), Academic Press: New York, **1976**; Vol. 10, p. 27.

[4] Z. Galus, *Fundamental of Electrochemical Analysis* (Ed. S. Marcinkiewicz), Halsted: New York, **1976**.

[5] A. J. Bard, L. R. Faulkner, *Electrochemical Methods*, 1st ed., Wiley: New York, **1980**, Chapter 8.

[6] D. P. Gregory and A. C. Riddiford, *J. Chem. Soc.*, **1956**, 3756.

[7] C. M. A. Brett, A. M. Oliveira Brett, *Comprehensive Chemical Kinetics* (Ed: C. H. Bamford, R. G. Compton), Elsevier: Amsterdam **1986,** Vol. 26, Chapter 5.

[8] J. Koutecky, V. G. Levich, *Zh. Fiz. Khim.*, **1956**, *32*, 1565.

[9] Z. Rongfeng, D. H. Evans, *J. Electroanal. Chem.*, **1995**, *385*, 201.

[10] M. Sakai, N. Ohnaka, *J. Electrochem. Soc.*, **1990**, *137(2)*, 576.

[11] J. Koutecky, R. Brdicka, *Coll. Czech. Chem. Comm.*, **1947**, *12*, 337.

[12] P. Delahay, *New Instrumental Methods in Electrochemistry*, Wiley-Interscience: New York, **1954**, p. 92.

[13] J. Koutecky, V. G. Levich, *Dokl. Akad. Nauk. SSSR*, **1957**, 117, 441.

[14] W. J. Albery, *Electrode Kinetics*, Clarendon Press: Oxford, **1975**; Chapter 5.

[15] R. G. Compton, R. G. Harland, *J. Chem. Soc., Faraday Trans. 1*, **1989**, *85(3)*, 761.

[16] S. Rebouillat, M. E. G. Lyons, T. Bannon, *J. Solid State Electrochem.*, **1999**, *3*, 215.

[17] Z. Galus, R. N. Adams, *J. Electroanal. Chem.*, **1962**, 4, 248.

[18] A. Bard, L. Faulkner, *Electrochemical Methods*, 1st ed., Wiley: New York, **1980**, 466.

[19] J. D. E. McIntyre, *J. Phys. Chem.*, **1967**, *71*, 1196.

[20] R. G. Compton, M. J. Day, M. E. Laing, R. J. Northing, J. I. Penman, A. M. Waller, *J. Chem. Soc., Faraday Trans. 1*, **1988**, *84(6)*, 2013.

[21] R. G. Compton, R. A. Spackman, P. R. Unwin, *J. Electroanal. Chem.*, **1989**, *264*, 1.

[22] C. Amatore, J.-M. Savéant, *J. Electroanal. Chem.*, **1977**, *85*, 27.

[23] C. Amatore, M. Gareil, J.-M. Savéant, *J. Electroanal. Chem.*, **1983**, *147*, 1.

[24] R. G. Compton, R. G. Harland, P. R. Unwin, A. M. Waller, *J. Chem. Soc., Faraday Trans. 1*, **1987**, *83*, 1261.

[25] R. Landsberg, R. Thiele, *Electrochim. Acta*, **1966**, *11*, 1243.

[26] F. Scheller, S. Müller, R. Landsberg, H.-J. Spitzer, *J. Electroanal. Chem.*, **1968**, *19*, 187.

[27] F. Scheller, R. Landsberg, S. Müller, *J. Electroanal. Chem.*, **1969**, *20*, 375.

[28] Y. M. Povarov, P. D. Lukovtsev, *Electrochim. Acta*, **1973**, *18*, 13.

[29] V. Y. Filinovskii, *Electrochim. Acta*, **1980**, *25*, 309.

[30] C. Amatore, J.-M. Savéant, D. Tessier, *J. Electroanal. Chem. Interfacial Electrochem.*, **1983**, *147(1-2)*, 39.

[31] O. Contamin, E. Levart, *J. Electroanal. Chem.*, **1982**, *136*, 259.

[32] E. Levart, *J. Electroanal. Chem.*, **1985**, *187*, 247.

[33] A. Caprani, J. P. Frayret, *J. Electroanal. Chem.*, **1982**, *138*, 155.

[34] D. C. Johnson and W. R. LaCourse, *Anal. Chem.*, **1990**, *62* 589A.

[35] W. R. LaCourse and D. C. Johnson, in *Advances in Ion Chromatography*, (Eds., P. Jandik, R. M. Cassidy, Vol. 2, Century International: Medfield, MA, **1990**, 353.

[36] W. R. LaCourse, *Pulsed Electrochemical Detection in High-Performance Liquid Chromatography*, John Wiley & Sons: New York, **1997**.

[37] S. Ranganathan, T.-C. Kuo, R.L. McCreery, *Anal. Chem.*, **1999**, *71(16)*, 3574.

[38] R. G. Compton, M. E. Laing, D. Mason, R. J. Northing, P. R. Unwin, *Proc. R. Soc. London A*, **1988**, *418(1854)*, 113.

III. SIMPLIFIED MODEL FOR ANODIC OXYGEN-TRANSFER REACTIONS WITHOUT AND WITH WEAK REACTANT ADSORPTION

Summary

We propose a mathematical model for two of the most commonly encountered types of oxygen-transfer reactions – those without and with weak reactant adsorption to the electrode surface. These models are meant to explain the variety of features observed in the rotated disk electrode voltammetry of organic compounds using doped metal oxide film anode. A new result indicates that the heterogeneous rate constant determined from Koutecky-Levich plots is not the rate constant for the water discharge reaction, but rather the rate constant for the oxygen transfer reaction. Significant strides were made to explain the variation of the half-wave potential, $E_{1/2}$, with the flux of reactant to the electrode surface. Experimental results show excellent agreement with theory for 0.33 Bi(V)-doped PbO_2 and 0.01 Fe(III)-doped PbO_2 electrodes.

Introduction

Metal oxide film electrodes have been used frequently in academic and industrial electrocatalysis because of their ability to facilitate the transfer of oxygen or hydrogen atoms in various electrode reactions [1-8]. Research in this laboratory has investigated the benefit of inorganic modifications of PbO_2 film electrodes for use in anodic O-transfer reactions. It was found that doped PbO_2 electrodes, formed by electrodeposition from acidic solutions of Pb(II) and foreign metallic ions, exhibit significant activity for oxygen transfer reactions.

The mechanism of oxygen-transfer reactions has been thoroughly addressed in numerous works [9-18]. However, there are few mathematical treatments offered in literature that apply to anodic oxidation reactions which occur through the transfer of oxygen from aqueous electrolyte to organic reactant molecules present in solution [19-20].

Dimethylsulfoxide (DMSO) has frequently been used as a model reactant for anodic O-transfer reactions for several reasons: a) DMSO is oxidized to $DMSO_2$ in a single 2-electron step, b) DMSO does not produce well-defined anodic voltammograms at undoped β-PbO_2 electrodes, and c) DMSO produces mass transport-limited response at a previously developed and well characterized Bi-doped PbO_2 electrode. The further refined mathematical model given below represents a thorough mathematical treatment of two related but distinct oxygen-transfer mechanisms with experimental evidence to support the theoretical implications of the model.

Experimental

Chemicals and solutions – Water was purified by deionization to 18 MΩ·cm in a Nanopure II purification system (Barnstead, Dubuque, IA) using water supplied through single-stage anion and cation exchange cartridges (Culligan, Northfield, MN). Reagent grade perchloric acid, dimethyl sulfoxide and iron powder (Fisher Scientific, Pittsburgh, PA) were used as received. Certified A.C.S. grade sulfuric acid (Fisher Scientific) was used as received. Bismuth nitrate (98+ %) and lead nitrate (99.9999+%) (Aldrich, Milwaukee, WI) were used as received.

Electrochemical apparatus and procedures – Voltammetric measurements were made

using a model AFCBP1 bipotentiostat and electrode rotator with MSRX control (Pine Instruments, Grove City, PA). Voltammetric measurements were performed in a double walled faraday cage in a laboratory maintained at 23 ± 1° C. All potentials were referenced to the saturated sodium calomel electrode (SSCE) for which the $E^{0'}$ for the ferricyanide-ferrocyanide redox couple was determined to be 0.45 V.

Films were deposited from 0.10 M $HClO_4$ using a RDE3 potentiostat and MSRX rotator (Pine Instruments). All voltammetric experiments were performed in 0.50 M H_2SO_4 using film electrodes deposited on a Au disk electrode (0.164 cm^2, Pine Instrument). Potential-time waveforms were generated and data were acquired by a PC utilizing LabView® 5.0 software and a 12-bit AT-MIO-16E-10 data acquisition board (National Instruments, Austin, TX).

Film electrodes. – The electrodeposition solution was prepared by dissolving Fe powder in deaerated 1.0 M $HClO_4$ with controlled heating. Sufficient $Pb(NO_3)_2$ powder was added to the cooled Fe(II) solution to produce 10 mM concentrations of each in 1.0 M $HClO_4$. Iron(III)-doped β-PbO_2 films were electrodeposited onto a Au rotated disk electrode (RDE: Pine Instruments) that had been thoroughly polished with alumina (5 μm: Dionex, Sunnyvale, CA) on microcloth (Buehler, Lake Bluff, IL) and rinsed thoroughly with distilled and deionized water. A potential of 1.70 V vs. SSCE was applied to the anode for a 15-min period while rotating the electrode at 105 rad s^{-1}. The current density observed for deposition was 6.0 - 6.5 mA cm^{-2}. It is important to note that evidence for incorporation of iron within the film is obtained when Fe(II) but not Fe(III) salts are used in the deposition solution. Bismuth(V)-doped β-PbO_2 films were electrodeposited from 1.0 M $HClO_4$ containing 10

mM $Pb(NO_3)_2$ and 5 mM $Bi(NO_3)_3$ at 1.6 V without stirring. Undoped β-PbO_2 films were similarly deposited in the absence of Bi(III).

Results and Discussion

Mechanisms which assume no reactant adsorption at the electrode surface - First, consider a mechanism which occurs without the adsorption of the reactant species:

$$S[\,] + H_2O \xrightarrow{k_{WDR}} S[OH] + H^+ + e^- \quad (1)$$

$$S[OH] + R \xrightarrow{k_{OTR}} S[\,] + RO + H^+ + e^- \quad (2)$$

Definitions:

R = the reactant in anodic O-transfer reactions.

RO = the product in anodic O-transfer reactions (2 eq/mol).

S = all surface sites at which anodic discharge of water can occur.

For Bi(V)-doped PbO_2-film electrodes, this can, presumably, correspond to Bi(V) sites as well as Pb(IV) sites.

Simplifying assumptions:

(i) Adsorption of R is ignored.

(ii) Rates of the WDR are assumed identical at all surface sites.

(iii) Reverse of the WDR is ignored.

(iv) The O_2-evolution reaction is ignored.

Current response - The total electrode current density (I_{tot}/FA) is given by:

$$\frac{I_{tot}}{FA} = k_{WDR}\theta_{S[\,]} + k_{OTR}\theta_{S[OH]}C_R^{\bullet} \tag{3}$$

where $\theta_{S[OH]}$ is the fractional surface coverage by OH species.

By definition:

$$\theta_{S[\,]} = 1 - \theta_{S[OH]} \tag{4}$$

Substituting $\theta_{S[\,]}$, the current is given by:

$$\frac{I_{tot}}{FA} = k_{WDR}\{1 - \theta_{S[OH]}\} + k_{OTR}\theta_{S[OH]}C_R^{\bullet}$$

$$= k_{WDR} - \{k_{WDR} - k_{OTR}C_R^{\bullet}\}\theta_{S[OH]} \tag{5}$$

Solving for $\theta_{S[OH]}$ using a steady-state assumption, we get:

$$\frac{d\theta_{S[OH]}}{dt} = 0 = k_{WDR}\theta_{S[\,]} - k_{OTR}\theta_{S[OH]}C_R^{\bullet} \tag{6}$$

Equation 6 can be rearranged to give:

$$k_{WDR} = (k_{WDR} + k_{OTR}C_R^{\bullet})\theta_{S[OH]} \tag{7}$$

From Equation 7 we get:

$$\theta_{S[OH]} = \frac{k_{WDR}}{k_{WDR} + k_{OTR}C_R^{\bullet}} \tag{8}$$

Substituting (8) into (5) gives:

$$\frac{I_{tot}}{FA} = k_{WDR} - \{k_{WDR} - k_{OTR}C_R^{\bullet}\}\left\{\frac{k_{WDR}}{k_{WDR} + k_{OTR}C_R^{\bullet}}\right\}$$

$$= 2k_{WDR}\left\{\frac{k_{OTR}C_R^s}{k_{WDR}+k_{OTR}C_R^s}\right\} \tag{9}$$

Alternatively, Equation 9 can be written as:

$$I_{tot} = \left\{\frac{2FAk_{WDR}k_{OTR}C_R^s}{k_{WDR}+k_{OTR}C_R^s}\right\} \tag{10}$$

Half-wave potential - Consider the unique relationship of the voltammograms exhibited in Figure 3.1. To examine the variation of $E_{1/2}$, we specify at $E = E_{1/2}$ that $k_{OTR} = k_{OTR,1/2}$. Furthermore, we define $I_{1/2} = I_{lim}/2$ which corresponds to $C_R^s = C_R^b / 2$. Therefore, $I_{tot,1/2}$ is given by:

$$I_{tot,1/2} = 2FAk_{WDR,1/2} = I_{lim}/2 = 2FA(D/\delta)C_R^b / 2 \tag{11}$$

where $D/\delta = 0.62D^{2/3}\upsilon^{-1/6}\omega^{1/2}$ (12)

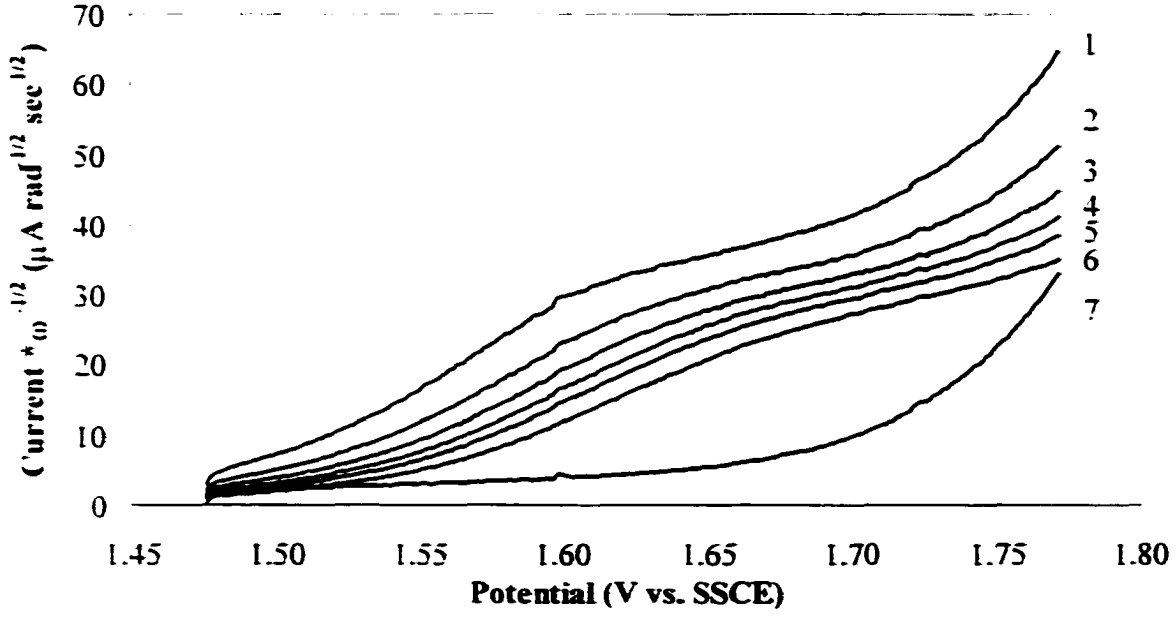

Figure 3.1. 5 mM DMSO at a 0.33 Bi-doped PbO_2 anode, 20 mV/s scan rate. Current has been normalized to the variation in rotation rate 1) 100 rpm 2) 225 3) 400 4) 625 5) 900 6) 1600 and 7) background (rotation independent).

We also can write:

$$k_{WDR,1/2} = 0.62D^{2/3}\upsilon^{-1/6}\omega^{1/2}C_R^b / 2 \quad (13)$$

Expanding the term for $k_{WDR,1/2}$, we write

$$k_{WDR}^0 \exp\{(\alpha F/RT)(E_{1/2} - E_{WDR}^{0'})\} = 0.62D^{2/3}\upsilon^{-1/6}\omega^{1/2}C_R^b / 2 \quad (14)$$

Finally, we solve for $E_{1/2}$ to get

$$E_{1/2} = E^0 - (RT/\alpha F)\mathrm{Ln}\{2k_{WDR}^0\} + (RT/\alpha F)\mathrm{Ln}\{0.62D^{2/3}\upsilon^{-1/6}\omega^{1/2}C_R^b\} \quad (15)$$

From Equation 15, we predict that a plot of $E_{1/2}$ vs. $\mathrm{Ln}\{0.62D^{2/3}\upsilon^{-1/6}\omega^{1/2}C_R^b\}$ is linear with a slope of + RT/αF. The potential must shift to larger values to achieve the increased OH flux required to match the increased reactant flux. Experimental evidence for this relationship can be observed in Figures 3.1-3.3.

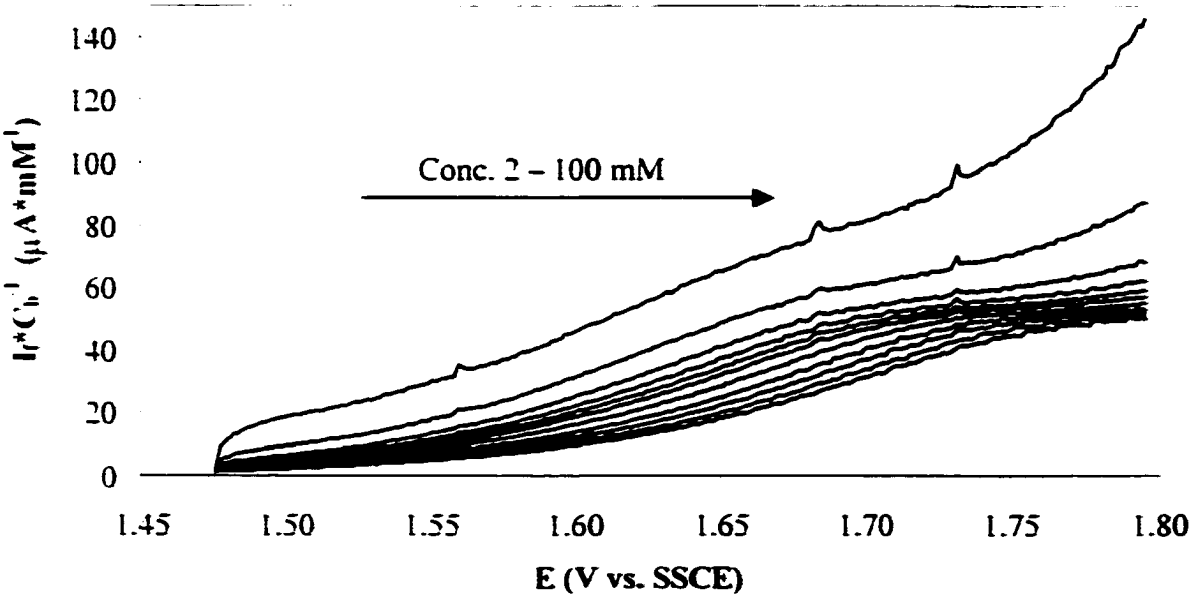

Figure 3.2. Forward sweep cyclic voltammograms of 2 – 100 mM DMSO at the same Bi-doped PbO_2 electrode as Figure 3.1. Again, the voltammograms have been normalized for differences in concentrations. Rotation rate: 100 rpm.

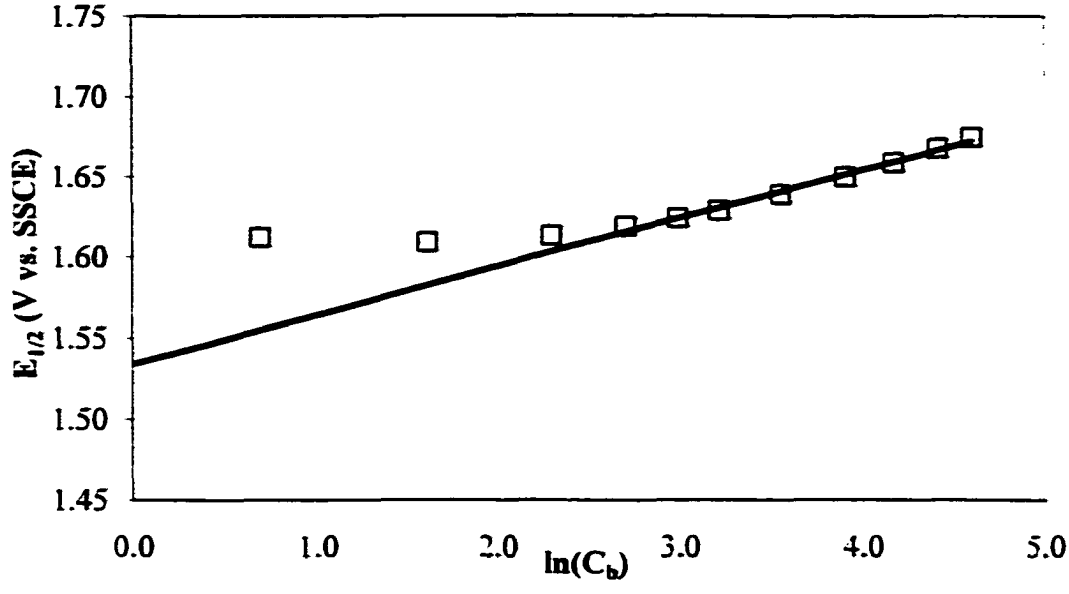

Figure 3.3. Dependence of $E_{1/2}$ on flux from Figure 3.2. Concentrations of DMSO 2-100 mM. 100 rpm rotation rate. 20 mV/s scan rate.

Calibration plots - Consider the calibration style plots shown in Figure 3.4. We consider the shape of plots of I_{lim} vs. C_R^*, as a function of k_{WDR}, i.e., as a function of potential. Again, we begin with Equation 10:

$$I_{lim} = \left\{ \frac{2FAk_{WDR}k_{(I)TR}C_R^*}{k_{WDR} + k_{(I)TR}C_R^*} \right\} \tag{10}$$

where C_R^* can be given by:

$$C_R^* = C_R^b - \left(\frac{I_{lim}}{2FA(D/\delta)} \right) \tag{16}$$

Combine Equation 10 and 16 and solve for I_{lim} to get:

$$I_{tot} = 2FAk_{WDR}\left\{\frac{k_{OTR}C_R^b - \left(\frac{k_{OTR}I_{tot}}{2FA(D/\delta)}\right)}{k_{WDR} + k_{OTR}C_R^b - \left(\frac{k_{OTR}I_{tot}}{2FA(D/\delta)}\right)}\right\}$$

$$= 2FAk_{WDR}\left\{\frac{2FA(D/\delta)k_{OTR}C_R^b - k_{OTR}I_{tot}}{2FA(D/\delta)(k_{WDR} + k_{OTR}C_R^b) - k_{OTR}I_{tot}}\right\} \quad (17)$$

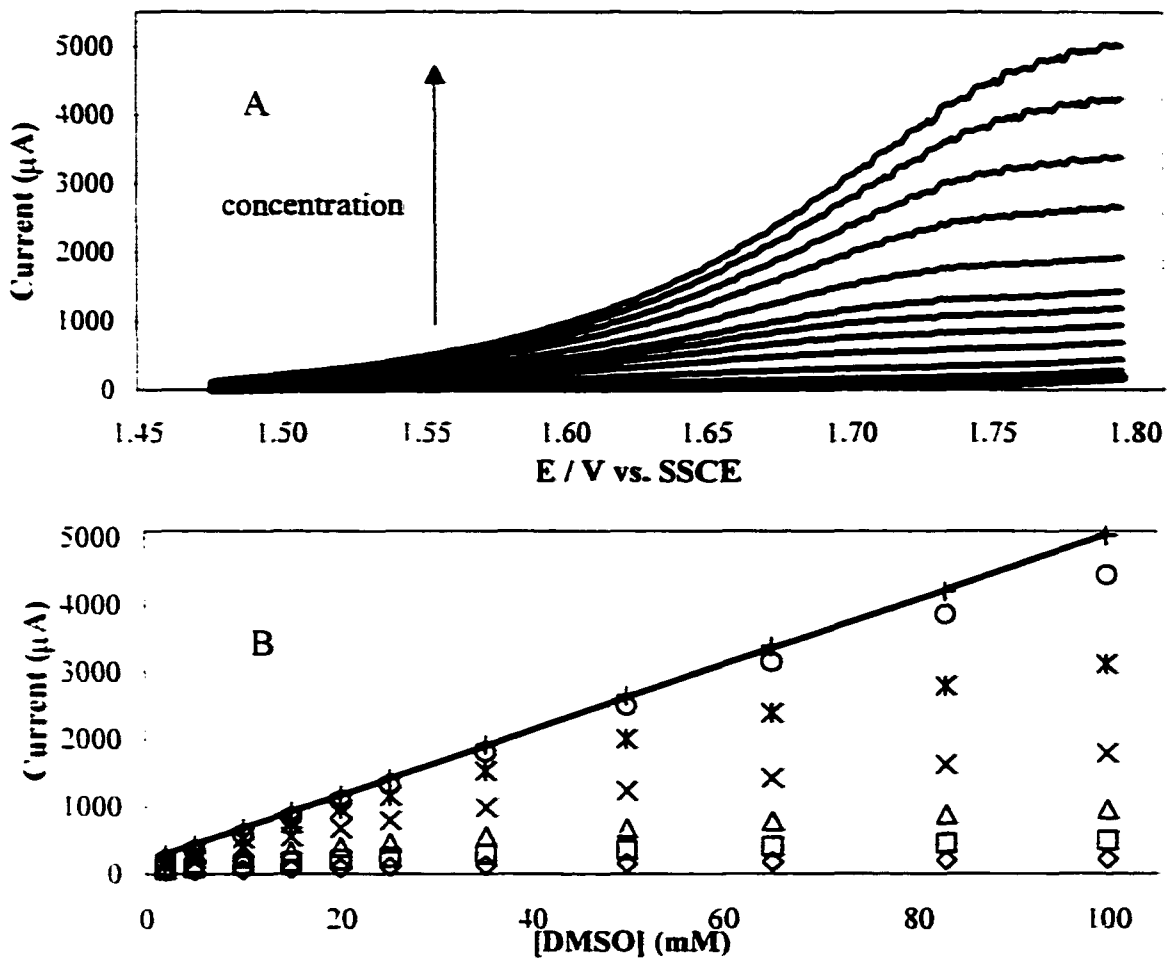

Figure 3.4. DMSO at a 0.33 Bi-doped PbO_2 electrode 1 M H_2SO_4, 0.02 V/s, 100 rpm, 0.164 cm^2. A: Cyclic voltammetric data, concentrations: 0, 2, 5, 10, 15, 20, 25, 35, 50, 65, 83, 100 mM. B: Calibration curve data from (A) at the potentials: ◊ - 1.50 V, □ - 1.55 V, △ - 1.60 V, x - 1.65 V, * - 1.70 V, ○ - 1.75 V, + - 1.79 V.

Cross multiply (17) to get:

$$2FA(D/\delta)k_{WDR}I_{tot} + 2FA(D/\delta)k_{OTR}C_R^b I_{tot} - k_{OTR}I_{tot}^2$$

$$= 2FAk_{WDR}2FA(D/\delta)k_{OTR}C_R^b - 2FAk_{WDR}k_{OTR}I_{tot} \quad (18)$$

Assume that $k_{OTR}I_{tot}^2$ can be ignored (due to the very low analytical currents employed) to eliminate the need for solving a quadratic equation. Solving for I_{tot} yields the *master equation*:

$$I_{tot} = \frac{2FAk_{WDR}(D/\delta)k_{OTR}C_R^b}{(D/\delta)k_{OTR}C_R^b + (D/\delta)k_{WDR} + k_{WDR}k_{OTR}} \quad (19)$$

To interpret Equation 19, we can consider several scenarios that cause different terms in the denominator of Equation 19 to predominate.

Case I: Let $(D/\delta)k_{OTR}C_R^b > (D/\delta)k_{WDR} + k_{WDR}k_{OTR}$, i.e., small values of potential for which k_{WDR} is small and the OH flux is virtually zero.

Then I_{tot} is given by:

$$I_{tot} = \frac{2FAk_{WDR}(D/\delta)k_{OTR}C_R^b}{(D/\delta)k_{OTR}C_R^b} = 2FAk_{WDR} \quad (20)$$

Based on Equation 20, we would predict that I_{tot} does not respond to the addition of reactant, R. This makes sense when k_{WDR} is small that there is virtually no generation of the OH species.

Case II: Let, $(D/\delta)k_{WDR} > (D/\delta)k_{OTR}C_R^b + k_{WDR}k_{OTR}$, i.e., the case of intermediate values of potential. This corresponds to the case represented by: O < OH flux < R flux. Then, I_{tot} is given by:

$$I_{tot} = \frac{2FAk_{WDR}(D/\delta)k_{OTR}C_R^b}{(D/\delta)k_{WDR}} = 2FAk_{OTR}C_R^b \quad (21)$$

Based on Equation 21, I_{tot} is predicted to be a linear function of C_R^b; however, there will be no effect of variations in rotational velocity. This response will show potential dependence because k_{OTR} corresponds to a charge-transfer process and, therefore, I_{tot} will be dependent on applied potential.

Case III: Let, $k_{WDR}k_{OTR} > (D/\delta)k_{WDR} + (D/\delta)k_{OTR}C_R^b$, i.e., the case of high potentials values. Then, I_{tot} is given by:

$$I_{tot} = \frac{2FAk_{WDR}(D/\delta)k_{OTR}C_R^b}{k_{WDR}k_{OTR}} = 2FA(D/\delta)C_R^b \quad (22)$$

This corresponds to the mass-transport limited response of the reactant, R.

Case IV: Consider the case when $(D/\delta)k_{WDR} + k_{WDR}k_{OTR} > (D/\delta)k_{OTR}C_R^b$.

Then, I_{tot} is given by:

$$I_{tot} = \left\{\frac{2FA(D/\delta)k_{OTR}C_R^b}{(D/\delta) + k_{OTR}}\right\} \quad (23)$$

According to Equation 23, the plot of I_{tot} vs. C_R^b is linear with a slope that reflects the combined values of D/δ and k_{OTR}. This corresponds to mixed control by transport and kinetic processes.

Equation 23 can be rearranged to the form:

$$I_{tot} = \left\{\frac{2FA(D/\delta)C_R^b}{1 + (D/\delta)(1/k_{OTR})}\right\} \quad (24)$$

Equation 24 can be rearranged to the form of the Koutecky-Levich equation given by:

$$\frac{1}{I_{tot}} = \left\{\frac{1}{2FAk_{OTR}C_R^b}\right\} + \left\{\frac{1}{2FA(D/\delta)C_R^b}\right\} \tag{25}$$

where $D/\delta = 0.62D^{2/3}\upsilon^{-1/6}\omega^{1/2}$.

Therefore, Equation 25 can be written as:

$$\frac{1}{I_{tot}} = \left\{\frac{1}{2FAk_{OTR}C_R^b}\right\} + \left\{\frac{1}{0.62(2)FAD^{2/3}\nu^{-1/6}\omega^{1/2}C_R^b}\right\} \tag{26}$$

According to Equation 26, a plot of $1/I_{tot}$ vs. $1/\omega^{1/2}$ is predicted to be linear with an intercept that is inversely proportional to k_{OTR}. Because k_{OTR} is expected to be an exponential function of applied potential, the natural logarithm of the intercept is expected to vary as a linear function of potential [20].

$$k = Ae^{-E_a/RT} \tag{27}$$

Figure 3.5 demonstrates experimental evidence from two different films that exhibit such behavior.

Mechanisms considering the weak adsorption of reactant species – Reactant adsorption to the electrode has only recently been considered a requirement for anodic O-transfer reactions to proceed at reasonably fast rates [22-24]. Consider the following reactions where the role of adsorption onto an electrode is considered:

$$S[\,] + H_2O \xrightarrow{k_{ox/rx}} S[OH] + H^+ + e^- \tag{28}$$

$$S'[\,] + R \underset{k_{-ads}}{\overset{k_{ads}}{=}} S'[R]; \text{ where } K_{ads} = k_{ads}/k_{-ads} \tag{29}$$

$$S[OH] + S'[R] \xrightarrow{k_{OTR}} S[\,] + S'[\,] + RO + H^+ + e^- \tag{30}$$

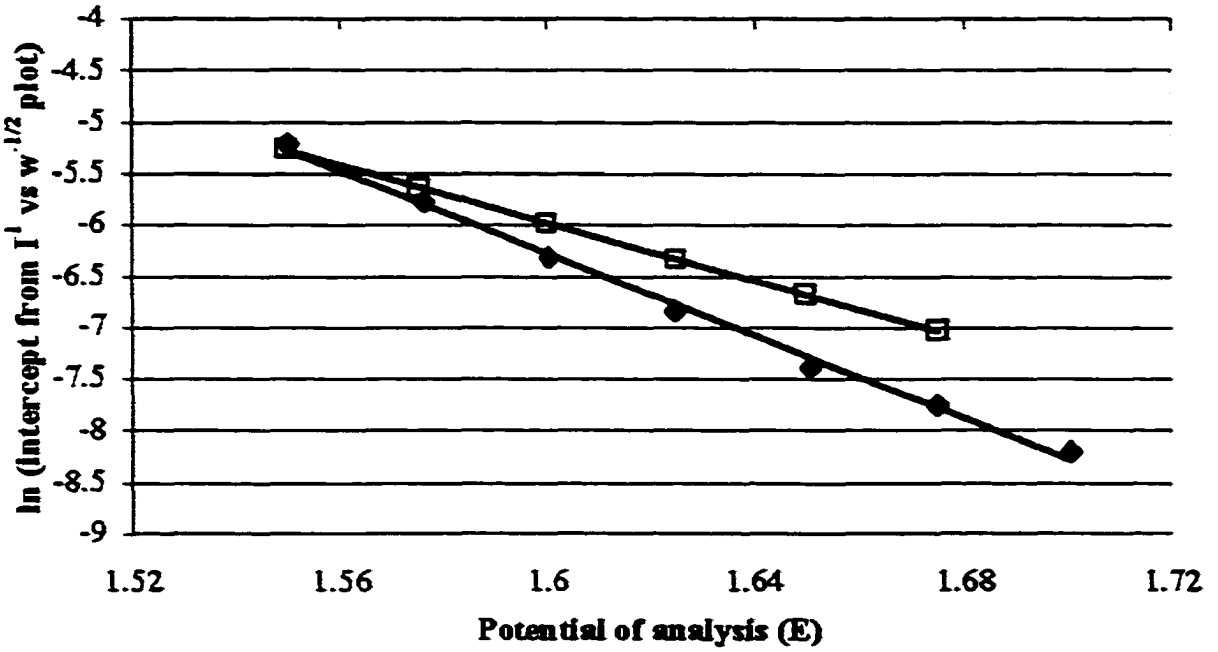

Figure 3.5. Arrhenius plots showing the variation in k_{OTR} (intercept) with Potential (E) as derived from the Koutecky-Levich analysis of 5 mM DMSO at ♦ - 0.33 Bi(V)-doped PbO_2 anode. □ - 0.01 Fe(III)-doped PbO_2 anode.

We define the additional variables above as:

Γ_0 = represents the surface density of S sites (mol/cm^2), i.e., $\Gamma_0 = \Gamma_{Pb(IV)} + \Gamma_{Bi(V)}$. In this mechanism, Γ_0 is assumed to be constant, independent of $\Gamma_{Bi(V)}/\Gamma_{Pb(IV)}$.

S′ = only those surface sites at which the reactant species (R) can be adsorbed. In this mechanism, S′ sites correspond to Bi(V) sites.

Γ_S = represents the surface density of S′ sites (mol/cm^2), i.e., $\Gamma_S = \Gamma_{Bi(V)}$.

The surface density of adsorption sites can be expressed:

$$\frac{\Gamma_{S'}}{\Gamma_0} = \frac{\Gamma_{Bi(V)}}{\Gamma_{Pb(IV)} + \Gamma_{Bi(V)}} = \frac{\rho}{1+\rho} \qquad (31)$$

where $\rho = \Gamma_{Bi(V)}/\Gamma_{Pb(IV)}$. Note: $\rho = C^b_{Bi(III)}/C^b_{Pb(II)}$ where C^b represents bulk concentrations of specified species in the film-deposition solution.

Simplifying assumptions:

(i) Rate of the WDR is assumed identical at all S sites.

(ii) Reverse of the WDR in Equation 28 is ignored.

(iii) The O_2-evolution reaction is ignored.

(iv) Equation 29 is assumed to be at equilibrium,

i.e., k_{ads} and k_{-ads} are large. Therefore,

$$k_{ads}\Gamma_{S'}\theta_{S'[]}C^*_R = k_{-ads}\Gamma_{S'}\theta_{S'[R]}$$

$$k_{ads}C^*_R - k_{ads}\theta_{S'[R]}C^*_R = k_{-ads}\theta_{S'[R]}$$

$$\theta_{S'[R]} = \frac{k_{ads}C^*_R}{k_{ads} + k_{ads}C^*_R} \tag{32}$$

Continuing,

$$\theta_{S'[R]} = \frac{(k_{ads}/k_{-ads})C^*_R}{(k_{ads}/k_{-ads}) + (k_{ads}/k_{-ads})C^*_R} = \frac{K_{ads}C^*_R}{1 + K_{ads}C^*_R} \tag{33}$$

This is the Langmuir adsorption isotherm.

A reasonable assumption can be made that $K_{ads}C^*_R < 1$, therefore

$$\theta_{S'[R]} = (k_{ads}/k_{-ads})C^*_R = K_{ads}C^*_R \tag{34}$$

Current response - The electrode current density (I_{tot} / FA) is given by:

$$\frac{I_{tot}}{FA} = k_{WDR}\Gamma_0\theta_{S[]} + k_{OTR}\Gamma_0\theta_{S[OH]}\Gamma_{S'}\theta_{S'[R]} \tag{35}$$

We note that:

$$\Gamma_0\theta_{S[\ ]} = \Gamma_0(1 - \theta_{S[OH]} - (\Gamma_{S'}/\Gamma_0)\theta_{S'[R]})$$

and, therefore, the current is given by

$$\frac{I_{tot}}{FA} = k_{WDR}\Gamma_0\{1 - \theta_{S[OH]} - (\Gamma_{S'}/\Gamma_0)\theta_{S'[R]}\} + k_{OTR}\Gamma_0\theta_{S[OH]}\Gamma_{S'}\theta_{S'[R]}$$

$$= k_{WDR}\Gamma_0 - k_{WDR}\Gamma_0(\Gamma_{S'}/\Gamma_0)\theta_{S'[R]} - \{k_{WDR}\Gamma_0 - k_{OTR}\Gamma_0\Gamma_{S'}\theta_{S'[R]}\}\theta_{S[OH]} \quad (36)$$

Solving for $\theta_{S[OH]}$ using a steady-state assumption, we get

$$\frac{d\theta_{S[OH]}}{dt} = 0 = k_{WDR}\Gamma_0\theta_{S[OH]} - k_{OTR}\Gamma_0\Gamma_{S'}\theta_{S'[R]}\theta_{S[OH]} \quad (37)$$

and, therefore,

$$k_{WDR}\Gamma_0 - k_{WDR}\Gamma_0(\Gamma_{S'}/\Gamma_0)\theta_{S'[R]} = (k_{WDR}\Gamma_0 + k_{OTR}\Gamma_0\Gamma_{S'}\theta_{S'[R]})\theta_{S[OH]}$$

or

$$k_{WDR} - k_{WDR}(\Gamma_{S'}/\Gamma_0)\theta_{S'[R]} = (k_{WDR} + k_{OTR}\Gamma_{S'}\theta_{S'[R]})\theta_{S[OH]} \quad (38)$$

Therefore, we can write:

$$\theta_{S[OH]} = \frac{k_{WDR} - k_{WDR}(\Gamma_{S'}/\Gamma_0)\theta_{S'[R]}}{k_{WDR} + k_{OTR}\Gamma_{S'}\theta_{S'[R]}} \quad (39)$$

Substituting Equation 39 into Equation 35 gives:

$$\frac{I_{tot}}{FA} = k_{WDR}\Gamma_0 - k_{WDR}\Gamma_0(\Gamma_{S'}/\Gamma_0)\theta_{S'[R]} - \{k_{WDR}\Gamma_0 - k_{OTR}\Gamma_0\Gamma_{S'}\theta_{S'[R]}\}\theta_{S[OH]}$$

$$= 2k_{WDR}k_{OTR}\Gamma_0\Gamma_{S'}\theta_{S'[R]}\left\{\frac{1 - (\Gamma_{S'}/\Gamma_0)\theta_{S'[R]}}{k_{WDR} + k_{OTR}\Gamma_{S'}\theta_{S'[R]}}\right\} \quad (40)$$

or, alternately,

$$I_{tot} = 2FAk_{WDR}k_{OTR}\Gamma_0\Gamma_{S'}\theta_{S'[R]}\left\{\frac{1-(\Gamma_{S'}/\Gamma_0)\theta_{S'[R]}}{k_{WDR}+k_{OTR}\Gamma_{S'}\theta_{S'[R]}}\right\} \tag{41}$$

Again, we apply the assumption $K_{ads}C_R^s < 1$, i.e., weak adsorption of reactant and, therefore, $\theta_{S'[R]} \approx K_{ads}C_R^s$. Now, Equation 41 is given by:

$$I_{tot} = 2FAk_{WDR}k_{OTR}\Gamma_0\Gamma_{S'}K_{ads}C_R^s\left\{\frac{1-(\Gamma_{S'}/\Gamma_0)K_{ads}C_R^s}{k_{WDR}+k_{OTR}\Gamma_{S'}K_{ads}C_R^s}\right\} \tag{42}$$

Let $(\Gamma_{S'}/\Gamma_0)K_{ads}C_R^s << 1$, then

$$I_{tot} = 2FAk_{WDR}k_{OTR}\Gamma_0\Gamma_{S'}K_{ads}C_R^s\left\{\frac{1}{k_{WDR}+k_{OTR}\Gamma_{S'}K_{ads}C_R^s}\right\} \tag{43}$$

Note that if we let $k_{WDR} << k_{OTR}\Gamma_{S'}K_{ads}C_R^s$, i.e., small applied potentials, then I_{tot} is given by:

$$I_{tot} = 2FAk_{WDR}\Gamma_0 \tag{44}$$

This case is not very interesting because it predicts that I_{tot} is not sensitive to changes in C_R^b. This reflects the consequence that k_{WDR} is small and, therefore, there is virtually no production of OH species. More interesting is the cases summarized below.

Let $k_{OTR}\Gamma_S K_{ads}C_R^s >> k_{WDR}$, i.e., intermediate to large values of applied potentials.

$$I_{tot} = 2FAk_{OTR}\Gamma_0\Gamma_S K_{ads}C_R^s \tag{45}$$

Now, make the substitution:

$$C_R^s = C_R^b - \frac{I_{tot}}{2FA(D/\delta)} \tag{46}$$

where $D/\delta = 0.62D^{2/3}\upsilon^{-1/6}\omega^{1/2}$, and solve for I_{tot} to get:

$$I_{tot} = \frac{2FA(D/\delta)k_{OTR}\Gamma_0\Gamma_{S'}K_{ads}C_R^b}{(D/\delta)+k_{OTR}\Gamma_0\Gamma_{S'}K_{ads}} \tag{47}$$

Take the reciprocal to get:

$$\frac{1}{I} = \frac{1}{2k_{OTR}\Gamma_0\Gamma_{S'}K_{ads}C_R^b} + \frac{1}{2FA(D/\delta)C_R^b} \tag{48}$$

This is of the form of the Koutecký-Levich equation.

Conclusions

It is surprising, upon first inspection, to find that Equation 26 does not contain the term k_{WDR}. Of course, this term was eliminated when we made the assumption $k_{WDR} > k_{OTR}C_R^*$, which resulted in Equation 22. Hence, it is assumed that the OH flux is sufficiently large to support the convective-diffusion limited flux of R.

For an O-transfer mechanism with no adsorption of the reactant species, Case I produces a plot of $1/I_{tot}$ vs. $1/\omega^{1/2}$ with a zero slope and an intercept that is independent of C_R^*. Case II produces a plot of $1/I_{tot}$ vs. $1/\omega^{1/2}$ with a zero slope and an intercept that decreases with increasing C_R^*. Case III produces a plot of $1/I_{tot}$ vs. $1/\omega^{1/2}$ with a non-zero slope with a zero intercept. Only Case IV produces a plot of $1/I_{tot}$ vs. $1/\omega^{1/2}$ with a non-zero slope that decreases with increasing C_R^* and a non-zero intercept that decreases with increasing C^b.

Equation 47 above describes I_{tot} as a function of C_R^b for the case of weakly adsorbed reactant:

$$I_{tot} = \frac{2FA(D/\delta)k_{OTR}\Gamma_0\Gamma_S K_{ads}C_R^b}{(D/\delta)+k_{OTR}\Gamma_0\Gamma_S K_{ads}} \quad (46)$$

This is to be compared to Equation 23 for the case of no adsorption under the condition $(D/\delta)k_{WDR} + k_{WDR}k_{OTR} > (D/\delta)k_{OTR}C_R^b$ as is given by:

$$I_{tot} = \left\{\frac{2FA(D/\delta)k_{OTR}C_R^b}{(D/\delta)+k_{OTR}}\right\} \quad (23)$$

Equation 23 is consistent with Equation 47 using the definition:

$$k_{OTR} = k_{OTR}\Gamma_0\Gamma_S K_{ads}$$

References

[1] J.A. Cox and P.J. Kulesza, *Anal. Chem.*, **1984**, *56*, 1021.

[2] M.K. Halbert and R.P. Baldwin, *Anal. Chem.*, **1985**, *57*, 591.

[3] I.-H. Yeo and D.C. Johnson, *J. Electrochem. Soc.*, **1987**,*134*, 1973.

[4] T.J. O'Shea and S.M. Lunte, *Anal. Chem.*, **1994**, *66*, 307.

[5] P.F. Luo and T. Kuwana, *Anal. Chem.*, **1994**, *66*, 2775.

[6] H. Lund, D. E. Danly, and C. J. H. King, in *Organic Electrochemistry*, 3rd ed., H. Lund and M. Baizer, Editors, p. 276, 1288, Marcel Dekkar Inc., New York, **1991**.

[7] D. Kyriacou and D. Jannakoudakis, *Electrocatalysis for Organic Synthesis*, p. 47, John Wiley & Sons, New York, **1991**.

[8] D. Pletcher and F. Walsh, *Industrial Electrochemistry*, 2nd ed., Chapman and Hall, New York, **1990**.

[9] P. Rueschi, P. Delahay, *J. Chem. Phys.*, **1955**, *23*, 556.

[10] J.O'M. Bockris, *J. Chem. Phys.*, **1956**, *23*, 817.

[11] N.I. Rosenthal, V.I. Veselovsky, *Dokl. Akad. Nauk SSSR*, **1956**, *111*, 637.

[12] A. Damjanovic, A. Dey, J.O'M. Bockris, *Electrochim. Acta*, **1966**, *11*, 791.

[13] A. Damjanovic, B. Jovanovic, *J. Electrochem. Soc.*, **1976**, *123*, 374.

[14] S. Trassatti, *J. Electroanal. Chem.*, **1980**, *111*, 125.

[15] A.G.C. Kobassen, G.H.J. Broers, *J. Electroanal. Chem.*, **1981**, *126*, 221.

[16] C.R. Churchill, D.B. Hibbert, *J. Chem. Soc., Faraday Trans.*, **1982**, *78*, 2937.

[17] T. Otagawa, J.O'M. Bockris, *J. Electrochem. Soc.*, **1982**, *129*, 2391.

[18] O. Simond, V. Schaller, C. Comninellis, *Electrochim. Acta*, **1997**, *42(13-14)*, 2009.

[19] N. . Popović, D.C. Johnson, *Anal. Chem.*, **1998**, *70*, 468.

[20] N. . Popović, J.A. Cox, D.C. Johnson, *J. Electroanal. Chem.*, **1998**, *456(1-2)*, 203.

[21] A.J. Bard, L.R. Faulkner, *Electrochemical Methods*, Wiley, New York, **1980**, p. 87.

[22] J.E. Vitt, D.C. Johnson, *J. Electrochem. Soc.*, **1992**, *139*, 774.

[23] L.J.J. Janssen, P.D.L. Van der Heyden, *J. Appl. Electrochem.*, **1995**, *25*, 126.

[24] C. Comninellis, A. De Battisti, *Chim. Phys.*, **1996**, *93*, 673.

IV. COMPARISON OF VOLTAMMETRIC RESPONSE OF PHENOL AND XYLENES AT IRON(III)-DOPED, BISMUTH(V)-DOPED AND UNDOPED β-LEAD DIOXIDE FILM ELECTRODES IN 0.50 M H_2SO_4

A paper submitted for publication in the Journal of the Electrochemical Society

Stephen E. Treimer, Jianren Feng, Marc D. Scholten, and Dennis C. Johnson[1], and Alison J. Davenport[2]

Abstract

Voltammetric activities are compared for the designated compounds in 0.50 M H_2SO_4 at the specified film electrodes configured as rotated disks. The effective number of electrons (n_{eff}, eq mol^{-1}) calculated from the Koutecky-Levich plot is 3.1±0.2 for toluene oxidation at the Fe-PbO_2 electrode, compared to 2.0±0.05 and 4.1±0.3 at the Bi-PbO_2 and PbO_2 electrodes, respectively. GC-MS data confirm that the primary product of toluene oxidation is benzyl alcohol (2 eq mol^{-1}) at the Fe-PbO_2 electrode with production of small amounts of benzaldehyde (4 eq mol^{-1}) and benzoic acid (6 eq mol^{-1}). XPS data indicate the ratio of Fe:Pb is ca. 1:100 (at:at) in the Fe-PbO_2 films. By comparison, a Bi:Pb ratio of 33:100 (at:at) is easily attained in Bi-PbO_2 films. Nevertheless, the apparent heterogeneous rate constant (k_{app}, cm s^{-1}) for toluene oxidation is larger at the Fe-PbO_2 electrode ($6.5\pm0.06\times10^{-3}$) compared to the Bi-PbO_2 electrode ($2.0\pm0.05\times10^{-3}$). XANES data confirm speculation that iron exists in the 3+ oxidation state with octahedral coordination by O-atoms

[1] Corresponding author.
[2] School of Metallurgy and Materials, The University of Birmingham, Edgbaston, Birmingham B15 2TT, U.K.

in Fe-PbO_2 films. The large activity of the Fe-PbO_2 electrode is attributed to the benefit of adsorption of aromatic molecules at Fe(III) sites.

Introduction

Research in this laboratory is directed to studies of the electrocatalytic properties of various pure, doped and mixed metal-oxide film electrodes. Reactions of interest include those oxidations of polar aliphatic and aromatic compounds in which the electrode reactions occur with transfer of oxygen atoms from H_2O in the solvent phase to the oxidation product(s). Based on thermodynamic data, numerous O-transfer reactions can be predicted to occur for aromatic compounds in aqueous media at electrode potentials below values for onset of rapid anodic discharge of H_2O with evolution of $O_2(g)$. However, the majority of these predicted O-transfer reactions are observed not to occur at common anode materials, e.g., Pt, Au and C, without co-evolution of O_2.

Metal oxide films have a long history of use as electrode materials applied to anodic O-transfer reactions of organic compounds. Of the metal oxide electrodes available, β-PbO_2 has received extensive attention both in industrial and academic applications.[1-5] Undoubtedly, the popularity of β-PbO_2 electrodes has resulted, at least in part, from observations of a large overpotential for anodic evolution of $O_2(g)$ at this electrode material. This fact permits application of potentials to ca. 2.0 V vs. SCE in acidic media without rigorous $O_2(g)$ evolution. Nevertheless, it is generally observed that O-transfer reactions of interest frequently are observed to occur only at large applied potentials (>2.0 V) with concomitant evolution of $O_2(g)$. Furthermore, oxidations of aromatic compounds at potentials below that required for $O_2(g)$ evolution have been observed to generate organic

surface films as a consequence of polymerization of radical products that are generated anodically but without concomitant transfer of O-atoms from H_2O. We interpret these observations based on the speculations summarized below.[6-8]

(i) Apparently, hydrolysis is not a rapid mechanism for the O-transfer step in the anodic reactions of interest. Instead, it is speculated that O-transfer occurs from adsorbed hydroxyl radicals (OH) that are generated by anodic discharge of H_2O, as described by:

$$S[\ ] + H_2O \underset{k_{-WDR}}{\overset{k_{WDR}}{\rightleftharpoons}} S[OH] + H^+ + e^- \qquad (1)$$

where S[ ] represents surface sites for adsorption of the OH species. Accordingly, the fundamental anodic O-transfer step occurs from S[OH] to the reactant species (R), as described by:

$$S[OH] + R \underset{k_{-OTR}}{\overset{k_{OTR}}{\rightleftharpoons}} S[\ ] + RO + H^+ + e^- \qquad (2)$$

(ii) We also speculate that electrocatalytic benefit comes from preadsorption of the reactant species, as described by:

$$S'[\ ] + R \underset{k_{-ads}}{\overset{k_{ads}}{\rightleftharpoons}} S'[R] \qquad (3)$$

where S'[ ] represents sites that might be the same or different from S[ ] in (1). Accordingly, the O-transfer step in this mechanism is described by:

$$S[OH] + S'[R] \underset{k_{-OTR}}{\overset{k_{OTR}}{\rightleftharpoons}} S[\ ] + S'[\ ] + RO + H^+ + e^- \qquad (4)$$

Benefit of reactant adsorption is expected to come as a consequence of the increased lifetime of these species at the electrode surface with a resulting increase in the probability of successful O-transfer steps.

(iii) It is apparent, from consideration of (1) to (4), that voltammetric waves for anodic O-transfer reactions can be expected to appear in the potential region corresponding to onset of $O_2(g)$ evolution, as represented by:

$$2S[OH] \underset{k_{-OER}}{\overset{k_{OER}}{\rightleftharpoons}} S[\ ] + O_2(g) + 2H^+ + 2e^- \qquad (5)$$

Research in this laboratory is directed specifically to the diagnosis of those electrocatalytic properties that minimize the overpotential necessary to achieve the desired anodic O-transfer reactions for aliphatic and aromatic compounds in aqueous media. Much work has been focused on variations in the electrocatalytic properties of β-PbO_2 film electrodes observed as a result of the incorporation of altervalent metallic species within these films.[6-15] Significant electrocatalytic activity has been reported for electrodeposited Bi(V)-doped β-PbO_2 films ("Bi-PbO_2").[6,9,16] Ratios of Bi:Pb can exceed 30:100 (at:at) in these highly active film electrodes. Of greatest significance has been the successful mathematical modeling of observed variations in the half-wave potential ($E_{1/2}$) for oxidation of dimethylsulfoxide (DMSO) to dimethylsulfone ($DMSO_2$) as a function of the Bi(V):Pb(IV) ratio in Bi-PbO_2 electrodes.[7] The incorporation of Fe(III) into β-PbO_2 films ("Fe-PbO_2") also has been the subject of recent manuscripts.[10-12,14,15,17-19] Probably of greatest significance is the enhanced current efficiency for the concomitant anodic generation of $O_3(g)$ during anodic evolution of $O_2(g)$.[14,16-19]

In this paper, the voltammetric activities for oxidation of toluene and xylene are compared for PbO_2, Bi-PbO_2, and Fe-PbO_2 film electrodes in acidic media. Results also are summarized from characterization of a Fe-PbO_2 film using x-ray absorption near edge spectroscopy (XANES).

Experimental

Chemicals and solutions. – Distilled water was purified further by deionization to 18 MΩ·cm in a Nanopure II purification system (Barnstead, Dubuque, IA) using water supplied through a single-stage anion- and cation-exchange cartridges (Culligan, Northfield, MN). Reagent grade perchloric acid, benzyl alcohol, benzaldehyde, benzoic acid, benzoquinone and iron powder (Fisher Scientific, Pittsburgh, PA) were used as received. Certified A.C.S. grade sulfuric acid and toluene (Fisher Scientific) were used as received. Bismuth nitrate (98– %), lead nitrate (99.9999+%), and *m*-, *o*-, and *p*-xylene isomers (99+%; Aldrich, Milwaukee, WI) were used as received. HPLC grade acetonitrile (Fisher Scientific) was used as received.

Stock solutions of organic compounds were made using acetonitrile as the diluent. Acetonitrile significantly enhanced the solubility of the non-polar hydrocarbons without adding to the faradaic signal at the electrodes.

Electrochemical apparatus and procedures. – Voltammetric measurements were made using a model AFCBP1 bipotentiostat and electrode rotator with MSRX control (Pine Instruments, Grove City, PA). Voltammetric measurements were performed in a double walled faraday cage in a laboratory maintained at 23±1° C. All potentials were referenced to

the saturated sodium calomel electrode (SSCE) for which the $E^{o'}$ for the ferricyanide-ferrocyanide redox couple was determined to be 0.45 V.

Films were deposited from 0.10 M $HClO_4$ using a RDE3 potentiostat and MSRX rotator (Pine Instruments). All voltammetric experiments were performed in 0.50 M H_2SO_4 using film electrodes deposited on a Au disk electrode (0.164 cm^2, Pine Instruments). Bulk electrolyses were performed using a coiled gold wire (17.1 cm^2) onto which the designated films had been deposited with stirring provided by a magnetic stirring bar.

Potential-time waveforms were generated and data were acquired by a PC utilizing LabView® 5.0 software and a 12-bit AT-MIO-16E-10 data acquisition board (National Instruments, Austin, TX).

Film electrodes. – The electrodeposition solution was prepared by dissolving Fe powder in deaerated 1.0 M $HClO_4$ with controlled heating. Sufficient $Pb(NO_3)_2$ powder was added to the cooled Fe(II) solution to produce 10 mM concentrations of each in 1.0 M $HClO_4$. Iron(III)-doped β-PbO_2 films were electrodeposited onto a Au rotated disk electrode (RDE; Pine Instruments) that had been thoroughly polished with alumina (5 μm; Dionex, Sunnyvale, CA) on microcloth (Buehler, Lake Bluff, IL) and rinsed thoroughly with distilled and deionized water. A potential of 1.70 V vs. SSCE was applied to the anode for a 15-min period while rotating the electrode at 105 rad s^{-1}. The current density observed for deposition was 6.0 - 6.5 mA cm^{-2}. It is important to note that evidence for incorporation of iron within the film is obtained when Fe(II) but not Fe(III) salts are used in the deposition solution. Bismuth(V)-doped β-PbO_2 films were electrodeposited from 1.0 M $HClO_4$ containing 10 mM $Pb(NO_3)_2$ and 5.0 mM $Bi(NO_3)_3$ at 1.6 V without stirring.[9] Undoped β-

PbO_2 films were similarly deposited in the absence of Bi(III). Caution: lead and bismuth salts must be considered to be toxic. Use and disposal of these compounds must follow accepted procedures.

Data analysis. – Values for the effective number of electrons transferred (n_{eff}, eq mol^{-1}) and the corresponding apparent heterogeneous rate constant (k_{app}, cm s^{-1}) were estimated from the slopes and intercepts, respectively, of plots of the reciprocal of observed current ($1/I_{obs}$, C^{-1} s) vs. the reciprocal of the square root of rotational velocity ($1/\omega^{1/2}$, $rad^{-1/2}$ $s^{1/2}$) according to the Koutecký-Levich equation given by:[20]

$$\frac{1}{I_{obs}} = \frac{1}{n_{eff} k_{app} F A_{geo} C^b} + \left(\frac{1}{0.62\, n_{eff} F A_{geo} D^{2/3}\, \nu^{-1/6} C^b}\right)\left(\frac{1}{\omega^{1/2}}\right) \qquad (6)$$

In (6), F is the faraday constant (C eq^{-1}), A_{geo} is the geometric area of the RDE (cm^2), C^b is the bulk concentration of reactant (mol cm^{-3}), D is the diffusion coefficient of the reactant (cm^2 s^{-1}), and ν is the kinematic viscosity of the solution (cm^2 s^{-1}).

Analytical apparatus and procedures. – Gas chromatography was performed on a Model 5890-series II chromatograph, using a capillary column (30-m length) coated with DB-5, with a detection by a Model 5972AMSD quadrupole mass selective detector (GC-MS: Hewlett-Packard, Palo Alto, CA). Helium was the mobile phase. Acquisition and analysis of GC-MS data was performed using Chemstation® software (Hewlett-Packard). Prior to injection into the GC-MS instrument, products from electrolysis solutions were extracted using diethyl ether, followed by evaporation of the combined extracts at 15°C under a slight vacuum to a volume of 1.0 mL. High performance liquid chromatography (HPLC) was achieved using a Nucleosil C18 column (140-mm length; Alltech, Deerfield, IL) and CH-150

column heater (Eldex, Napa, CA). The mobile phase was a 50:50 mixture of H_2O and acetonitrile delivered by a GPM-2 pump (Dionex). Photometric detection was performed with a VDM-2 UV-Vis detector (Dionex). Data acquisition was controlled by ASYST software and data acquisition board. Table 4.1 summarizes separation conditions for gas chromatographic and liquid chromatographic analyses.

Table 4.1. Chromatographic conditions used in the analyses of electrolysis product solutions by gas chromatography with mass spectrometry (GC-MS) and high performance liquid chromatography (HPLC).

Technique	GC/MS	HPLC
Make	J & W	Alltech
Packing	DB-5	Nucleosil C18
Pore size	capillary	5 μm
Length	30 m	140 mm
Diameter (mm)	0.25	4.6
Eluent	He	50/50 H_2O/MeCN
Flow rate (mL/min)	14	1.0
Initial T (°C)	50	35
Initial t (min)	1	-
Rate (°C / min)	20	-
Final T (°C)	250	35
Final t (min)	10	-
Inlet T (°C)	250	-
Detector T (°C)	280	-
λ_{det} (nm)	-	280, 254

X-ray absorption measurements were made using the National Synchrotron Light Source using Beamline X10C at Brookhaven National Laboratory. A two-crystal monochrometer employing Si(III) crystals was used. X-ray fluorescence spectra were collected by a Canberra 13 element solid-state detector whose face was nearly parallel to the cell and at a distance of 2-3 cm. To improve energy resolution, the third order harmonic Si(333) reflection was used in which $\Delta E/E = 8.8 \times 10^{-6}$. When the third order harmonic was

set to the Fe K edge at 7.112 eV, the fundamental occurred at 2.371 eV and the fifth order reflection occurred at 11.853 eV. The third order fundamental was fully attenuated by a 0.3-m air path and the fifth order harmonic was rejected by a rhodium-coated refocusing mirror. Horizontal and vertical slit positions were adjusted to optimize the resolution of the double pre-edge peaks of α-Fe_2O_3. Further details of these measurements are given elsewhere.[21]

Results and Discussion

XANES data. – Figure 4.1A shows low resolution XANES data for a Fe-PbO_2 film electrodeposited from 1.0 $HClO_4$ containing equimolar concentrations of Fe^{2+} and Pb^{2+} (———). Also shown in this figure are data obtained for standard samples of Fe (· · · · ·), FeO (– · – · –), and α-Fe_2O_3 (– · · – · · –). It is apparent in Figure 4.1A that the sharp peak for the electrodeposited Fe-PbO_2 film at 7132 eV corresponds approximately to the peak for the α-Fe_2O_3 standard. Figure 4.1B contains high resolution XANES data obtained in the pre-edge region for the Fe-PbO_2 film (———) in addition to the standard samples of FeO (– · – · –), α-Fe_2O_3 (– · · – · ·) and γ-Fe_2O_3 (– · · · – · · · –). There is a close similarity in the shapes of the spectra for the Fe-PbO_2 and α-Fe_2O_3 samples. More specifically, both of the indicated spectra exhibit a shoulder at 7.113 eV on the main pre-edge peak at 7.115 eV. Therefore, we conclude that iron in the Fe-PbO_2 film exists in the 3+ oxidation state with octahedral coordination by O-atoms from the octahedral lattice of the β-PbO_2 matrix. It is somewhat surprising that Fe(III) is incorporated within the rutile matrix of β-PbO_2 given the fairly large discrepancy between the radii for Fe^{3+} (0.64 Å) and Pb^{4+} (0.84 Å).[22] Previous research results obtained from x-ray diffractometry have indicated that Bi^{5+} (0.74 Å)[22] in

electrodeposited Bi-PbO_2 films also is incorporated within the octahedral lattice of β-PbO_2.[23] X-ray photoelectron spectroscopy (XPS) was used for semi-quantitative determination of Fe^{3+} in the Fe(III)-doped β-PbO_2 films. The maximum concentration was determined to be ca. 1% (at:at wt). This is considerably less than those concentrations claimed by Velichenko et al. resulting from addition of fluoride ion into the deposition solutions.[17-19] However, in our hands, addition of fluoride ion did not result in an increased Fe^{3+} as determined by XPS.

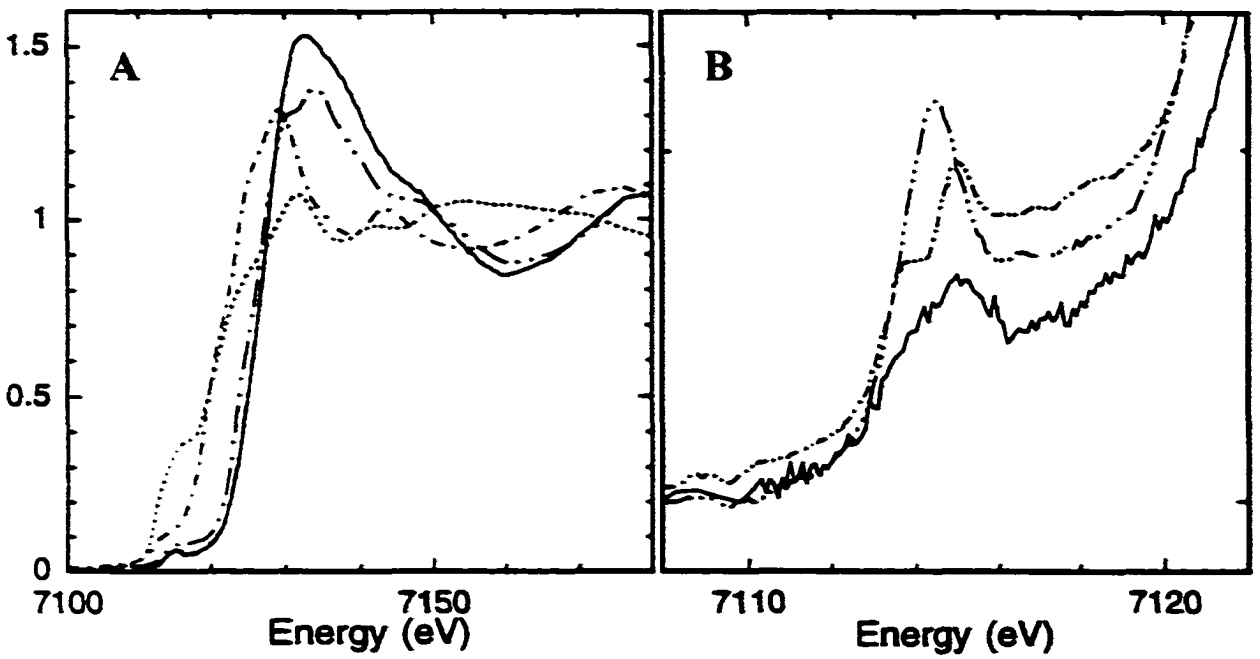

Figure 4.1. Low resolution (A) and high resolution (B) XANES data for the pre-edge region of the spectrum. Spectra: (———) electrodeposited Fe-PbO_2 film. (· · · · ·) Fe standard. (– – – –) FeO standard. (– · · – · · –) α-Fe_2O_3 standard. (– · · · – · · · –) γ-Fe_2O_3 standard. Solution for electrodeposition of Fe-PbO_2 film: 1.0 M $HClO_4$ containing 10.0 mM Fe^{2+} and 10.0 mM Pb^{2+}.

Anodic response for DMSO. – Values of n_{eff} and k_{app} obtained for the anodic voltammetric wave for DMSO are given in Table 2. This anodic O-transfer reaction has been well characterized at Bi-PbO_2 electrodes and the product determined to be $DMSO_2$ (n_{eff} = 2 eq mol^{-1}). The value of n_{eff} determined for DMSO oxidation at the Fe-PbO_2 electrode is consistent with that determined using the Bi-PbO_2 electrode. Having greatest significance is the observation that k_{app} at the Bi-PbO_2 electrode ($18.0\pm0.1\times10^{-3}$ cm s^{-1}) is substantially larger than that for the Fe-PbO_2 electrode ($5.4\pm0.1\times10^{-3}$ cm s^{-1}). The high reactivity of Bi-PbO_2 electrodes for DMSO oxidation has been attributed to a mechanism in which preadsorption of DMSO occurs at Bi(V) sites via the lone-pair electrons on the S-atom of DMSO.[7,8] The benefit of adsorption is believed to result from the increased residence time of

Table 4.2. Summary of electrochemical parameters for anodic oxidations of toluene and xylene at iron-doped, bismuth-doped and undoped β-PbO_2 film electrodes. Uncertainties indicated represent ±1.0 standard deviation.

Electrode	Parameter	DMSO	Toluene	*m*-Xylene
Fe-PbO_2	n_{eff} (eq mol^{-1})	2.1 ± 0.01	3.1±0.2[a]	1.2±0.02
	$10^3 k_{eff}$ (cm s^{-1})	5.4 ± 0.09	6.5±0.06[a]	11.0±0.5
Bi-PbO_2	n_{eff} (eq mol^{-1})	2.0 ± 0.01	2.0±0.05[b]	1.7±0.04
	$10^3 k_{eff}$ (cm s^{-1})	1.8 ± 0.07	2.0±0.05[b]	4.0±0.1
PbO_2	n_{eff} (eq mol^{-1})	NR	4.1±0.32[d]	1.0±0.03
	$10^3 k_{eff}$ (cm s^{-1})	NR	0.42±0.003[d]	5.0±0.2

[a] Based on data for $1/\omega^{1/2} = 0.20 - 0.45$ $s^{1/2}$ $rad^{-1/2}$.
[b] Based on data for $1/\omega^{1/2} = 0.11 - 0.45$ $s^{1/2}$ $rad^{-1/2}$.
[c] NR = no reaction.
[d] Based on data for $1/\omega^{1/2} = 0.14 - 0.45$ $s^{1/2}$ $rad^{-1/2}$.

the reactant species at the electrode surface and, therefore, the increased probability of successful oxidation. The smaller value of k_{app} for DMSO oxidation at the Fe-PbO_2 electrode is suspected be a consequence of the smaller density of Fe(III)-sites in the surface of this electrode as compared to Bi(V)-sites in the Bi-PbO_2 surface.

Anodic response for toluene. – Figure 4.2 compares the cyclic voltammetric response (positive scan) of 5.0 mM toluene at β-PbO_2 (A), Bi-PbO_2 (B), and Fe-PbO_2 (C) film electrodes. The positive scan limits were 1.80 V for all voltammetric experiments; however, the curve C in Figure 4.2 is truncated at potential less than 1.80 V to facilitate the matter of scaling in the current axis. Some difference in the potentials necessary to achieve a specified rate of O_2 evolution can be attributed to differences in surface roughness; however, we attribute the large difference observed for the Fe-PbO_2 (C) and Bi-PbO_2 (B) electrodes to be an indication of a larger rate for anodic discharge of H_2O at Fe(III) sites in comparison to Bi(V) sites.

The voltammetric responses shown in Figure 4.2 for toluene at the three electrodes are very characteristic of an anodic O-transfer mechanism in which anodic discharge of H_2O to produce OH is a prerequisite. During the initial rising portion of the waves, e.g., ca. 1.50 – 1.60 V for Fe-PbO_2 (C), the anodic current exhibits virtually no variation as a result of increases in rotational velocity. This is consistent with the requirement of anodic discharge of H_2O to produce OH in this mechanism. More specifically, at low applied overpotentials, the current is controlled by the rate of OH generation and, therefore, the current is independent of the flux of reactant arriving at the electrode surface.[8] At higher potential values, pseudo current plateaus are apparent for the lowest rotational velocity at the Bi-PbO_2 and Fe-PbO_2 electrodes. However, it can be expected for increasing values of reactant

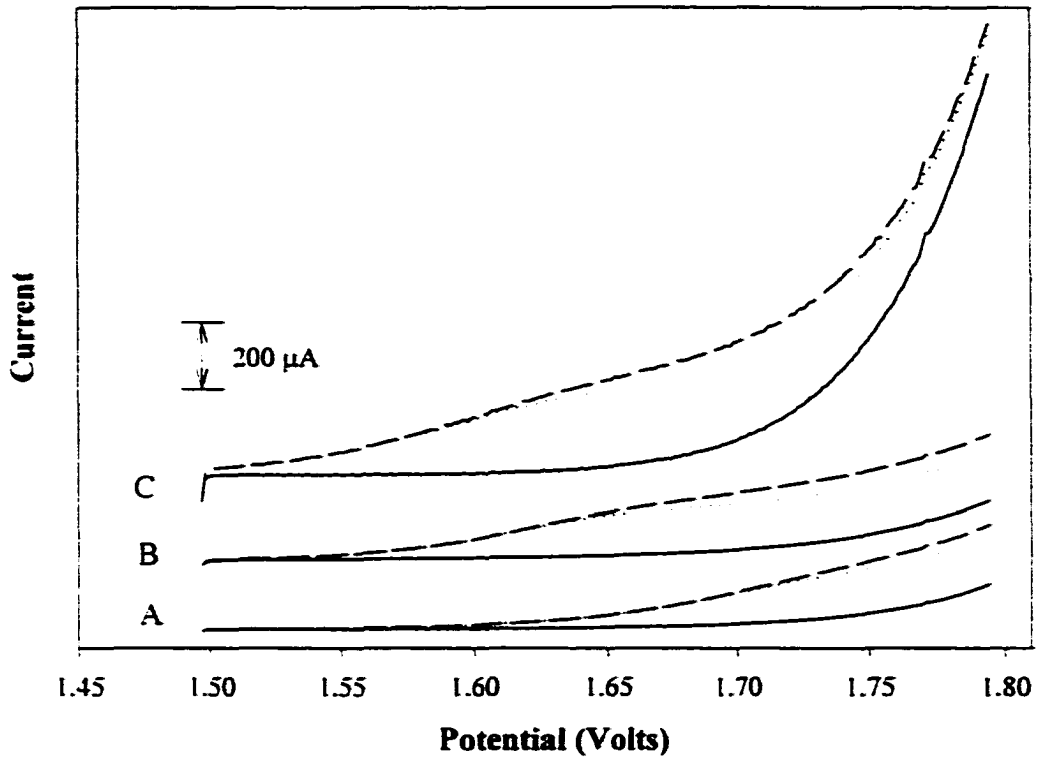

Figure 4.2. Comparison of voltammetric activity (positive scan) of pure β-PbO_2 (A), Bi-PbO_2 (B), and Fe-PbO_2 (C) film electrodes for oxidation of 5.0 mM toluene under identical conditions. Scan rate: 20 mV s^{-1}. Scan limits: 1.50 V - 1.80 V vs. SSCE. Toluene concentration (mM): (——) 0, (····– –) 5.0. Rotation rate (rad s^{-1}): (——) 94.2, (····) 5.24, (– –) 10.5.

concentration, even when using at high applied overpotentials, that the electrode current will shift from control by reactant flux, with corresponding dependence on rotational velocity, to control by OH flux, without dependence on rotational velocity.[8] Therefore, applications of (6) for estimation of n_{eff} and k_{app} values from plots of $1/i_{obs}$ vs. $1/\omega_{1/2}$ are not considered relevant for treatment of current values obtained at low overpotential and/or high reactant fluxes.

In spite of the caution cited above, we contend that the comparison of voltammetric data shown in Figure 4.2 can be useful for evaluation of relative activities of these electrodes

for anodic oxidation of toluene. First, the larger anodic currents observed at the Fe-PbO_2 electrode (C) in the potential region ca. 1.60 - 1.65 V are indicative of larger values of n_{eff} and/or k_{app} at this electrode as compared to the Bi-PbO_2 (B) and β-PbO_2 (A) electrodes. Second, the negative shift in $E_{1/2}$ to successively lower values progressing from β-PbO_2 (1.67 V) to Bi-PbO_2 (1.62 V) to Fe-PbO_2 (1.57 V) is an indication of catalytic effectiveness for the various metallic sites within this anodic O-transfer mechanism increasing in the order Pb(IV) < Bi(V) << Fe(III). Because of the low surface excess of Fe(III) sites compared to the Bi(V) sites, it is apparent that the inherent activity of the Fe(III) sites is significantly larger than that of Bi(V) sites within this mechanism.

Koutecky-Levich plots were constructed for further comparison of the voltammetric data shown in Figures 4.2A-C. More specifically, anodic current values were measured at potentials chosen to correspond to identical residual currents of 20 μA for the three electrodes. Accordingly, the rate of anodic discharge of H_2O was expected to be identical for the three electrodes, i.e., equal values for the maximum rate of production of the OH species. The Koutecky-Levich plots for toluene are shown in Figure 4.3 for the β-PbO_2 ( ), Bi-PbO_2 (●) and Fe-PbO_2 (Δ) electrodes, and values of n_{eff} and k_{eff} calculated from these plots are given in Table 3. The error bars in Figure 4.3 represent ±1 standard deviation for three determinations ($N = 3$). The plot for Fe-PbO_2 (Δ) exhibits two regions of linearity designated the low flux region ($1/\omega^{1/2} \geq 0.20$ $s^{1/2}$ $rad^{-1/2}$) and high flux region ($1/\omega^{1/2} < 0.2$ $s^{1/2}$ $rad^{-1/2}$). As discussed above, this change in slope can be attributed to the shift in the rate-controlling step from that of toluene transport (low flux region) to OH generation (high flux region).[8] Using 9.7×10^{-6} cm^2 s^{-1} for the diffusion coefficient (D) of toluene,[24] n_{eff} was calculated to be

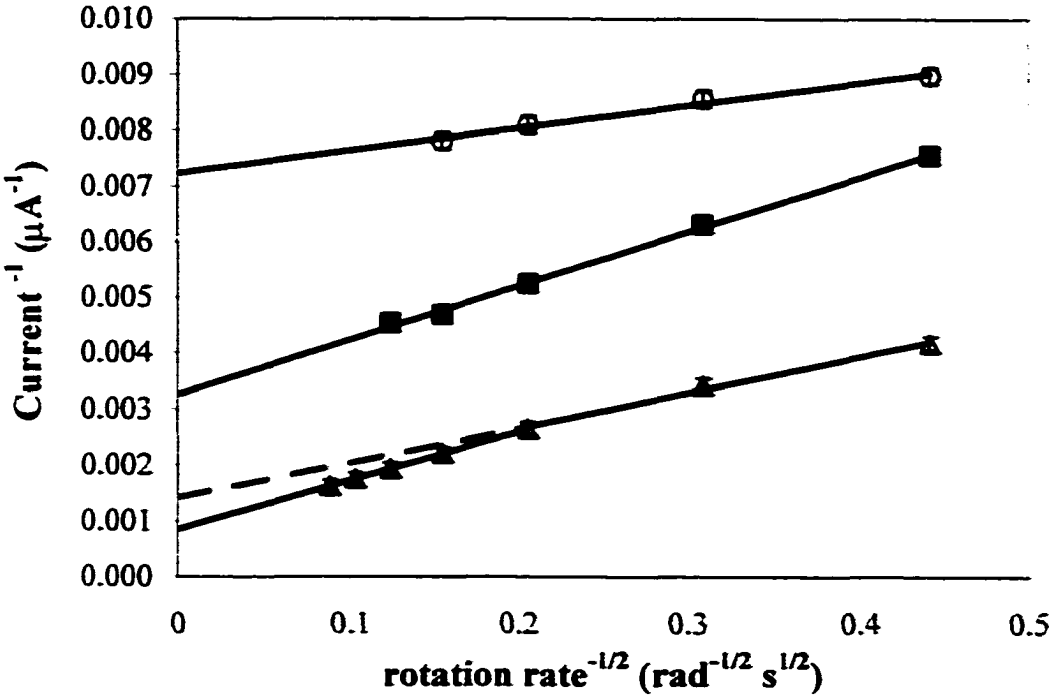

Figure 4.3. Koutecky-Levich plots for oxidation of 5.0 mM toluene at Fe(III)-doped [Δ], Bi(V)-doped [■], and undoped [○] β-PbO_2 rotated disk electrodes. Detection potential: 1.70 V vs. SSCE. Error bars denote ±1.0 standard deviation.

3.1±0.2 eq mol^{-1} using data obtained for the low-flux region ($1/\omega^{1/2} = 0.20 - 0.45\ s^{1/2}\ rad^{-1/2}$) at the Fe-$PbO_2$ electrode. Values of n_{eff} for toluene oxidation at the β-PbO_2 and Bi-PbO_2 electrodes were determined to be 4.1±0.3 and 2.0±0.05 eq mol^{-1}, respectively. The fact that the smallest currents are obtained at the β-PbO_2 electrode, despite the large value of n_{eff}, is attributed to a small value for k_{app} at this electrode.

Values of k_{app} were calculated for toluene oxidation at the three electrodes represented in Figure 4.3 from the intercepts of these Koutecky-Levich plots and these values are included in Table 2. The intercept used for the Bi-PbO_2 electrode corresponded to the linear extrapolation from the low flux region of the plot. The values calculated for k_{app} (cm s^{-1}) are 0.42±0.03x10^{-3} (β-PbO_2), 2.0±0.05x10^{-3} (Bi-PbO_2) and 6.5±0.06x10^{-3} (Fe-PbO_2).

Further evidence of the lack of activity of the β-PbO_2 and Bi-PbO_2 for the anodic O-transfer reaction(s) of toluene was the observation that these electrode surfaces became fouled after very short time periods (< 30 min) when operated at a constant potential under conditions of high analyte flux ($\omega \geq 94.2$ rad s^{-1}). Evidence for fouling was a rapid decay of current. In contrast, Fe-PbO_2 electrodes exhibited no evidence for fouling during much longer periods of use (> 1 h) in the high flux region.

Anodic response for xylenes. – The film electrodes were used to obtain voltammetric data for the anodic oxidation of *o*-, *m*-, and *p*-xylene as a function of rotational velocity. Again, the activity of the Fe-PbO_2 electrode was significantly larger than that of the other electrodes. The Koutecký-Levich plots of the background-corrected voltammetric response at 1.675 V (positive scan) for *m*-xylene at the Fe-PbO_2 electrode are shown in Figure 4.4. The values of n_{eff} and k_{app} calculated from these plots are included in Table 2.

A 10 mM solution of *m*-xylene was electrolyzed for a 1.0-hr period at a potential of 1.675 V vs. SSCE. The major product of oxidation was determined to be 3-methyl benzaldehyde (12%, $n_{eff} = 4$ eq mol^{-1}). The presence of a trace amount (<1%) of 3-methyl benzoic acid also was identified. This indicates that once one of the methyl groups is oxidized, the resulting aldehyde functionality is more susceptible to further oxidation than the remaining methyl group. This behavior may give some indication of molecular orientation at the electrode surface. These results were further verified by the electrolysis of a solution of 2-methyl benzaldehyde for which the only product discovered was 2-methyl benzoic acid.

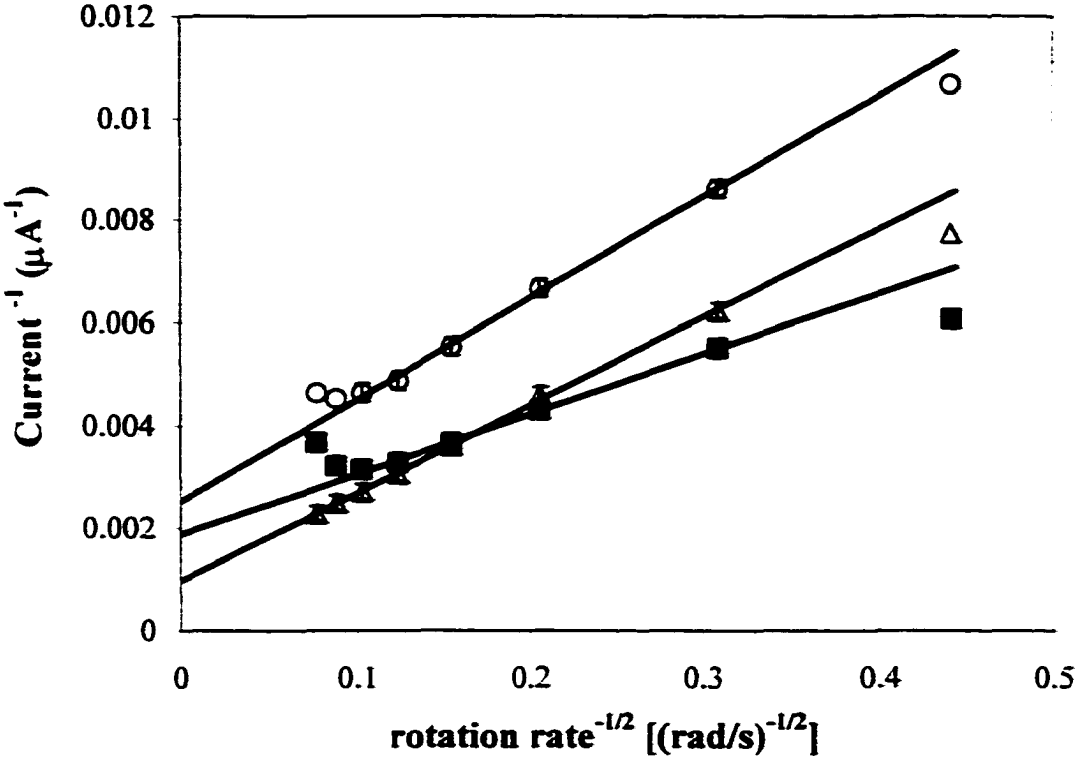

Figure 4.4. Koutecky-Levich plots for oxidation of 5.0 mM *m*-xylene at Fe(III)-doped [Δ], Bi(V)-doped [■], and undoped [○] β-PbO_2 film rotated disk electrodes. Detection potential: 1.675 V vs. SSCE. Error bars denote ±1.0 standard deviation.

Mechanical stabilities of films. – It is important to note that the mechanical stability of Fe-PbO_2 films was inferior to that of Bi-PbO_2 and undoped β-PbO_2 films. In spite of the low concentrations of Fe(III) in Fe-PbO_2 films (ca. 1%), these films were easily removed from the Au substrates simply by rubbing with a tissue. In comparison, the undoped β-PbO_2 and Bi-PbO_2 films were not removed by such action.

Conclusions

All three film electrodes tested were observed to exhibit voltammetric waves for oxidation of toluene. However, of greatest significance is the observation that k_{app} for this

anodic reaction is larger at the Fe-PbO_2 electrode ($6.5\pm0.06\times10^{-3}$ cm s^{-1}) than at the Bi-PbO_2 ($2.0\pm0.05\times10^{-3}$ cm s^{-1}) and pure β-PbO_2 ($0.42\pm0.03\times10^{-3}$ cm s^{-1}) electrodes. This is especially noteworthy because of the small amount of Fe(III) in the Fe-PbO_2 film (ca. 1%) as compared to the large amount of Bi(V) in the Bi-PbO_2 film (ca. 33%). We conclude that the higher catalytic activity of Fe(III) sites as compared to Bi(V) and Pb(IV) sites is the beneficial consequence of stronger adsorption of aromatic molecules at the Fe(III) sites. This adsorption is expected to occur via interaction of π-electrons in the aromatic compound with partially filled d-orbitals at the Fe(III) sites.

Experimental results for toluene are consistent with the step-wise reaction sequence shown below leading to benzoic acid as the final product.

$$\phi\text{-}CH_3 + H_2O \rightarrow \phi\text{-}CH_2OH + 2H^+ + 2e^- \quad (7)$$

$$\phi\text{-}CH_2OH \rightarrow \phi\text{-}CHO + 2H^+ + 2e^- \quad (8)$$

$$\phi\text{-}CHO + H_2O \rightarrow \phi\text{-}COOH + 2H^+ + 2e^- \quad (9)$$

It is interesting to compare values of n_{eff} calculated from the Koutecky-Levich plots for the three electrodes with the above reaction sequence in mind. For the β-PbO_2 electrode, n_{eff} = ca. 4 eq mol^{-1} in spite of the small value of k_{app} whereas, in comparison, n_{eff} = ca. 2 eq mol^{-1} for the Bi-PbO_2 electrode. We speculate that ϕ-CH_2OH molecules produced in (7) remain adsorbed at the β-PbO_2 electrode but not the Bi-PbO_2 electrode. With this possibility in mind, it is interesting to note for m-xylene that n_{eff} = 1.0 eq mol^{-1} at the β-PbO_2 electrode in comparison to 1.7 eq mol^{-1} at the Bi-PbO_2 electrode and 1.2 eq mol^{-1} at the Fe-PbO_2 electrode.

Future research must focus on the perceived importance of increasing the Fe(III) content in β-PbO_2 films as well as increasing their adherence to the substrates. Velichenko *et al.* have described some success in addressing the first of these goals by the addition of fluoride ion to the deposition solutions.[17-19] An alternate approach might be the choice of metal oxide hosts having smaller lattice constants than that for β-PbO_2.

Acknowledgements

The authors are grateful to T. J. Barton for the loan of the GC-MS instrument. Also, Ames Laboratory for funding of this project. Ames Laboratory is a division of the U.S. Department of Energy and operated under Contract W-7405-Eng-82.

References

1. N. L. Weinberg and H. R. Weinberg, Chem. Rev., **68**, 449 (1968).
2. D. Pletcher and F. Walsh, Industrial Electrochemistry, 2nd ed., Chapman and Hall, New York (1990).
3. H. Lund, D. E. Danly, and C. J. H. King, in Organic Electrochemistry, 3rd ed., pp. 276, 1288, H. Lund and M. Baizer, Editors, Marcel Dekker Inc., New York (1991).
4. D. Kyriacou and D. Jannakoudakis, Electrocatalysis for Organic Synthesis, p. 47, John Wiley & Sons, New York (1991).
5. K. Scott, Electrochemical Processes for Clean Technology, p. 233, The Royal Society of Chemistry, Cambridge, (1995).
6 N. Đ. Popović and D. C. Johnson, Anal. Chem. **70**, 468 (1998).
7 N. Đ. Popović, J. A. Cox and D. C. Johnson, J. Electroanal. Chem., **455**, 153 (1998).
8 N. Đ. Popović, J. A. Cox and D. C. Johnson, J. Electroanal. Chem., **456**, 203 (1998).

9. D. C. Johnson, N. Đ. Popović, J. Feng, L. L. Houk, and K. T. Kawagoe, Proc. Electrochem. Soc., **95-26**, 176 (1996).

10 J. Feng and D. C. Johnson, J. Appl. Electrochem., **20**, 116 (1990).

11 J. Feng and D. C. Johnson, J. Electrochem. Soc., **137**, 507 (1990).

12 J. Feng and D. C. Johnson, J. Electrochem. Soc., **138**, 3328 (1991).

13 D. C. Johnson, H. Chang, J. Feng, and W. Wang, in Electrochemical Technology for a Cleaner Environment; D. Genders and N. Weinberg, Editors, p. 331, Electrosynthesis Co., Inc.: East Amherst (1992).

14 J. Feng, D. C. Johnson, S. N. Lowery, and J. J. Carey, J. Electrochem. Soc., **141**, 2708 (1994).

15 J. Feng, L. L. Houk, D. C. Johnson, S. N. Lowery, and J. J. Carey, J. Electrochem. Soc., **142**, 3626 (1995).

16 N. Belhadj Tahar and A. Savall, J. Appl. Electrochem., **29**, 277 (1999).

17 A. B. Velichenko, D. V. Girenko, S. V. Kovalyov, A. N. Gnatenko, R. Amadelli, and F. I. Danilov, J. Electroanal. Chem. **454**, 203 (1998).

18. R. Amadelli, L. Armelao, A. B. Velichenko, N. V. Nikolenko, D. V. Girenko, L. V. Kovalyov, and F. I. Danilov, *Electrochim. Acta*, **45**, 713 (1999).

19. A. B. Velichenko, R. Amadelli, G. L. Zucchini, D. V. Girenko, and F. I. Danilov, *Electrochim. Acta*, **45**, 4341 (2000).

20. J. Koutecky and V. G. Levich, Zh. Fiz. Khim., **32**, 1565 (1956).

21 A. J. Davenport and M. Sansone, J. Electrochem. Soc. **142**, 725 (1995).

22. D. R. Lide (Ed.), CRC Handbook of Chemistry and Physics, 71st ed., CRC Press: Boca Raton, FL, p. 12-1.

23. I.-H. Yeo, S. Kim, R. Jacobson and D.C. Johnson, J. Electrochem. Soc., **136**, 1395 (1989).

24. C. L. Yaws, *Handbook of transport property data : viscosity, thermal conductivity, and diffusion coefficients of liquids and gases*. Gulf Pub. Co., Houston, (1995).

V. ELECTROCHEMICAL INCINERATION OF SELECTED ORGANIC COMPOUNDS

A paper being reviewed for patent and to be submitted for publication in Environmental Science and Technology

Stephen E. Treimer, Jianren Feng, Linda L. Houk, Dennis C. Johnson[1], and Nebojša Avdalović[2]

Abstract

Numerous organic solvents, including those commonly used as mobile phase modifiers in liquid chromatography, can be oxidatively degraded at a Pt anode in acidic media. Single-pass and multi-pass degradations utilizing flow-through electrolysis cells are demonstrated for dilute solutions of methanol, acetonitrile, tetrahydrofuran, 1,4-dioxane, methylene chloride, chloroform, and methyl *tert*-butyl ether in 0.10 M H_2SO_4. Efficiencies of the electrolytic processes are improved in all cases by the presence of thin films of $MnO_2(s)$ on the Pt anodes. These films are easily prepared by electrodeposition of Mn^{2+} added to the solutions as $MnSO_4 \cdot H_2O(s)$.

Introduction

The challenge of providing clean drinking water becomes more difficult as the population of the world increases and industrialization continues. An example of the growing problem is the recent discovery of methyl *tert*-butyl ether (MTBE) in the drinking waters of some regions in California. Chlorinated and non-chlorinated solvents are

---

[1] Corresponding author.
[2] Dionex Corporation, 1228 Titan Way, Sunnyvale, CA 94088-3603

commonly used in liquid-liquid extraction processes and high-performance liquid chromatography (HPLC) [1]. It is known that chlorinated hydrocarbons can be carcinogenic [2] and the removal of these compounds from their aqueous solutions and mixtures can be problematic. Given the magnitude of the use of these and other solvents in industry and academia, a strategy must be developed for the remediation of these wastes before they enter the ecosystem.

Numerous studies have reported on various biological, physical and chemical methods for treatment of agricultural and industrial wastes. These techniques include adsorption onto activated carbon, biological degradation, wet air oxidation, supercritical water oxidation, photocatalytic oxidation, phytoremediation, combustion, and solid-phase catalyst oxidation [3-5]. Each technique has its unique advantages and disadvantages with regard to applicability, effectiveness, and cost [6]. So-called electrochemical incineration (ECI) is a viable alternative to these waste treatment processes [7,8]. ECI is especially appealing for applications in academic and industrial laboratories that generate small volumes of organic wastes. The ECI process is more expensive than biological and phytochemical treatments; however is considerably faster and can be performed on site or on-line with minimal waste storage.

The goal of ECI is the complete degradation of organic substances to innocuous products, e.g., CO_2 , H_2O, NO_3^-, ClO_3^-, etc. Prior efforts related to electrolytic degradation of chlorinated hydrocarbons have focused on cathodic dehalogenation processes [9,10]. To illustrate, the cathodic dehalogenation of methyl chloride results in production of methane:

$$CH_3Cl(aq) + 2H^+ + 2e^- \rightarrow CH_4(g) + H^+ + Cl^- \qquad (1)$$

One advantage claimed for this process is a low power requirement. However, cathodic dehalogenation of polychlorinated hydrocarbons is known to generate harmful intermediate products, e.g., the dehalogenation of CCl_4 occurs in a step-wise fashion with production of $CHCl_3$, CH_2Cl_2, and CH_3Cl as intermediate products. Anodic degradation processes are described as "anodic O-transfer reactions" because O-atoms from H_2O in the solvent phase are transferred to the reactants. The anodic degradation of chlorinated hydrocarbons is expected to yield the desired innocuous products, as illustrated for CH_2Cl_2 by:

$$CH_2Cl_2(aq) + 2H_2O \rightarrow CO_2(g) + 2Cl^- + 6H^+ + 4e^- \quad (2)$$

Data obtained in our laboratory support speculations that prerequisites to successful anodic O-transfer reactions include: (i) anodic discharge of H_2O to produce adsorbed OH radicals which are the immediate source of O-atoms transferred in these mechanisms [11], and (ii) preadsorption of reactant species to increase their lifetime within the applied electric field at the electrode-solution interface [12,13]. The kinetics of ECI processes are slow at traditional anode materials e.g., Au, Pt, and glassy carbon. Recent efforts have yielded more active anode materials, e.g. synthetic diamond and various doped metal oxides [14-20]. Coupling electrolytic oxidations with Fenton's reagent ($H_2O_2 + Fe^{2+}$) or with photocatalytic oxidation also has been demonstrated to improve the efficiency of some waste remediation processes [21-23].

Much work in this laboratory has focused on the use of anodes consisting of thin films of mixed metal oxides on conductive substrates to improve the efficiency of the ECI process. Iron(III)-doped β-PbO_2(*s*) films on Ti substrates have been used for the electrolytic degradation of benzoquinone with a current efficiency exceeding that obtained at Au, Pt, and glassy carbon electrodes [24]. Mixed metal-oxide films consisting of the oxides of Sb, Ti,

and Ru in $SnO_2(s)$ have been successfully employed for electrolytic degradation of benzoquinone and 4-chlorophenol [8,25]. However, low levels (*ca.* ppb) of the constituent metals have been detected in the product solutions following use of these anodes. Therefore, the goal of on-going research is the discovery of effective catalytic electrode materials that are not based on the toxic elements lead and tin. Recently, we have successfully applied electrolysis at $MnO_2(s)$-coated electrodes for the degradation of several organic solvent modifiers used in HPLC, including methylene chloride. Manganese(II) is a non-toxic metallic species present as a co-factor in important enzymatic processes that occur in living systems with an RDA in humans of 2-5 mg day^{-1}. Furthermore, $MnO_2(s)$ is well known as an oxidizing agent in organic chemistry and in catalytic abatement of aqueous pollutants [6,26-30].

Here we report on the effective use of $MnO_2(s)$-coated Pt anodes for the electrolytic degradation of several chlorinated and non-chlorinated organic compounds commonly used as solvent modifiers n high performance liquid chromatography (HPLC). The compounds include methanol, tetrahydrofuran, 1,4-dioxane, acetonitrile, chloroform, methylene chloride, and methyl *tert*-butyl ether. The goal of this research is the development toward an on-line, single pass solvent incinerator for chromatographic and other industrial waste streams.

Experimental

Reagents - The organic solvents chosen for electrochemical incineration were methanol, tetrahydrofuran, 1,4-dioxane, acetonitrile, methyl *tert*-butyl ether, chloroform and methylene chloride (HPLC grade, Fisher Scientific Pittsburgh, PA). Other chemicals were formaldehyde, $MnSO_4 \cdot H_2O(s)$ and reagent grade concentrated H_2SO_4 (Fisher Scientific). All

aqueous solutions were prepared from distilled water that had been purified further by deionization (Millipore, Bedford, MA).

Electrolysis apparatus and conditions - The undivided H-cell is shown in Figure 5.1 with a glass tube (1.0-cm i.d.) connecting the anode and cathode compartments. A total of 50 mL of sample was sufficient to fill both compartments to a level above the connecting tube. The anode was a Pt plate (2.0 cm^2) and the cathode was a Pt wire (ca. 2 cm^2). Reflux condensers maintained at 10 °C were positioned above each cell to minimize the loss of volatile organic compounds with low boiling points. The anode compartment was stirred with a magnetic stirring bar.

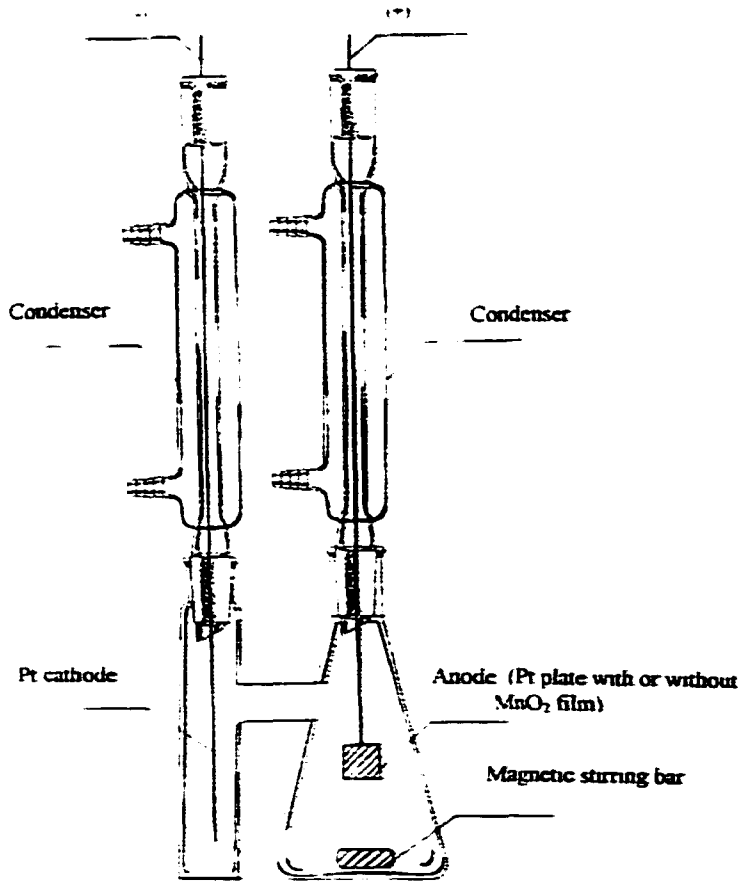

Figure 5.1. Diagram of H-shaped undivided electrolysis cell.

The laboratory-scale undivided flow-through Electrocell AB cell (The Electrosynthesis Co., Lancaster, NY) is shown in Figure 5.2. Electrolysis solutions were repeatedly circulated through the cell from a three-necked flask (150 mL min^{-1}) using a MasterFlex peristaltic pump (Cole-Parmer, Vernon Hills, IL). A chilled reflux condenser mounted above the flask was used to condense and return water vapor and mist containing volatile components from the electrolysis solutions. The two Ti blocks labeled C and G had been machined to permit control of their temperatures by the passage of thermostated water [31]. However, in experiments reported here, the anode and cathode were operated at ambient temperatures. The Pt-foil anode (D, 4.0 cm x 3.5 cm) was pressed against the face of block C in the assembled cell by Ti block E (6-mm thick). Block G served as the cathode.

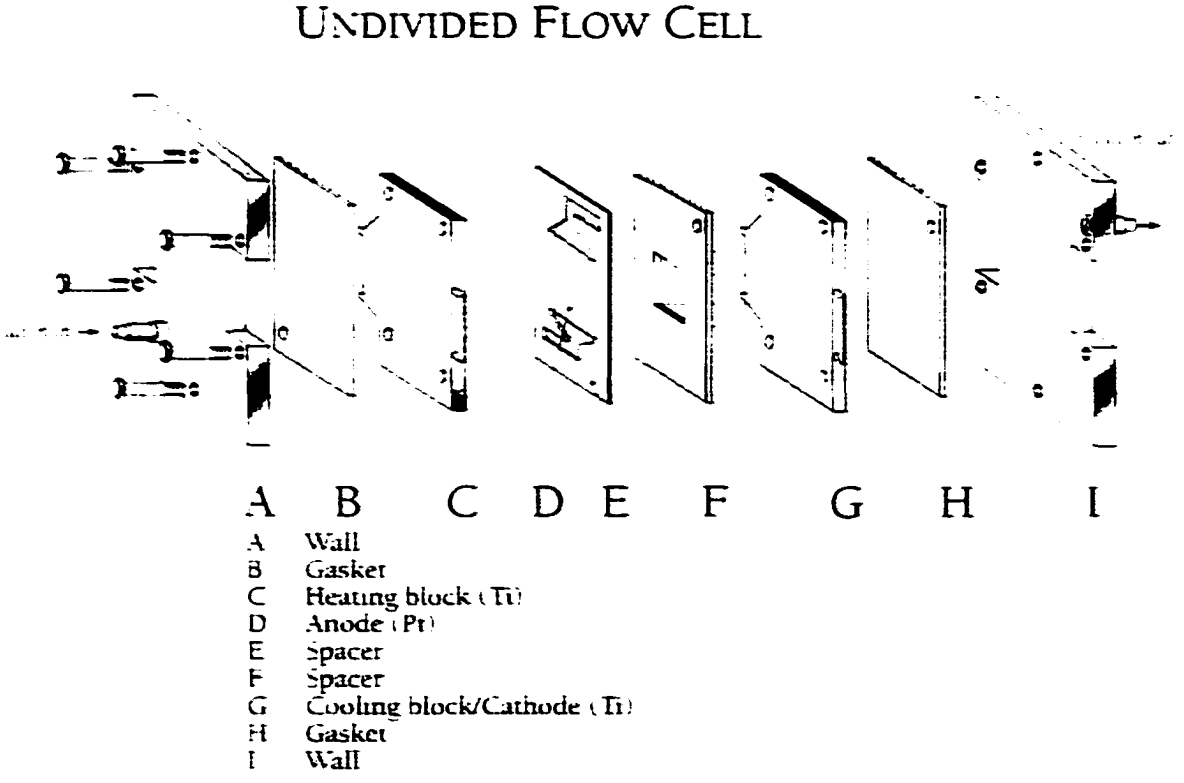

Figure 5.2. Diagram of the undivided, multi-pass flow-through cell.

The window cut into silicon spacer F (2.5 x 3.0 cm, McMaster-Carr, Chicago, IL) defined the outer dimensions of the electrolysis zone in the flow-through cell. The thickness of the electrolysis zone in the assembled apparatus, defined by spacers E and F, was ca. 3 mm.

The miniaturized cell shown in Figure 5.3 was used to minimize the time necessary to achieve electrolytic degradation of test samples in conjunction with off-line gas chromatographic analysis of the gas mixture generated during electrolysis [31]. In this cell, a coiled Pt wire (*ca.*3 cm^2) was tightly wrapped around a porous stainless steel cathode

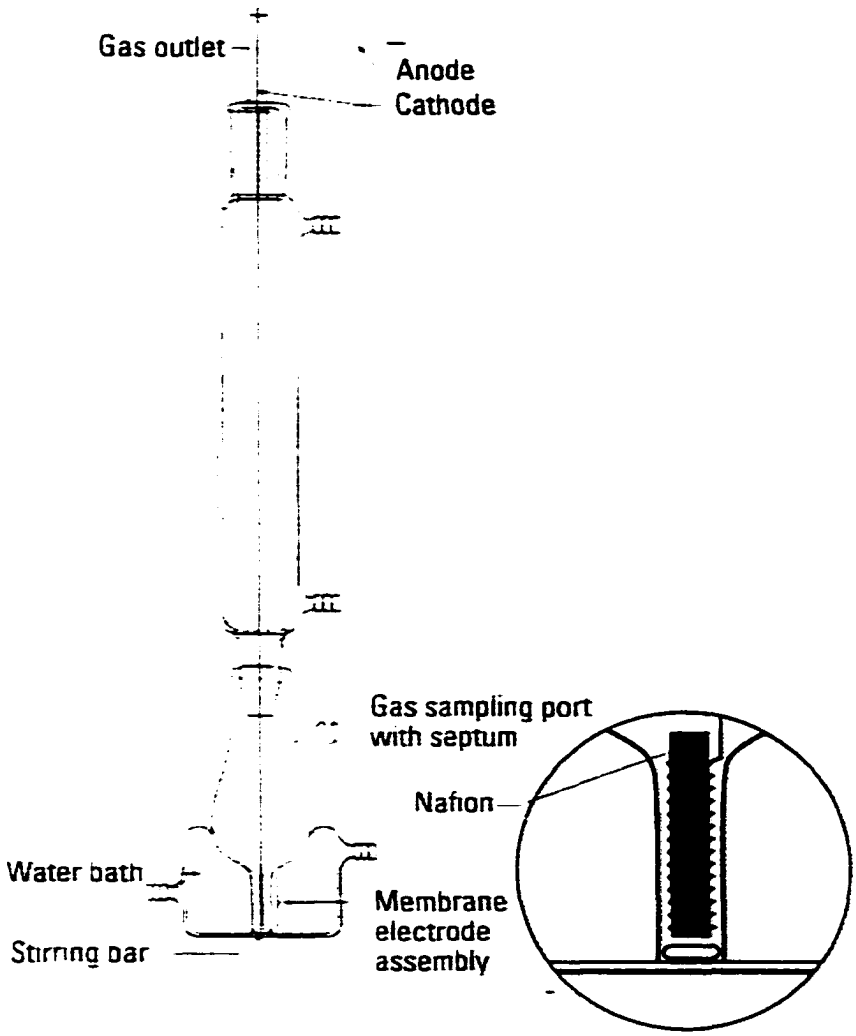

Figure 5.3. Diagram of the miniature electrolysis cell with membrane electrode assembly.

covered with a rectangular piece of Nafion 117 covering the porous stainless steel cathode. The cell temperature was controlled by a Model 90 Refrigerated & Heated Bath (Fisher Scientific, Itasca, IL). Headspace gas samples (100 μL) were obtained through the rubber septum at the top of the electrolysis cell using a Gastight® syringe (Hamilton Co., Reno, NV).

The single-pass ECI cell (Figure 5.4) was a modified Cation Self-Regenerationg Suppressor CSRS-I (Dionex Corp., Sunnyvale, CA). The CSRS-I is supplied with Pt screen working electrodes (14.5 cm x 1.5 cm) that were replaced with Pt foil sheets of the same geometry and the ion-exchange membrane was removed. The anode and cathode were separated by a 3-mm silicon rubber gasket (McMaster-Carr) which had a 1.0 cm x 12.0 cm portion removed to define the cell volume. Thus, the modified CSRS-I was operated in the so-called "undivided mode". During operation, the cell was positioned vertically, with the outlet port above the inlet port to enable gas bubbles to be swept out of the cell by the effluent stream (see Figure 5.4). Test solutions were contained in a closed flask chilled to 13 ± 1 °C and pumped through the cell by a Minipuls-2 peristaltic pump (Gilson, Inc., Milano, Italy) at 1.0 mL/min. Processed solutions were collected in a jacketed, three-neck flask fitted with two high efficiency reflux condensers mounted in series and maintained at 5 °C to minimize losses of any unreacted organic compounds or volatile products remaining in the waste stream.

The power supply was a Model 420X operating a Model 415 High Power Potentiostatic Controller (Electrosynthesis) operated in the galvanostatic mode at 1.0 amp (85 mA/cm^2) unless otherwise stated.

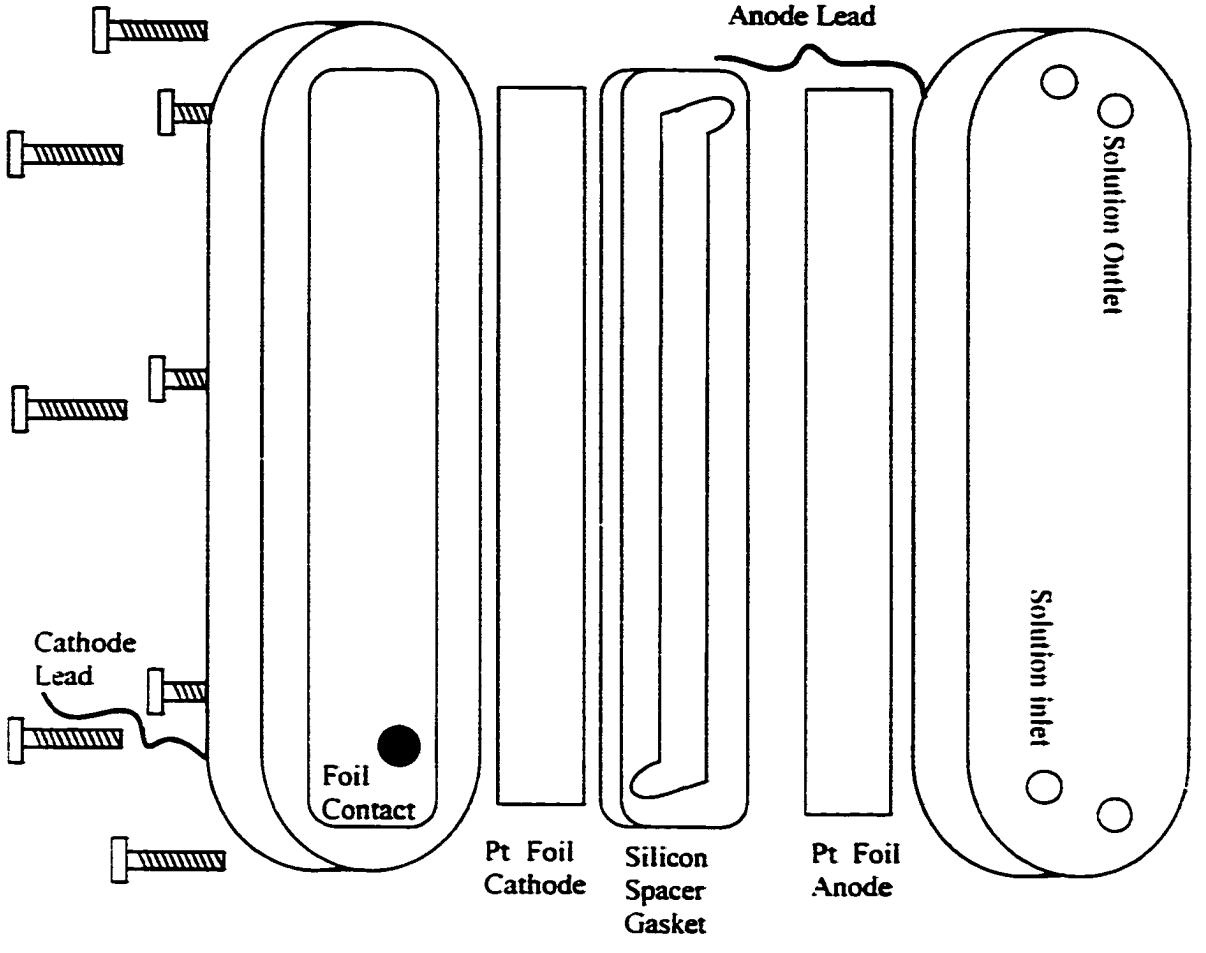

Figure 5.4. Modified Dionex CSRS-I electrochemical cell used for the single-pass destruction of selected organic compounds.

Electrode preparation - The Pt substrates were submerged in a 1:1 (v/v) mixture of ethanol and 1.0 M NaOH to remove adsorbed organic materials. Then, following a thorough rinse with deionized water, the electrodes were roughened by immersion into aqua regia (2 h). Finally, the electrodes were again rinsed with water. When specified, the Pt anode in the H-cell (Figure 5.1) was coated with a thin rose-colored film of $MnO_2(s)$ by electrodeposition at constant current (1.0 A, 10 min) from 1.0 M H_2SO_4 containing 0.10 M Mn^{2+} added as

$MnSO_4 \cdot H_2O(s)$. The Pt anode in the miniature cell (Figure 5.2) was coated with $MnO_2(s)$ by deposition (20 mA, 10 min) from 1.0 M H_2SO_4 containing 10 mM Mn^{2+}. The Pt anode in the multi-pass and single-pass flow-through cells were coated with $MnO_2(s)$ by electrodeposition from 1.0 M H_2SO_4 containing 5.0 mM and 1.0 mM Mn^{2+} respectively, present in the solutions of the organic samples being processed.

Chemical analyses - Chemical oxygen demand (COD) was determined using a DR2000 analyzer (Hach Chemical, Loveland, CO). Carbon dioxide was detected using a gas chromatograph (GC) with a thermal conductivity detector (GOW-MAC, Bridgewater, NJ) and 8'x¼" Carboxen 1004 column (Supelco, Bellefonte, PA).

The analysis of organic compounds in gaseous samples was performed using a Model 550 (Tracor) GC equipped with a flame ionization detector (Marconic, Austin, TX). The chromatographic column (1/8 in x 10 ft) was packed with 3% SP-1500 on 80/120 Carbopack B (Supelco). Gas samples were obtained using a Gastight® syringe (Hamilton). Data were collected by a serial interface to a PC and Logger Pro software (Tufts University and Vernier Software, Portland, OR).

For the single-pass ECI experiments utilizing the modified CSRS-I cell, pre- and post-ECI aliquots (5.0 mL) of the target compound were pipetted from the respective chilled reservoirs to standard vials (Hach) and capped with rubber septa (Aldrich). Pre-ECI aliquots were taken at 1-hour intervals to monitor possible evaporation. Post-ECI aliquots (5.0 mL) were taken at 30-min intervals to identify possible intermediates. After 1-hour equilibration time, a sample of the headspace was withdrawn from the sealed vial with the Gastight® syringe and injected for chromatographic analysis (in triplicate). The ECI efficiency of the

designated organic compound was calculated by comparison of the integrated chromatographic peaks obtained from the pre- and post-ECI solutions.

Results and discussion

Preliminary tests using the H-cell (Figure 5.1) - Initial comparisons of the activities of bare and $MnO_2(s)$-coated Pt anodes for electrolytic degradation of the target compounds were made using the H-cell (Figure 1). These results, summarized in Table 5.1, correspond to COD values determined before and after 20-hour electrolysis periods in 50-mL aliquots of 0.10 M H_2SO_4 containing 10% (v/v) of the specified organic compounds. In all cases, a larger reduction in COD is achieved using $MnO_2(s)$-coated Pt anodes. Because COD values for acetonitrile and methylene chloride decreased by 100% for the trials represented, the electrolyses were repeated for shorter electrolysis periods. After 1.5-hour electrolyses at Pt and MnO_2 coated Pt anodes, the COD for 0.10 M H_2SO_4 containing 10% (v/v) acetonitrile were decreased by 3% and 81%, respectively. After 3-hour electrolyses at Pt and MnO_2 coated Pt anodes, the COD of 0.10 M H_2SO_4 containing 10% (v/v) methylene chloride were decreased by 31% and 98%, respectively. It is readily apparent that the presence of thin films of $MnO_2(s)$ on the Pt anode results in a significant enhancement of the degradation rates for the organic compounds tested. Because ECI at constant current maintains a constant flux of OH radicals regardless of the anode material (albeit at perhaps different potentials), we speculate that the enhancement of degradation rates is a direct result of enhanced adsorption of organic compounds onto the $MnO_2(s)$ surface as compared to the oxide-covered Pt surface.

The solutions changed color during electrolyses at the $MnO_2(s)$-coated Pt anode. In all cases, solutions were colorless at the start of the electrolyses; however, they quickly turned to a light purple color after electrolysis started with a concomitant loss of a majority of the $MnO_2(s)$ films from the Pt surface. The solutions then turned to a muddy brown color, undoubtedly from the formation of suspended particles of $MnO_2(s)$. We speculate further that a small amount of MnO_4^- is generated during redeposition of Mn^{2+} as $MnO_2(s)$ at the Pt and $MnO_2(s)$/Pt surfaces. Furthermore, MnO_4^- can react with Mn^{2+} in acidic solution to form a suspension of $MnO_2(s)$, the source of the muddy brown appearance. As time elapsed, the solutions again became colorless, as $MnO_2(s)$ is known to oxidize organic compounds with the production of Mn^{2+} [32]. Ultimately, all Mn^{2+} is redeposited on the anode surfaces in the form of $MnO_2(s)$ and the fully processed solutions are colorless.

Table 5.1. Chemical oxygen demand (COD) determined before and after 20-h periods of electrolysis of 50-mL aliquots of 0.10 M H_2SO_4 containing 10 % (v/v) of the designated organic solvents using an H-cell (Figure 5.1). Anodic current: 1.0A (0.50 A/cm^2).

Compound	COD before electrolysis (mg/L)	COD after electrolysis at Pt anode (mg/L)	Decrease in COD (%)	COD after electrolysis at MnO_2/Pt (mg/L)	Decrease in COD (%)
Methanol	93,700	36,300	61	0	100
Tetrahydrofuran	143,000	60,300	58	22,200	84
Dioxane	140,000	54,900	61	11,700	92
Acetonitrile	21,900	0	100	0	100
Methylene chloride	23,300	16,000	31	0	100

Multi-pass flow-through electrolysis cell (Figure 5.2) - The multi-pass flow-cell (Figure 5.2) was applied for batch-wise electrolytic degradations of the target compounds from Table 5.1. Formaldehyde was also included in this study because it was suspected to be an intermediate product of the step-wise oxidation of methanol. There was no deposition of $MnO_2(s)$ films on the Pt anode prior to addition of the organic compounds to the acidic media. Instead, 5 mM $MnSO_4(s)$ was dissolved in the acidic solution following addition of the organic compounds to enable electrodeposition of the desired $MnO_2(s)$ films during the ECI process.

Table 5.2 contains COD values for the test solutions determined before and after the 20-hour electrolysis periods. Except for acetonitrile, the electrolyses achieved >90% reduction in the COD values. Undoubtedly, extended electrolysis periods will result in 100% reduction of COD for all organic compounds represented in Table 5.2.

We speculate that an increase in the rate of the anodic degradation process might be achieved by increasing the rate of convective mass transfer at the anode surface in the flow-cell. Therefore, a 1-mm thick plastic-mesh insert (The Electrosynthesis Co., Inc.) was positioned next to the Pt anode in the flow cell to enhance turbulence at the electrode surface. Table 5.3 summarizes COD data for electrolysis solutions in the presence and absence of the plastic-mesh insert. Only a slight increase in degradation rate (ca. 4 %) was obtained using the insert. Perhaps the benefit of increasing turbulence was offset by the decrease in effective area of the anode resulting from contact with the insert. Additional experimentation is needed to determine the appropriate cell design to maximize the rate of convective mass transfer and, therefore, to minimize the time required for total degradation of target compounds.

Table 5.2. Chemical oxygen demand (COD) determined before and after 20-h periods of electrolysis of 100-mL aliquots of 0.10 M H_2SO_4 containing 10 % (v/v) of the designated organic solvent with 5.0 mM $MnSO_4$ using the flow cell (Figure 2). Anodic current: 1.0 A (0.070 A/cm^2).

Compound	COD before electrolysis (mg/L)	COD after electrolysis at Pt anode (mg/L)	Decrease in COD (%)
Methanol	93,700	124	99.9
Tetrahydrofuran	148,000	9,730	93.4
Dioxane	140,000	11,000	92
Acetonitrile	21,200	5,030	76.3
Methylene chloride	23,300	0	100
Formaldehyde	111,000	0	100

Table 5.3. Values of chemical oxygen demand (COD) determined before and after 10-h periods of electrolysis of 100-mL aliquots of 0.10 M H_2SO_4 containing 10 % (v/v) of the designated organic solvents with 5.0 mM Mn(II) using the flow cell (Fig. 2) with and without the plastic-mesh insert. Anodic current: 1.0 A (0.070 A/cm^2).

Compound	Plastic Mesh Insert?	COD before electrolysis (mg/L)	COD after electrolysis at Pt anode (mg/L)	Decrease in COD (%)
Methanol	No	93,700	14,000	85
Methanol	Yes	93,700	10,400	89
Methylene chloride	No	23,300	1,200	95
Methylene chloride	Yes	23,300	300	99

The effect of larger variations in pH, as determined by choice of supporting electrolyte, was examined for the electrolytic degradation of the target compounds at the uncoated Pt anode in the flow-cell equipped with the plastic-mesh insert. The use of $MnO_2(s)$-coated Pt was avoided in this study because Mn^{2+} is known to precipitate as $Mn(OH)_2(s)$ in highly alkaline media and as $MnHPO_4(s)$ in phosphate buffer. Typical data are shown for methanol and tetrahydrofuran in Table 5.4. The largest degradation efficiencies for these compounds using the uncoated Pt anode were obtained in the acidic medium.

Miniaturized cell (Figure 5.3) - Total electrochemical incineration of organic compounds results in production of $CO_2(g)$. Therefore, it was expected that off-line determination of $CO_2(g)$ in the solution headspace would be an effective basis for comparison of the catalytic activities of various anode materials. The miniaturized cell shown in Figure 5.3 was applied, in conjunction with gas chromatography using thermal conductivity detection (TCD), to determine qualitatively the relative rates of $CO_2(g)$ production during the electrolysis of 5.0-mL aliquots of 0.10 M H_2SO_4 containing 10% (v/v) methanol.

Figure 5.5 contains plots of the chromatographic peak height for $CO_2(g)$ as a function of the electrolysis time corresponding to the absence (–●–) and presence (··○··) of 5 mM Mn^{2+} in the electrolysis solution. The $CO_2(g)$ concentration reached its maximum at *ca.* 20 min for the presence of Mn^{2+} as compared to *ca.* 80 min for the absence of Mn^{2+}. The area under the curve obtained in the presence of Mn^{2+} is *ca.* 45% larger than the area under the

Table 5.4. Chemical oxygen demand (COD) determined before and after a 20-h period of electrolysis for 100-mL aliquots of the designated solutions containing 10% (v/v) of the specified organic solvents using an uncoated Pt anode in the flow cell (Fig. 2) with a plastic-mesh insert. Anodic current: 1.0 A (0.070 A/cm^2).

Compound	Medium	COD before electrolysis (mg/L)	COD after electrolysis at Pt anode (mg/L)	Decrease in COD (%)
MeOH[a]	0.1 M H_2SO_4	93.700	14.000	85
MeOH	0.1 M Na_2SO_4 (pH 7)	93.800	22.900	76
MeOH	0.02 M KH_2PO_4/ 0.08 M Na_2HPO_4 (pH 7)	93.300	61.100	34
MeOH	0.1 M NaOH	94.200	35.100	63
THF[b]	0.1 M H_2SO_4	143.000	16.700	88
THF	0.1 M Na_2SO_4 (pH 7)	143.000	25.000	82
THF	0.02 M KH_2PO_4/ 0.08 M Na_2HPO_4 (pH 7)	143.000	108.000	24
THF	0.1 M NaOH	144.000	50.800	65

[a] Methanol [b] Tetrahydrofuran

curve obtained without the addition of Mn^{2+}. This is evidence that more $CO_2(g)$ was formed using the $MnO_2(s)$-coated Pt anode. However, $CO_2(g)$ production in both examples decreased to negligible values by 120 min. indicating that both solutions are virtually devoid of all methanol and intermediate oxidation products. We tentatively conclude that, in the case of the bare Pt anode, the slow rate of oxidative degradation allowed for the loss of some the volatile methanol through the condenser without return to the electrolysis cell.

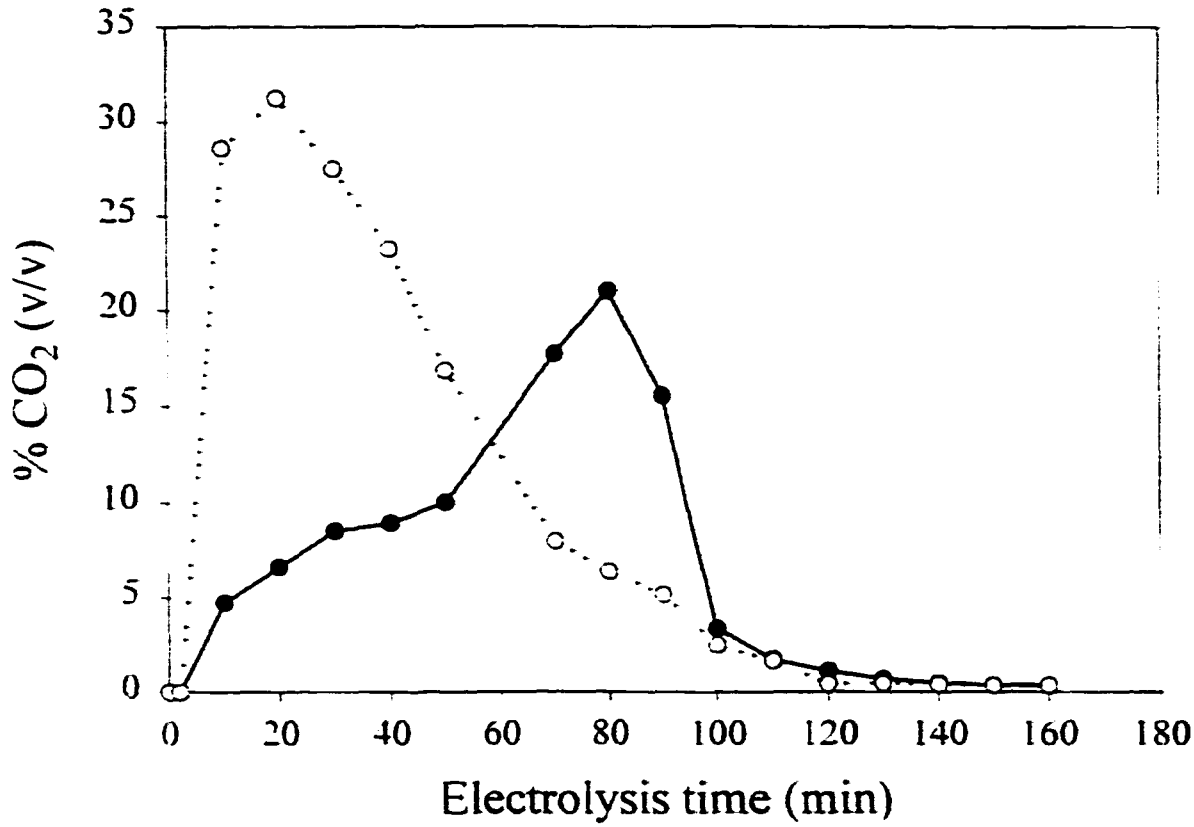

Figure 5.5. Chromatographic peak height for $CO_2(g)$ in gas stream during electrolytic degradation of 10% methanol in a 5.0-mL aliquot of 0.10 M H_2SO_4 using the miniature electrolysis cell (Figure 3) without (–●–) and with (··○··) addition of 5 mM Mn(II).

Gas chromatography with flame ionization detection (FID) or thermal conductivity detection (TCD) was applied to monitor the variations of $CO_2(g)$ and methanol in the gas phase above the electrolysis solution in the miniaturized cell. A new chromatographic peak was observed to develop immediately following onset of electrolysis of 5.0-mL aliquots of 0.10 M H_2SO_4 containing 10% methanol. This peak was assigned to formaldehyde on the basis of matching retention times with peaks obtained for standard formaldehyde solutions. Formaldehyde represents the first stable degradation product (n = 2 eq mol^{-1}) in the stepwise

oxidation of methanol to $CO_2(g)$ and its appearance is concluded to be evidence for a stepwise degradation mechanism. Figure 5.6 contains plots of the chromatographic peak heights for methanol (●), formaldehyde (○) and $CO_2(g)$ (▲) for the electrolytic degradation of methanol at a Pt-wire anode without (Fig. 5.6a) and with (Fig. 5.6b) addition of 5 mM Mn^{2-} to the electrolysis mixture. Whereas the appearance of $CO_2(g)$ peaks persisted for a longer time in the absence of Mn^{2+}, no evidence for $CO_2(g)$ production existed after 300 min for the use of Mn^{2+}. Furthermore, the maximum peak heights for formaldehyde are significantly greater when Mn^{2+} was added. These data are strong evidence that the rate of the anodic degradation of methanol is catalyzed by the $MnO_2(s)$ film on the Pt anode surface.

Temperature variations - The miniature cell (Figure 5.3) was used in studies of the effect of temperature variations (5 to 95°C) on the rate of degradation for 8.0-mL aliquots of 0.10 M H_2SO_4 containing 1% dioxane and 1.0 mM Mn^{2+}. Dioxane was chosen for this study because it has the highest boiling point of the organic compounds studied (101°C) to minimize loss of the organic reactant by volatilization. Figure 5.7 shows plots of concentrations of $CO_2(g)$ in the gas stream above the electrolysis solution. As the temperature of the solution increased, the peak concentration of $CO_2(g)$ was achieved at decreasing times in the electrolysis periods. More specifically, the $CO_2(g)$ level peaked at *ca.* 80 min for 95°C as compared to 240 min for 35°C. As expected, these data demonstrate that the rate of oxidative degradation of methanol to $CO_2(g)$ is increased with increasing electrode temperature. It is interesting to note that the maximum $CO_2(g)$ concentrations represented in Figure 5.7 for temperatures in the range 35 - 95 °C are approximately equivalent. This seems to be contrary to the assertion that increased temperature results in an increased rate of $CO_2(g)$ production. We speculate that a limited value for the rate of $CO_2(g)$

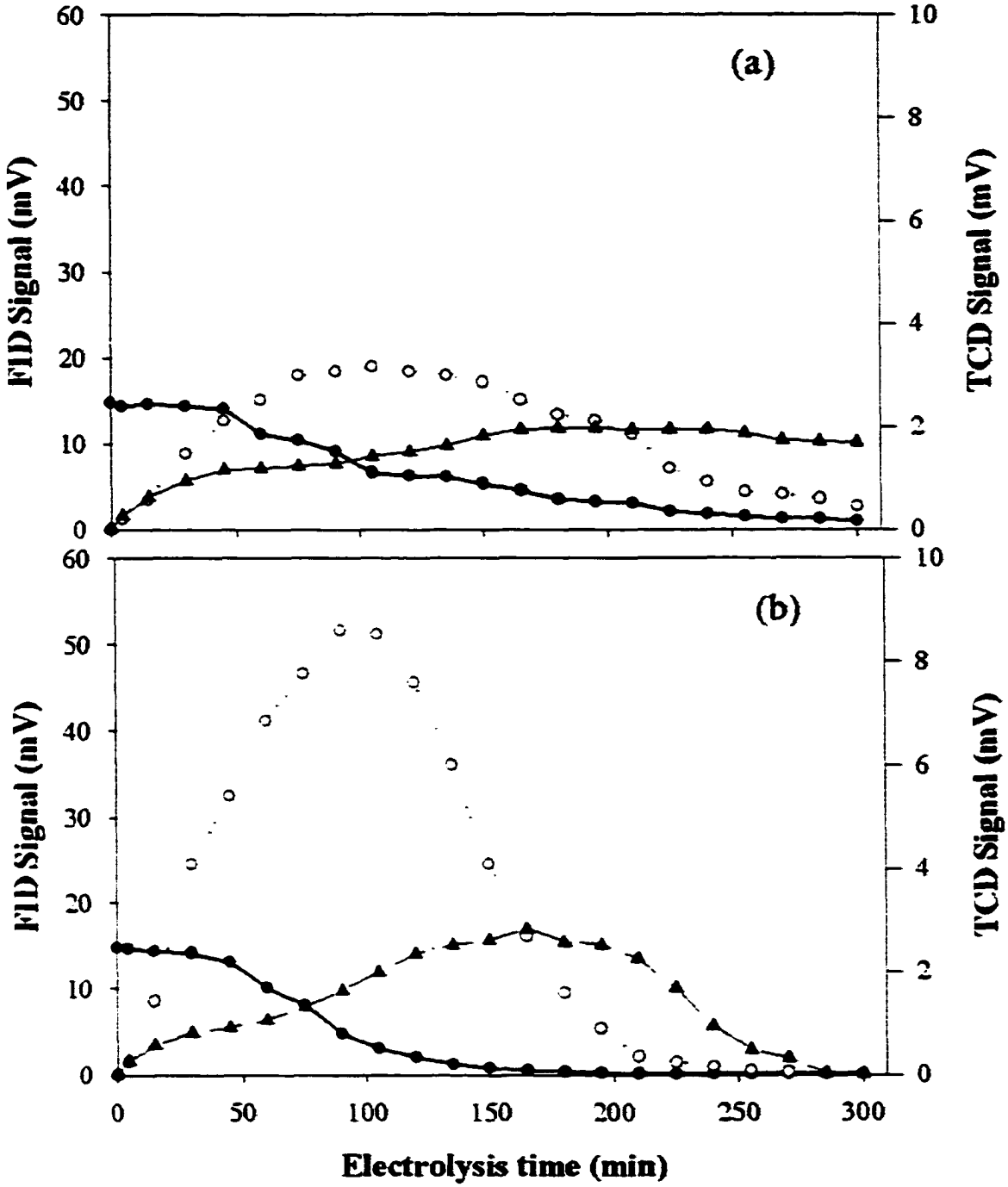

Figure 5.6. Chromatographic peak signal for selected compounds in headspace of miniature cell (Fig. 5.3) during electrolysis of 10% methanol in 5.0 mL of 0.10 M H_2SO_4 without (a) and with (b) addition of 5 mM Mn(II). Temperature: 5 °C. Anode area: 5.0 cm^2. Anode current: 1.0 A (0.20 A cm^{-2}). Curves: (●) methanol, (○) formaldehyde, (▲)carbon dioxide.

production occurs when the rate of methanol degradation becomes limited by: (i) the flux of OH species generated by anodic discharge of H_2O and/or (ii) the rate of convective-diffusional mass transport of methanol at the electrode surface. Future research will examine this speculation by altering the current density and methanol concentration.

Single-pass flow cell (Figure 5.4) - Representative data are shown in Table 5.5 from tests of the extent of electrochemical degradation in the modified CSRS-I cell during a single pass of the designated compounds in 0.10 M H_2SO_4 containing 1 mM $MnSO_4(s)$.

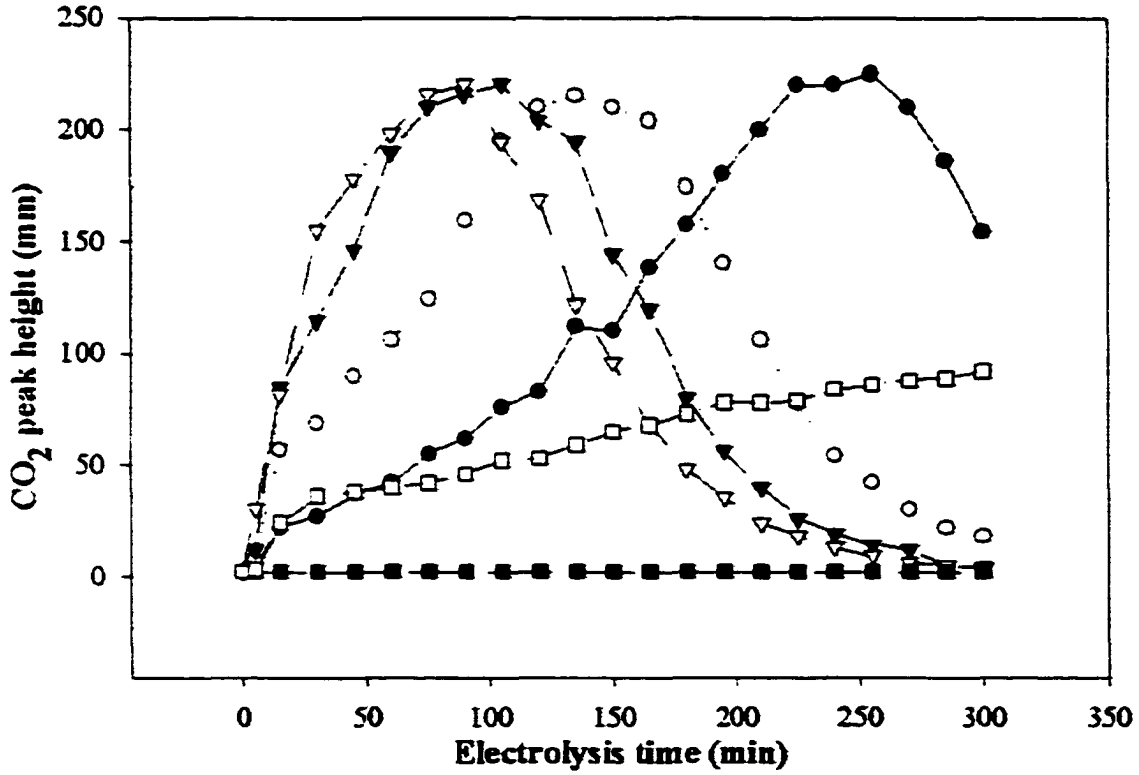

Figure 5.7. Chromatographic peak height for $CO_2(g)$ in gas stream during electrolytic degradation of 1% dioxane in an 8.0-mL aliquot of 0.10 M H_2SO_4 using the miniaturized cell (Figure 5.3) placed in a thermostated water bath. Anode current: 1.0 A (0.33 A cm^{-2}). Temperature (°C): (□) 5, (●) 35, (○) 55, (▼) 75, (▽) 95. Blank (°C): (■) 95.

Data from Table 5.5 confirm the conclusion that chlorinated and non-chlorinated hydrocarbons can be efficiently degraded by anodic (oxidative) degradation. When an undivided cell was used, cathodic dechlorination occurred; however, the products of cathodic dechlorination ultimately were anodically degraded to relatively benign compounds.

Use of a flow-through cell fabricated from the modified CSRS-I cell demonstrated that this apparatus holds promise for the continuous on-line or in-process stream degradation of chlorinated and non-chlorinated hydrocarbon solvent in acidic aqueous solutions or possibly neutral solutions if the electrode spacing is minimized and/or ionic membrane is employed.

Table 5.5. Summary of the results of single-pass ECI of the following solvents through the modified Dionex CSRS-II cell (Figure 5.4). Anodic current: 1.0 A (0.085 A/cm^2), flow rate 1 mL min^{-1}.

Compound	% efficiency	S.D.	comments
Methanol	53.0	4.0	
Tetrahydrofuran	83.0	10.3	
1,4 Dioxane	77.7	13.7	
Acetonitrile	8.6	1.1	an additional 8.0% decrease with 2nd pass
Methylene chloride	64.9	12.2	
Chloroform	84.6	8.0	
Methyl *tert*-butyl ether	71.6	14.1	

The Pt electrodes in the CSRS-I cell and other electrolysis cells used in this research are appropriate for the specified electrolytic degradation processes. However, the activity of the anode is increased by the presence of a $MnO_2(s)$ film. This catalytic film is easily prepared *in situ* by electrodeposition of $MnO_2(s)$ from $MnSO_4(s)$ dissolved in the solutions prior to electrolytic processing. The use of alkaline media is not appropriate because addition of $MnSO_4(s)$ to alkaline media results in formation of a brown "muddy" appearance from dispersed $Mn(OH)_2(s)$.

Future Research

Definite advantage can come from operation of the CSRS-I cell in a "divided" mode with the anode and cathode separated by a cation-exchange membrane. The primary advantage of the divided mode is the elimination of intermediate products of partial dechlorination processes at the cathode. However, the cation-exchange membrane must be chosen with large pore diameters to minimize joule heating, which, in excess, causes unwanted thermal degradations of the membrane and evaporation (rather than remediation) of the process stream. Future research will compare a variety of cation-exchange membranes, optimize cell path length, and the thickness of electrode separation.

Acknowledgements

This research was made possible by financial contributions from Dionex Corp., Sunnyvale, CA. The authors also are grateful to Ekaterina Kadnikova and Hajime Takano for translations of several journal publications.

References

[1] C.F. Poole, S.A. Shuette, *Contemporary Practice of Chromatography*, Elsevier, New York, **1984**, p. 257.

[2] W. Cooper, *Journal of the Air & Waste Management Association*, **1993**, *43*, 1358.

[3] A. Adachi, T. Kobayashi, *Jpn. J. Toxicol. Environ. Health*, **1993**, *39*, 63.

[4] M.M. Halmann, *Photodegradation of Water Pollutants*, CRC Press, New York, **1995**, p. 113-180.

[5] R.B. Winter, K.M. Yen, B.D. Ensley, *Bio/Technology*, **1989**, *7*, 282.

[6] Y.I. Matatov-Meytal, M. Sheintuch, *Ind. Eng. Chem. Res.*, **1998**, *37*, 309.

[7] R. Cossu, A.M. Polcaro, M.C. Lavagnolo, M. Mascia, S. Palmas, F. Renoldi, *Environ. Sci. Technol.*, **1998**, *32*, 3570.

[8] S.K. Johnson, L.L. Houk, J. Feng, R.S. Houk, D.C. Johnson, *Environ. Sci. Technol.* **1999**, *33*, 2638.

[9] N. Sonoyama, T. Sakata, *Environ. Sci. Technol.*, **1999**, *33*, 3438.

[10] A.P. Tomilov, S.G. Mairanovskii, M. Ya. Fioshin, V.A. Smirnov, *Electrochemistry of Organic Compounds*, Chap. VI, Halsted Press, NewYork, **1968**.

[11] N.Đ. Popović, D.C. Johnson, *Anal. Chem.*, **1998**, *70*, 468.

[12] N.Đ. Popović, J.A. Cox, D.C. Johnson, *J. Electroanal. Chem.*, **1998**, *455*, 153; *1998*, *456*, 203.

[13] D.C. Johnson, N. Popović, J. Feng, L.L. Houk, K.T. Kawagoe, *Proc. Electrochem. Soc.*, **1996**, *95-26*, 176.

[14] J.J. Carey, W. Henrietta, C.S. Christ, S.N. Lowery, U.S. Pat. 5,399,247; **1995**.

[15] I-H. Yeo, D.C. Johnson, *J. Electrochem. Soc.*, **1987**, *134*, 1973.

[16] K.T. Kawagoe, D.C. Johnson, *J. Electrochem. Soc.*, **1994**, *141*, 3404.

[17] R. Kotz, S. Stucki, B. Carcer *J. Appl. Electrochem.*, **1991**, *21*, 14.

[18] C. Comninellis, C. Pulgarin, *J. Appl. Electrochem.*, **1993**, *23*, 108.

[19] F. Vicent, E. Vazquez, E. Morallon, F. Cases, J.L. Vazquez, A. Aldaz, *Port. Electrochim. Acta.*, **1995**, *13*, 423.

[20] J.M. Kesselman, O. Weres, N.S. Lewis, M.R. Hoffman, *J. Phys. Chem. B.*, **1997**, *101*, 2637.

[21] E. Brillas, J. Casado, *J. Electrochem. Soc.*, **1998**, *145*, 759.

[22] I.U. Haque, J.F. Rusling, *Chemosphere*, **1993**, *26*, 1301.

[23] K. Vinodgopal, U. Stafford, K.A. Gray, P.V. Kamat, *J. Phys. Chem.*, **1994**, *98*, 6797.

[24] J. Feng, L.L. Houk, D.C. Johnson, *J. Electrochem. Soc.*, **1995**, *142*, 3626.

[25] L.L. Houk, S.K. Johnson, J. Feng, R.S. Houk, D.C. Johnson, *J. Appl. Electrochem.*, **1998**, *28*, 1167.

[26] A.T. Stone, H.-J. Ulrich, *Env. Sci. Technol.*, **1989**, *23*, 421.

[27] L.A. Kulski, A.A. Ivanyuk, E.S. Matskevich, O.A. Mumina, *Doklady Akademii Nauk Ukrainsko I Ssr.*, **1988**, *5*, 41.

[28] O.A. Mumina, E.S. Matskevich, *Khim. Teknol. Vody*, **1985**, *7*, 35.

[29] A. Watanabe, H. Takahishi, *J. Nat'l. Chem. Lab. for Ind.*, **1990**, *85*, 275.

[30] Y. Li, W. Xu, Y. Sun, *Sel. Papers of Eng. Chem. and Metal.*, **1997**, *9*, 40.

[31] D.C. Johnson, J. Feng and L.L. Houk, *Electrochim. Acta*, accepted.

[32] F.A. Cotton, G. Wilkinson, *Advanced Inorganic Chemistry*, 3rd ed.: Interscience Publishers: New York, **1972**, chap. 25.

VI. PHOTO ASSISTED ELECTROCHEMICAL INCINERATION OF SELECTED ORGANIC COMPOUNDS

A paper accepted for publication in Journal of the Electrochemical Society[1]

Stephen E. Treimer, Jianren Feng[2], and Dennis C. Johnson[3]

Abstract

The decrease in chemical oxygen demand (COD) of mildly acidic (pH 3.5) aqueous solutions of phenol, aniline, *n*-propanol and acetic acid was observed to be significantly larger at $PbO_2(s)$-coated Pt electrodes ("PbO_2/Pt") in comparison to bare Pt electrodes in a flow-through reactor. Furthermore, the rate of $CO_2(g)$ production during electrolysis of phenol solutions at PbO_2/Pt electrodes (4.6 cm^2) also was determined to be significantly larger when these electrode surfaces were illuminated by a 14-W UV lamp (254 nm). The total amount of $CO_2(g)$ produced over a 4-h electrolysis period at an illuminated PbO_2/Pt electrode in a flow-through cell was equal to 90% of the theoretical amount corresponding to stoichiometric conversion of the phenol to $CO_2(g)$. Elemental analysis of the $PbO_2(s)$ films demonstrated that they were doped slightly with iron presumably in the Fe(III) state, i.e., Fe(III)/Pb(IV) = 0.010. The source of Fe(III) was concluded to be the stainless steel used in construction of the flow-through electrolysis vessel. It is speculated that the Fe(III) sites in the surfaces of the $PbO_2(s)$ films can function as Lewis acid sites for adsorption of reactant molecules via non-bonded electrons as an initial step in the anodic degradation mechanisms.

---

[1] Reprinted with permission of the Journal of the Electrochemical Society, in press.
[2] Present address: Pollution Control Division, Galveston County Health District, La Marque, TX 77568
[3] Corresponding author.

The advantage of pre-adsorption of reactant molecules is thought to be the result of longer residence times for these molecules within the applied electric field at the electrode-solution interfacial region. The observed effect of UV illumination is speculated to be associated with absorption of the photons within the surface of the $PbO_2(s)$ films.

Introduction

The oxidative remediation of toxic organic wastes in industrial effluents has been the subject of intense investigation. The US Environmental Protection Agency estimates that in 1998 >130 million pounds of phenol and >28 million pounds of aniline waste were released to the environment.[1] Phenol is used in the industrial production of numerous compounds, including pharmaceuticals, disinfectants, germicides, and slimicides.[2,3] Aniline is used as the starting material for the manufacture of many azo compounds used to dye cloth. Reference 1 also reports the disposal of the groundwater contaminants Atrazine® (>1.8 million pounds) and Trifluralin® (>0.2 million pounds) herbicides, and naphthalene (>49 million pounds), a representative of the general class of compounds known as *polycyclic aromatic hydrocarbons* (PAHs). The controversial oxidation of PAH compounds in the body has received significant attention in the study of human carcenogenesis.[4,5]

The large environmental burden resulting from phenol waste has resulted in extensive studies of photocatalytic processes for the oxidative degradation of this class of compound. Direct photocatalytic oxidation of phenol has been attempted.[6-17] Photocatalytic electrochemistry has been developed and primarily makes use of colloidal suspensions of semiconductor particles at which the rate of oxidation processes is increased when irradiated by ultraviolet (UV) light. Subsequent removal of the colloidal suspension of semiconductor

particles from remediated waste solutions, if necessary, can be difficult. On-going research in this and other laboratories also is focused on alloy and metal oxide anode materials that support the direct anodic degradation of organic compounds.[3,18–32] The objective in the degradation of phenol and related compounds is the quantitative conversion to carbon dioxide, a technique referred to here as *electrochemical incineration*.

Prior to the study reported here, our attention has been given to comparisons of electrode materials for the purpose of determining those anode compositions that exhibit maximum activity for oxidative processes[28]; the role of altervalent metallic dopants in PbO_2-film electrodes, with emphasis on Bi(V);[33,34] and the identification of the intermediate products of electrochemical incineration.[31] Here, we describe results from an investigation to determine possible benefits of direct illumination of anode surfaces by UV light (254 nm) to enhance the rates of the electrochemical incineration of selected organic compounds. In previous related work, Vinodgopal *et al.* demonstrated the benefit of UV illumination of a thin particulate film of TiO_2 on an optically transparent, conductive anode maintained at a constant anodic bias for the anodic degradation of 4-chlorophenol.[35,36] In the study reported here, a Pt-wire anode was wrapped tightly around a quartz tube into which a UV lamp was inserted.

Experimental

Reactor – A diagram of the flow-through photoelectrochemical reactor is shown in Figure 6.1. In this reactor, UV light (254 nm) was generated by a GPH-274 low-pressure 14-watt Hg-vapor lamp (15 mm o.d. x 21 cm length) from Southern New England Ultraviolet (Branford, CT). This pencil-shaped lamp was placed inside a quartz tube (22-mm o.d. x 31-

cm length) wrapped with 284 cm of 51-μm Pt wire (4.6-cm^2 area) to serve as the anode during electrolyses. This assembly was then placed inside a stainless steel cylinder (2.5-cm i.d. x 30.5-cm length) that defined the dimensions of the flow-through reactor and also functioned as the cathode during electrolyses. Analyte solutions were circulated continuously within the closed-loop reactor for the designated periods.

The temperature of the stainless steel cylinder was maintained at 40 ± 1 °C using

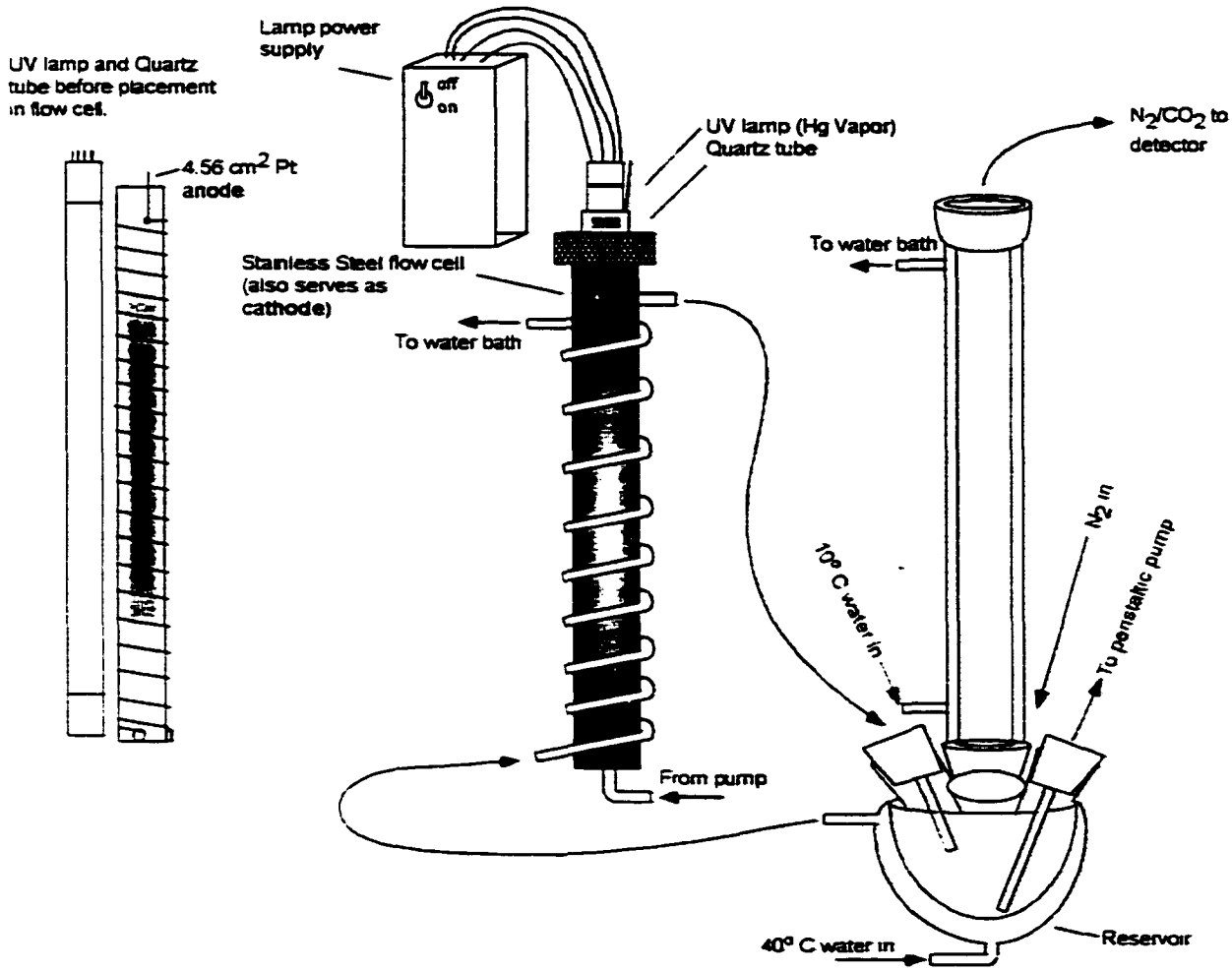

Figure 6.1. Schematic diagram of the flow-though electrochemical cell for photo-assisted electrochemical incineration of organic compounds in aqueous media.

water pumped by a Lauda controlled-temperature bath from Scientific Apparatus (Chicago, IL) through copper tubing (5-mm o.d. x 120-cm length) wrapped tightly around the stainless steel cylinder.

Instrumentation – Electrolyses were performed at a constant current of 1.0 A (0.22 A cm^{-2}) from a Model 415 potentiostat, operated in the galvanostatic mode, and Model 420X power supply from Electrosynthesis (Lancaster, NY) connected in-series with a Model 8012A current meter from Fluke (Everett, WA).

The concentration (v/v) of $CO_2(g)$ within the headspace above the glass reservoir was determined by a Binos 100 NDIR flow-through detector from Fisher-Rosemont (Baar, Switzerland) using pure $N_2(g)$ to purge the headspace.[37] The rate of $N_2(g)$ flow was dynamically measured and regulated at 210 ± 5 mL min^{-1} by an in-line Model 110 digital flow meter from Cole-Parmer (Vernon Hills, IL). The temperature of the headspace was maintained at 10 ± 1 °C using a second Lauda controlled temperature water bath and multiple condensers. Labview software (Version 5.1) from National Instruments (Austin, TX) was written for data collection using a 16-bit AT-MIO16-XE50 interface board.

Solutions of the selected organic compounds were circulated between the reactor and a glass reservoir (350 mL) using a Masterflex® Model L peristaltic pump from Cole-Parmer operated at a flow rate of 230 mL min^{-1}. The glass reservoir was constructed with a water jacket through which water at 40 ± 1 °C was pumped from the Lauda controlled temperature bath.

Chemical oxygen demand (COD) was determined using apparatus and procedures from Hach Chemical Company (Ames, IA).[38]

Reagents – All solutions were prepared from reagents used as received from Fisher Scientific (Pittsburgh, PA). Tap water was deionized using anion- and cation-exchange towers from Culligan (Owatonna, MN), and purified further to achieve 18-MΩ resistivity using a Milli-Q system from Millipore (Bedford, MA). Except where specified to the contrary, electrolyses were applied to 5.0 mM solutions of designated organic compounds in 0.10 M $NaNO_3$ adjusted to pH 3.5 by addition of 0.1 M HNO_3.

Metal oxide films – Where specified, films of $MnO_2(s)$, $PbO_2(s)$ or MnO_2-$PbO_2(s)$ were electrodeposited on the Pt-wire anode simultaneously with electrochemical incineration of selected organic compounds by addition of 1.0 mM $MnSO_4$, 1.0 mM $Pb(NO_3)_2$, or 0.5 mM $MnSO_4$ with 1.5 mM $Pb(NO_3)_2$, respectively. Following completion of electrolysis procedures, the electrodeposited films were cathodically stripped from the Pt-wire anode, and the inner surfaces of the reactor cell were cleaned, using *aqua regia*.

Elemental compositions of metal oxide films employed as electrodes in this study were determined using a series 4500 inductively coupled plasma mass spectrometer (ICP-MS) from Hewlett-Packard (Wilmington, DE) *without* the Shield Torch® system. The metal oxide films were electrochemically stripped from the Pt substrates in 0.1 M HNO_3 electrolyte. Electrolyte blanks were analyzed for interferences and subtracted and then compared to standard solutions prepared from NIST certified Fe, Mn, and Pb standards (1000 ppm) from SPEX CertiPrep (Metuchen, NJ).

Analysis of Results –Values of current efficiency (CE) for conversion of organic compounds to CO_2 were calculated using the following equation:

$$CE = \frac{\text{moles } CO_2 \text{ produced/coulombs passed}}{\text{theoretical moles } CO_2 \text{ achievable/theoretical coulombs required}} * 100 \qquad (1)$$

Results and Discussion

Selected aromatic compounds – Table 6.1 contains a summary of results for the electrochemical incineration of acidic solutions (pH 3.5) containing 5.0 mM phenol and 5.0 mM aniline. Listed in the table are percentage values for the decrease in chemical oxygen demand (COD) for these solutions (350 mL) resulting from electrolysis at the designated anodes for the indicated time periods. Also listed are values of current efficiency calculated by Equation 1 on the basis of complete degradation of organic compounds to CO_2 as described by Equations 2 and 3 for phenol and aniline, respectively.

$$C_6H_5OH + 11H_2O \rightarrow 6CO_2 + 28H^+ + 28e^- \qquad (2)$$

$$C_6H_5NH_3^+ + 15H_2O \rightarrow 6CO_2 + NO_3^- + 38H^+ + 36e^- \qquad (3)$$

As implied, it was assumed that there was no build up of partially oxidized intermediate products. The anodic oxidation of phenol, including identification of intermediate products and suggested reaction pathways, have been discussed previously.[3,17,20,31]

Based on results in Table 6.1 for the decrease in COD for phenol solutions, the inherent activity of anode surfaces without UV illumination increased in the order: Pt (57%) < MnO_2/Pt (64%) < PbO_2/Pt (86%) < MnO_2-PbO_2/Pt (92%). The application of UV illumination increased the activity of all anode surfaces with the highest activity observed for the PbO_2/Pt anode (98%). Therefore, further testing did not include the MnO_2/Pt and MnO_2-PbO_2/Pt electrodes.

Table 6.1. Decrease in COD and current efficiency for CO_2 production for phenol and aniline at designated anodes with and without UV illumination.

Organic Compound	Anode	Electrolysis Period (h)	UV Illumination	Decrease in COD (%)	Current Efficiency (%)
Phenol[a]	Pt	4.0	No	57	4.8
	Pt	4.0	Yes	59	6.7
	MnO_2/Pt	4.0	No	64	8.1
	MnO_2/Pt	4.0	Yes	79	13
	PbO_2/Pt	4.0	No	86	13
	PbO_2/Pt	4.0	Yes	98	17
	MnO_2-PbO_2/Pt	3.0	No	92	23
	MnO_2-PbO_2/Pt	3.0	Yes	93	22
Aniline[b]	Pt	4.0	No	53	5.1
	Pt	4.0	Yes	68	5.8
	PbO_2/Pt	4.0	No	64	9.2
	PbO_2/Pt	4.0	Yes	80	12.8

[a] Assumes a 28-electron process.
[b] Assumes a 36-electron process.

Data for the decrease in COD given in Table 6.1 for aniline solutions are similar to those for phenol. More specifically, the inherent activity without UV illumination is higher for the PbO_2/Pt (64%) electrode than for the Pt electrode (53%). Furthermore, application of UV illumination resulted in the largest decrease in COD for the PbO_2/Pt anode (80%). Kirk *et al.* reported a current efficiency of 13% with 80% conversion to CO_2 for a 5-h period of electrolysis using a current of 1.0 A at an electrode having an area of 237 cm^2 (4.2 mA cm^{-2}).[18] Under similar experimental conditions (data not shown), our results also indicate approximately 13% current efficiency, but 90% conversion to CO_2 after a 4-h electrolysis period when using the PbO_2/Pt anode under UV illumination.

Two mechanisms appear feasible for the photo-assisted degradation processes. First, adsorbed aromatic molecules are expected to undergo π-π^* electronic transitions as a result of the absorption of UV photons and the rate constants for anodic degradation of these electronically excited molecules are suspected to be larger than that for ground-state molecules. Second, the observed benefit of UV illumination might be photocatalytic in nature resulting from absorption of UV photons within the surface layer of the electrodes and the resultant promotion of electrons from the valence band to the conduction band. Results are presented below for anodic degradation of non-aromatic compounds as a test of the validity of the first speculation above.

Selected non-aromatic compounds – The initial mechanistic speculation considered the possibility that the observed photo effect is associated with electronic activation of adsorbed aromatic molecules as a result of absorption of UV photons. Therefore, data were obtained for anodic degradation of *n*-propanol, an aliphatic compound. These results are summarized in Table 6.2. Regardless of the absence of a strong chromophore in *n*-propanol,

the benefit of UV illumination was very evident in the degradation of this compound. More specifically, for the PbO_2/Pt electrode, a 61% decrease in COD was achieved during electrolytic degradation with simultaneous UV illumination in comparison to only 33% for the absence of UV illumination. These results are concluded to demonstrate that photo-activation of adsorbed organic molecules is not a significant component of the photo-assisted electrolytic degradation mechanism.

Our laboratory has encountered difficulty in achieving total electrochemical incineration of aromatic compounds, i.e., complete oxidation to CO_2 as the final product.

Table 6.2. Decrease in COD and current efficiency for CO_2 production for *n*-propanol and acetic acid at designated anodes with and without UV illumination.

Organic Compound	Anode	Electrolysis Period (h)	UV Illumination	Decrease in COD (%)	Current Efficiency (%)
n-Propanol[c]	Pt	4.0	No	0.0	0.0
	Pt	4.0	Yes	0.4	31
	PbO_2/Pt	4.0	No	1.3	33
	PbO_2/Pt	4.0	Yes	6.0	61
Acetic Acid[d]	Pt	4.0	No	0.0	0.0
	Pt	4.0	Yes	0.2	6.0
	PbO_2/Pt	4.0	No	1.1	1.2
	PbO_2/Pt	4.0	Yes	1.4	14

[c] Assumes an 18-electron process.
[d] Assumes an 8-electron process.

Analyses of product solutions have indicated a build-up of acetic acid or acetate anion, depending on pH.[31] It is apparent that acetic acid is kinetically resistant to further degradation. It can be conjectured that these hydrophilic compounds are not adsorbed into the electrode-solution interface and, therefore, the requisite anodic O-transfer step from adsorbed OH radicals to solvated hydrophilic species is slow or non-existent. Data shown in Table 6.2 verifies the virtual inertness of acetic acid under these conditions, albeit there is a slightly greater reactivity at the PbO_2/Pt electrode, as compared with the bare Pt electrode, particularly when illuminated with UV light.

Elemental analysis of oxide films – The PbO_2 films in this study were observed to exhibit a slightly *rusty* hue in comparison to the dark black color characteristic of pure β-PbO_2. The *rusty* hue was suspected to result from the presence of Fe(III) in PbO_2 ("Fe-PbO_2").

A PbO_2 film typical of those used to generate data in Table 6.2 was dissolved and the resulting solution was analyzed using ICP-MS. Indeed, this film was determined to contain 0.8% Fe(III) calculated relative to the Pb(IV) content. Analysis of a film of MnO_2 by ICP-MS indicated the presence of 1.0% Fe(III) relative to Mn(IV). It is anticipated that Fe(III), with its low d-orbital occupancy, functions as Lewis acid sites in the surfaces of Fe(III)-doped PbO_2 films ("Fe-PbO_2") and Fe(III)-doped MnO_2 films ("Fe-MnO_2"). Catalytic benefit of Fe(III) in β-PbO_2 films has been described for oxidation of CN^- to CNO^- in alkaline media.[39] In comparison, virtually no voltammetric response was observed for CN^- at a pure PbO_2-film electrode. The catalytic activity of the Fe-PbO_2/Au surface was speculated to result from weak adsorption of the CN^- species at the Fe(III) surface sites

within the oxidation mechanism. A similar function Fe(III) sites has been offered to explain the higher current efficiencies for anodic production of O_3 during O_2 evolution at Fe-PbO_2/Au electrodes in comparison to PbO_2/Au electrodes.[40-43] It is anticipated in the present work that the Fe(III) sites can adsorb phenol and aniline by the formation of weak coordination bonds with the organic molecules via their π-electrons. The benefit expected from reactant adsorption is an increased time of residence at the electrode surface with a resulting increase in probability for the desired anodic reaction.

The only possible source of Fe(II/III) in the electrolysis solutions was the stainless steel cylinder of the electrolytic reactor that functions as a cathode during electrolysis. However, the mechanism for dissolution of the stainless steel is not clear. In a separate experiment using electrolyte solution free of organic compound, the Fe(II/III) content of the solution was determined to increase approximately as a linear function of time to 0.070 ppm at 2.2 h when the stainless steel cathode was at its "open-circuit" potential. Subsequently, the concentration of Fe(II/III) was determined to decrease only to 0.040 ppm during a 2-h period under the electrolysis conditions (1.0 A). We suspect that very thin films of protective oxide formed under open-circuit conditions are dissolved into the acidic electrolyte.

Rate of $CO_2(g)$ generation for phenol – It has been stated that "deep oxidation of any hydrocarbon should yield CO_2 though this is seldom achieved".[43] Figure 6.2 shows the percent $CO_2(g)$ (v/v) in the gas mixture coming from the void space above the solution reservoir as a function of time (t) during electrolytic degradation of phenol at the Pt electrode and the Fe(III)-doped PbO_2 on the Pt electrode ("Fe-PbO_2/Pt") with and without UV illumination of the electrode surfaces. Clearly for the uncoated Pt anode, the rate of $CO_2(g)$ generation is low in the absence (●) and presence (▽) of UV illumination for t < ca. 5000 s

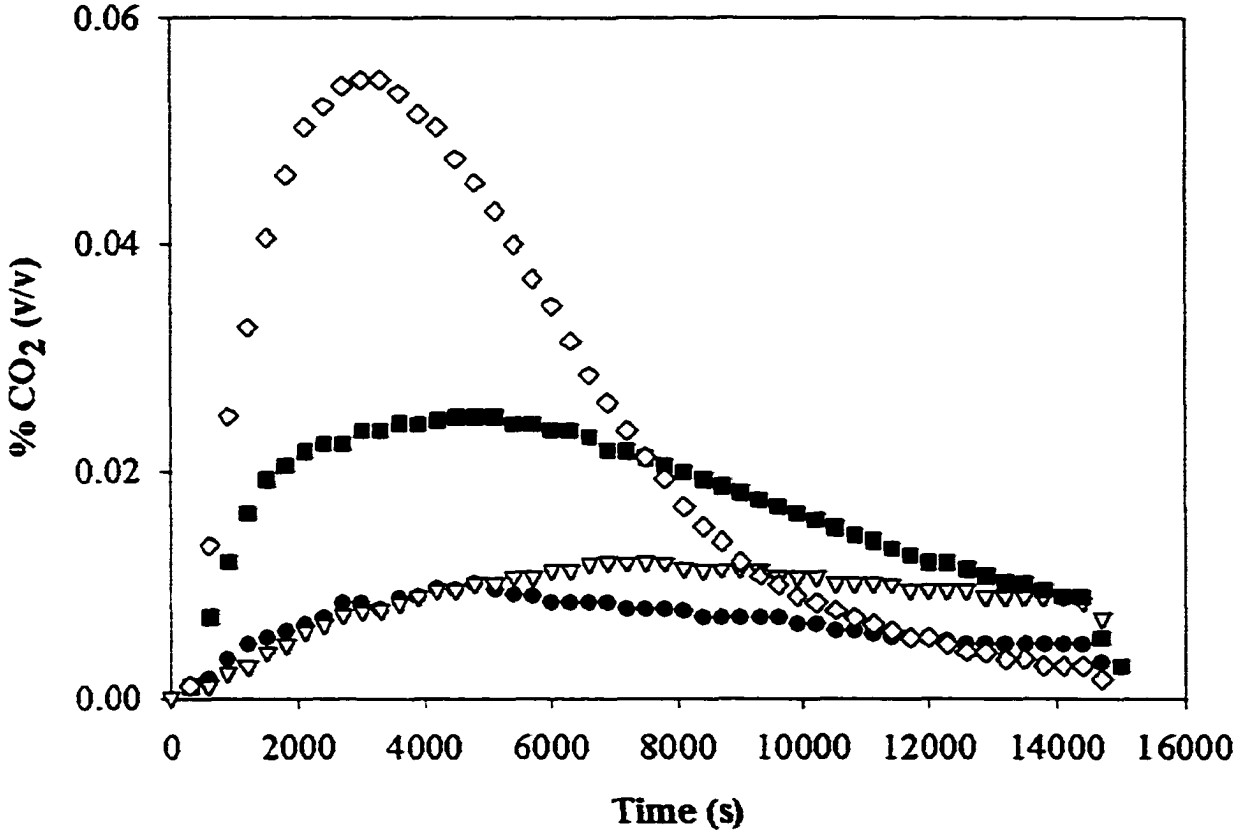

Figure 6.2. Percent $CO_2(g)$ as a function of time in the $N_2(g)$ stream coming from the electrochemical cell during the electrochemical incineration of 5.0 mM phenol at bare Pt and Fe(III)-doped PbO_2/Pt electrodes with and without UV illumination. Anodes: (■, ◇) Fe-PbO_2/Pt, (●, ▽) Pt. Conditions: (◇, ▽) with UV illumination, (■, ●) without UV illumination.

with only a slight increase caused by UV illumination for $t > 5000$ s. Use of the Fe-PbO_2/Pt anode resulted in a significantly higher rate of $CO_2(g)$ production (■), as compared with the uncoated Pt (●), in the absence of UV illumination. Furthermore, with application of UV illumination, a significant increase in $CO_2(g)$ was observed with UV illumination (◇) for $1000 < t < 6000$ s. The rate of $CO_2(g)$ production at the PbO_2/Pt electrode under UV illumination (◇) rapidly diminishes toward zero for $t > 7000$ s. This behavior undoubtedly

reflects the significant decrease in the concentration of phenol in the bulk solution as a result to the rapid degradation process.

Figure 6.3 shows the time-integrals of the plots from Figure 6.2 plotted as moles $CO_2(g)$ vs. time. In the case of the Fe-PbO_2/Pt electrode under UV illumination, the production of $CO_2(g)$ reached 76% of the theoretical limit at 9000 s (2.5 h) and 90% of the theoretical limit at 14,400 s (4 h). These yields are significantly larger than the values 21% at 2.5 h and 46% at 10 h reported by Sharifan and Kirk for 3.5 mM phenol in 1.0 M H_2SO_4 using a larger anode (237 cm^2) with a current of 1.0 A (0.42 A cm^{-2}).[19] Results reported by

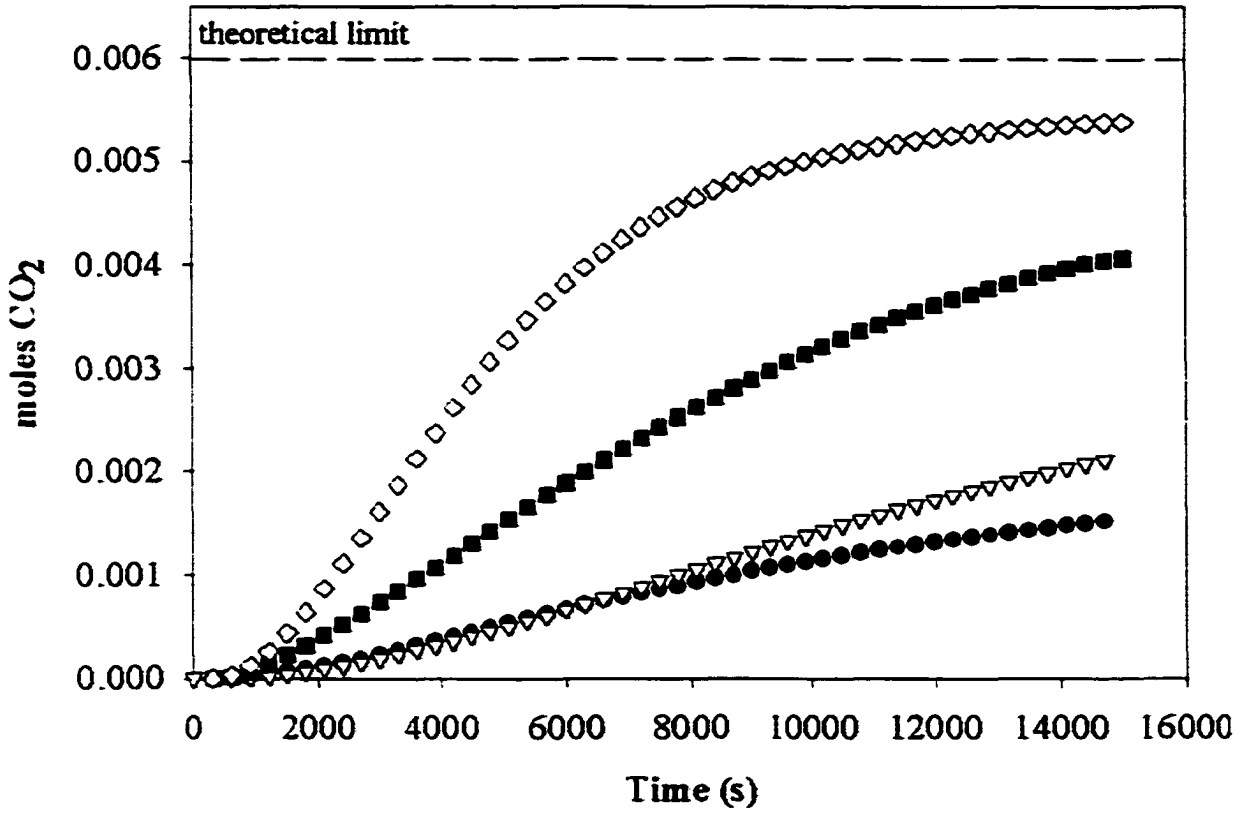

Figure 6.3. Moles of $CO_2(g)$ generated as a function of time during the electrochemical incineration of 5.0 mM phenol at bare Pt and Fe(III)-doped PbO_2/Pt electrodes with and without UV illumination. Theoretical maximum is 6.0×10^{-3} moles CO_2. Anodes: (■,◇) Fe-PbO_2/Pt, (●, ▽) Pt. Conditions: (◇, ▽) with UV illumination, (■, ●) without UV illumination.

these workers were obtained using an anode consisting of lead pellets with a stainless steel cathode; however, no mention was made of iron content in the $PbO_2(s)$ film generated on the Pb pellets during passage of anodic current.

Figure 6.4 contains a comparison of the moles of $CO_2(g)$ generated vs. time during use of the Fe(III)-doped $MnO_2(s)$ film on the Pt electrode ("Fe-MnO_2/Pt") without (●) and with (▽) UV illumination. The Fe-MnO_2/Pt electrode exhibited kinetics only slightly more favorable than that for the Pt electrode; however, illumination of the electrode with UV light

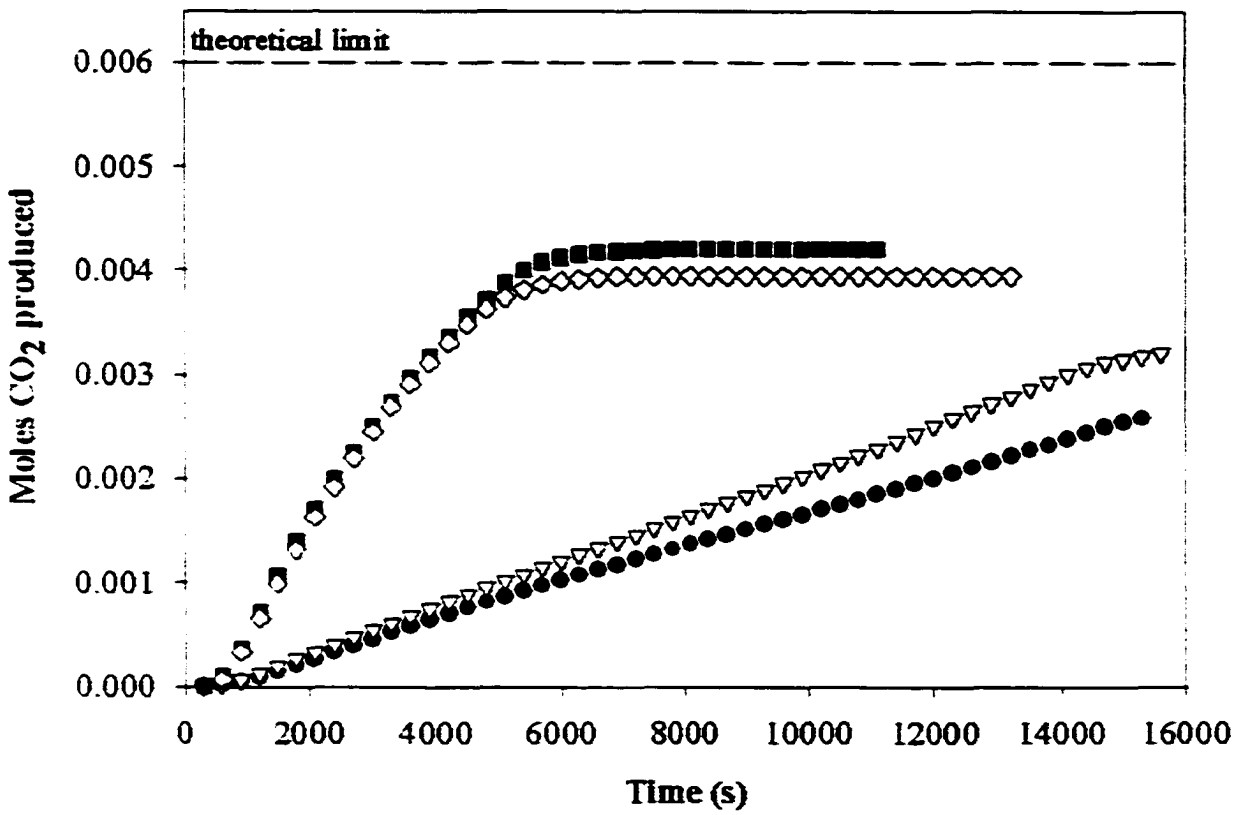

Figure 6.4 Moles of $CO_2(g)$ generated as a function of time during the electrochemical incineration of 5.0 mM phenol at Fe(III)-doped MnO_2-PbO_2/Pt and MnO_2/Pt anodes with and without UV illumination. Theoretical maximum is 6.0×10^{-3} moles CO_2. Anodes: (■, ◇) Fe-MnO_2-PbO_2/Pt, (●, ▽) Fe-MnO_2/Pt. Conditions: (◇, ▽) with UV illumination, (■, ●) without UV illumination.

had a more pronounced effect than for the Pt electrode. Also shown in Figure 6.4 are plots for a Fe(III)-doped MnO_2-PbO_2/Pt electrode ("Fe-MnO_2-PbO_2/Pt") without (■) and with (◇) UV illumination. It is apparent for this electrode that there is no benefit from UVillumination. The Fe-MnO_2-PbO_2/Pt electrode exhibited more rapid onset of $CO_2(g)$ production (t < 1000 s) than observed for the Fe-PbO_2/Pt electrode. However, the Fe-MnO_2-PbO_2/Pt electrode was unable to drive the incineration reaction to the same degree of completeness as achieved using the Fe-PbO_2/Pt electrode, reaching only approximately 70% completeness.

Additional experimental results demonstrated that the UV illumination of anodes under open-circuit conditions did not result in significant degradation of the aromatic

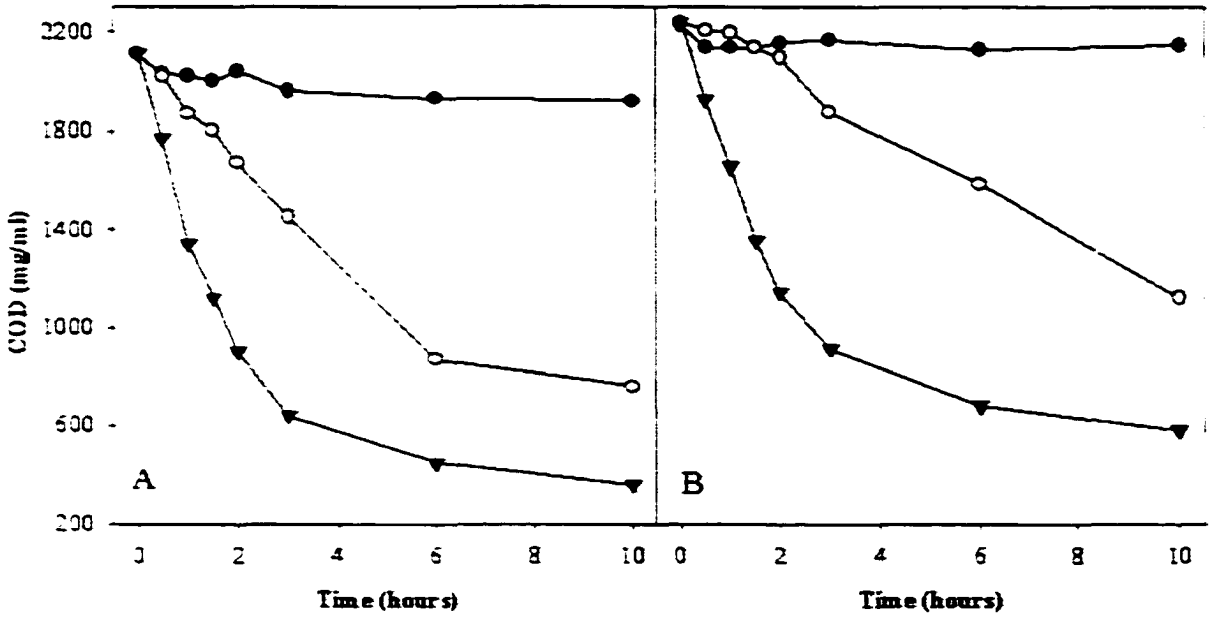

Figure 6.5 Comparison of the electrochemical incineration of (A) 5.0 mM 4-chlorophenol and (B) 5.0 mM phenol with/without UV illumination in 0.10 M NaOH. Anode: Pt. Conditions: (●) UV illumination under open-circuit conditions, (○) electrolysis without UV illumination, and (▼) electrolysis with UV illumination.

compounds tested. As representative data, Figures 6.5A&B contains COD values obtained during the processing of 0.10 M NaOH containing 5.0 mM 4-chlorophenol (A) and 5.0 mM phenol (B) using the bare Pt-wire anode. Clearly, the change of COD is insignificant in comparison to experimental uncertainty during UV illumination of the anode without the passage of anodic current (●). Hence, it is concluded that photocatalytic degradation without simultaneous electrolysis is negligible using the UV lamp tested in these experiments. Also shown are COD values for the electrochemical incineration of these solutions with (▼) and without (○) simultaneous UV illumination of the Pt anode. As already demonstrated, simultaneous illumination of the anode during electrolysis results in a significant increase in the rate at which COD decreases with time.

Conclusion

Illumination of anode surfaces with low intensity UV light was observed to result in faster $CO_2(g)$ production during electrochemical incineration of selected organic compounds. We conclude that the use of photo-assisted electrochemical incineration can be important for oxidative degradations of toxic organic wastes, especially at the site of origin.

Based on observations of this photo effect for both aromatic (phenol and aniline) and non-aromatic (*n*-propanol and acetic acid) compounds, we speculate that the photo mechanism results from absorption of UV photons in the surface of the electrode rather than absorption by reactant molecules. The consequence of adsorption of UV photons in the electrode surface might be an increased rate for generation of •OH radicals as is proposed to explain the photocatalytic process at TiO_2 particles.[35,36,44,45] Future research will test this speculation for the PbO_2-film electrodes by determining possible differences in the apparent

overpotential for anodic discharge of H_2O with and without illumination UV light. Future research also will test the possible benefit of emulsifying agents to increase the solubility of insoluble compounds in the aqueous media.

Acknowledgement

The authors would like to thank Ames Laboratory for funding of this project. Ames Laboratory is a division of the U.S. Department of Energy and operated under Contract W-7405-Eng-82.

References

1. *1998 Toxic Release Inventory Public Data Release*. U.S. Environmental Protection Agency. Washington. D.C. (2000).

2. *Merck Index*. p. 7205. Merck & Co., Inc., Rahway, NJ (1989).

3. K. Rajeshwar and J. G. Ibanez. *Environmental Electrochemistry*. p. 370. Academic Press. San Diego (1997).

4. E. Cavalieri and E. Rogan. in *Polycyclic Hydrocarbons and Carcinogenesis*. R. G. Harvey. Editor. p. 289. American Chemical Society. Washington. D.C., (1985).

5. E. Cavalieri and E. Rogan. *Environ. Health Perspect.*, **64**. 69 (1985).

6. D. F. Ollis. E. Pelizzetti and N. Serpone. in *Photocatalysis: Fundamentals and Applications*. N. Serpone and E. Pelizzetti. Editors. Chapter 18. Wiley Interscience. New York (1989).

7. R. W. Matthews, in *Photochemical Conversion and Storage of Solar Energy*, E. Pelizzetti and M. Schiavello, Editors, p. 427, Kluwer Academic Publishers, Dordrecht (1991).

8. T-Y. Wei and C-C. Wan, *J. Photochem. Photobiol.* A: Chem., **69**, 241 (1992)

9. M. A. Fox and M. T. Dulay, *Chem. Rev.*, **93**, 341 (1993).

10. A. Mills, R. H. Davies and D. Worsley, *Chem. Soc. Rev.*, **22**, 417 (1993).

11. A. Mills, S. Morris and R. Davies, *J. Photochem. Photobiol. A: Chem.*, **70**, 183 (1993).

12. I. U. and J. F. Rusling, *Chemosphere*, **26**, 1301 (1993).

13. C. Richard and P. Boule, *New J. Chem.*, **18**, 547 (1994).

14. J. Theurich, M. Lindner and D. W. Bahnemann, *Langmuir*, **12**, 6368 (1996).

15. J. M. Kesselman, O. Weres, N. S. Lewis and M. R. Hoffmann, *J. Phys. Chem. B*, **101**, 2637 (1997).

16. X. Li, J. W. Cubbage, T. A. Tetzlaff, and W. S. Jenks, *J. Org. Chem.*, **64**, 8509 (1999).

17. X. Li, J. W. Cubbage, and W. S. Jenks, *J. Org. Chem.*, **64**, 8525 (1999).

18. D. W. Kirk, H. Sharifian, and F. R. Foulkes, *J. App. Electrochem.*, **15**, 285 (1985).

19. H. Sharifan and D. W. Kirk, *J. Electrochem. Soc.*, **133**, 921 (1986).

20. O. Hammerich and B. Svensmark, in *Organic Electrochemistry*, 3rd ed., H. Lund and M. Bazier, Editors, p. 615, Marcel Dekker, New York (1991).

21. R. Kotz, S. Stucki and B. Carcer, *J. Appl. Electrochem.*, **21**, 14 (1991).

22. S. Stucki, R. Kotz, B. Carcer and W. Suter, *J. Appl. Electrochem.*, **21**, 99 (1991).

23. C. Comninellis and C. Pulgarin, *J. Appl. Electrochem.* **23**, 108 (1993).

24. K. Rajeshwar, J. G. Ibanez, and G. M. Swain, *J. App. Electrochem.*, **24**, 1077 (1994).

25. C. Comninellis in *Environmental Oriented Electrochemistry*, C. A. C. Sequeira, Editor, p. 77, Elsevier, New York (1994).

26. C. Comninellis and A. Nerini, *J. Appl. Electrochem.*, **25**, 23 (1995).

27. A. Savall, *Chimia*, **49**, 23 (1995).

28. J. R. Feng, L. L. Houk, D. C. Johnson, S. N. Lowery and J. J. Carey, *J. Electrochem. Soc.*, **142**, 3626 (1995).

29. C. Comninellis and D. Battisti, *J. Chim. Phys.*, **93**, 673 (1996).

30. L. L. Houk, S. K. Johnson, J. Feng, R. S. Houk and D. C. Johnson, *J. Appl. Electrochem.*, **28**, 1167 (1998).

31. S. K. Johnson, L. L. Houk, J. Feng, R. S. Houk and D. C. Johnson, *Environ. Sci. & Tech.*, **33**, 2638 (1999).

32. D. C. Johnson, J. Feng and L. L. Houk, *Electrochim. Acta*, **46**, 323 (2000).

33. N. Đ. Popović, D. C. Johnson, *Anal. Chem.*, **70**, 468 (1998).

34. N. Đ. Popović, J. A. Cox and D. C. Johnson, *J. Electroanal. Chem.*, **455**, 153 (1998).

35. K. Vinodgopal, S. Hotchandani and P. V. Kamat, *J. Phys. Chem.*, **97**, 9040 (1993).

36. K. Vinodgopal, U. Stafford, K. A. Gray and P. V. Kamat, *J. Phys. Chem.*, **98**, 6797 (1994).

37. U. Schumann and P. Grundler, *Wat. Res.*, **32(9)**, 2835 (1998).

38. *Water Analysis Handbook*, G. A. Walters, Editor, p. 468, Hach Company, Loveland, CO (1989).

39. J. Feng and D. C. Johnson, *J. Electrochem. Soc.*, **137**, 507 (1990).

40. J. Feng, D. C. Johnson, S. N. Lowery and J. J. Carey, *J. Electrochem. Soc.*, **141**, 2708 (1994).

41. A. B. Velichenko, D. V. Girenko, S. V. Kovalyov, A. N. Gnatenko, R. Amadelli, and F. I. Danilov, *J. Electroanal. Chem.*, **454**, 203 (1998).

42. R. Amadelli, L. Armelao, A. B. Velichenko, N. V. Nikolenko, D. V. Girenko, L. V. Kovalyov, and F. I. Danilov, *Electrochim. Acta*, **45**, 713 (1999).

43. A. B. Velichenko, R. Amadelli, G. L. Zucchini, D. V. Girenko, and F. I. Danilov, *Electrochim. Acta*, **45**, 4341 (2000).

44. K. Rajeshwar and J. G. Ibanez, *Environmental Electrochemistry*, p. 136. Academic Press, San Diego (1997).

45. *Ibid.*, p. 500.

VII. THE POSSIBILITY OF CONTROLLED PARTIAL ANODIC DEGRADATION OF PHENOL

A paper submitted for publication in Electrochemical and Solid State Letters

Stephen E. Treimer and Dennis C. Johnson[1]

Abstract

A metal oxide film electrode has been identified that is speculated to be useful for selective anodic conversion of phenol to acetic acid in weakly acidic (pH 3.5) 0.10 M $NaNO_3$ under galvanostatic conditions (0.18 A cm^{-2}) with irradiation from an 18-W UV light (254 nm). The film composition corresponds to 1.2% (at/at) Fe^{3+} and 0.8% (at/at) Mn^{4+} in a β-PbO_2 matrix.

Introduction

The removal of phenol and related aromatic compounds from waste effluents and contaminated ground waters is a primary initiative of the Environmental Protection Agency. Various methodologies have been developed for degradation of phenol and the oxidative pathway for phenol has been thoroughly elucidated;[1-8] however, few technologies oxidize phenol in a controlled or selective manner. A goal of preliminary research described here is the controlled oxidation of phenol to generate a product that might have commercial value.

[1] Corresponding author

Experimental

Instrumentation.– The flow-through photoelectrochemical reactor and associated instrumentation have been described.[9] To summarize, the reactor utilized a low-pressure Hg-vapor lamp (15 mm o.d. x 21 cm length, 254 nm) operated at 18-watts power and inserted into a quartz tube (22-mm o.d. x 31-cm length). The tube was wrapped with a 284-cm length of 51-μm Pt wire (5.4 cm^2) that served as the anode. This assembly was placed in a stainless steel cylinder (2.5-cm i.d. x 30.5-cm length) that functioned as the cathode. Electrolyses were performed at a constant current (0.22 A cm^{-2}) at 40±1 °C. The concentration (v/v) of $CO_2(g)$ in the reactor headspace was determined with a Binos 100 NDIR flow-through detector from Fisher-Rosemont (Baar, Switzerland) using a $N_2(g)$ purge (210±5 mL min^{-1}). Chemical oxygen demand (COD) was determined using a procedure from Hach Chemical Company (Ames, IA).[10]

Reagents.– Solutions were prepared from reagents as received from Fisher Scientific (Pittsburgh, PA) using tap water purified by passage through anion- and cation-exchange towers from Culligan (Owatonna, MN), and a Milli-Q system from Millipore (Bedford, MA). Electrolyses solutions contained 0.10 M $NaNO_3$ adjusted to pH 3.5 using 0.10 M HNO_3.

Metal oxide films.– Films of Fe(III)-doped β-$PbO_2(s)$ ("Fe-PbO_2") or the mixed Fe(III)-doped and Mn(IV)-doped β-$PbO_2(s)$ ("Fe/Mn-PbO_2") were electrodeposited on the Pt-wire anode simultaneously with electrochemical incineration of selected organic compounds by addition of 1.0 mM $Pb(NO_3)_2$ or 0.50 mM $MnSO_4$ with 1.5 mM $Pb(NO_3)_2$, respectively. Iron(III) in the films originated from the stainless steel cylinder under the slightly acidic conditions.

Analysis of films.– Elemental analysis of films was achieved via energy dispersive spectroscopy (EDS) using a Link Isis Model-200 x-ray analyzer from Oxford Instruments (High Wycombe, Bucks, United Kingdom) equipped with a high-purity Ge light-element x-ray detector. A take-off angle of 30° was used with ca. 4,000 x-ray counts per second for a 60-s acquisition time. The resolution was ca. 140 eV at 5.9 keV.

Results and Discussion

Significant activity was demonstrated in previous research for the anodic oxidation of phenol at Fe-PbO_2 film electrodes in dilute acidic electrolyte.[9] Subsequently, the activity of an Fe/Mn-PbO_2 film electrode was compared with that of an Fe-PbO_2 film electrode for phenol oxidation. Figure 7.1 shows the %CO_2 (v/v) in the headspace of the reactor system as a function of time (t) during electrolyses of 200-mL aliquots of slightly acidic (pH 3.5) 0.10 M $NaNO_3$ containing 5.0 mM phenol (1.0 mmol). The solid line (——) corresponds to use of the Fe-PbO_2 electrode with illumination by the UV light. This curve has the expected shape for exhaustive conversion of an organic compound to CO_2. More specifically, the CO_2 level rises from zero to a maximum at ca. 3,000 s (0.8 h) and then decreases with an asymptotic approach to zero for t > 14,000 s (4.0 h). The time-integral of this curve over the 3.9-h electrolysis period corresponds to production of 5.4 mmol CO_2, i.e., 90% of the yield expected for complete conversion to CO_2 as described by Equation [1].

$$C_6H_5OH + 11\ H_2O \rightarrow 6\ CO_2 + 28\ H^+ + 28\ e^- \qquad [1]$$

The dashed line (- - -) in Figure 7.1 corresponds to use of the Fe/Mn-PbO_2 electrode with illumination by the UV light. The shape of this curve is significantly different from that obtained for the Fe-PbO_2 electrode. More specifically, there is a more rapid rise in CO_2 level

to its maximum value at ca. 1000 s (0.3 h). This is evidence of faster kinetics at the Fe/Mn-PbO_2 electrode in comparison to the Fe-PbO_2 electrode. More significant is the sharp termination of CO_2 production in the region $1.4 < t < 1.7$ h. This feature indicates the cessation of CO_2 production prior to complete anodic degradation of phenol according to Equation [1].

Table 7.1 contains values for expected yields of CO_2, for complete incineration of the designated compounds. Included in Table 1 are the observed yields of CO_2, calculated from the time-integrals of plots of $\%CO_2$ vs. time, for 3-h electrolyses of the designated

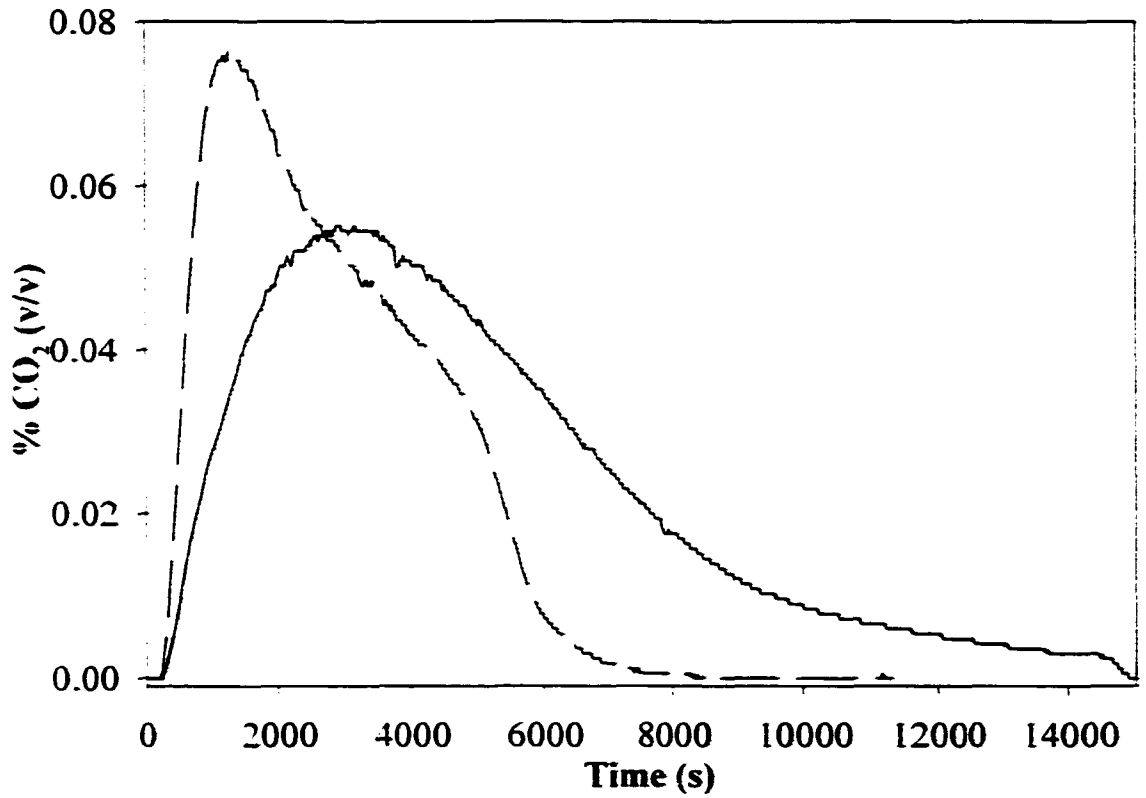

Figure 7.1. Typical electrochemical incineration curves for 200 mL aliquots of 5.0 mM Phenol in pH 3.5 0.1 M $NaNO_3$ electrolyte at a Fe,Mn-doped β-PbO_2 (— —) and Fe-doped β-PbO_2 (——) anodes with illumination of 18 W UV light.

compounds at Fe/Mn-PbO_2 film electrodes under UV illumination. Also included in Table 7.1 are COD values for the solutions at the start and end of the electrolyses. For phenol, the quantity of CO_2 produced was 4.05±0.19 mmoles for five repetitions ($N = 5$). This yield is 67.5% of the theoretical yield based on Equation [1]. This CO_2 yield is consistent with anodic degradation of phenol to CO_2 and acetic acid or formic acid, as described by Equations [2] and [3], respectively.

$$C_6H_5OH + 9\,H_2O \rightarrow 4\,CO_2 + CH_3COOH + 20\,H^+ + 20\,e^- \quad [2]$$

$$C_6H_5OH + 11\,H_2O \rightarrow 4\,CO_2 + 2\,HCOOH + 22\,H^+ + 22\,e^- \quad [3]$$

In view of these speculations, aliquots of formic acid and acetic acid were electrolyzed according to the procedure applied for phenol. A summary of these results is included in Table 7.1. Anodic degradation of formic acid was very rapid and the COD

Table 7.1. Yield of CO_2 and decrease in COD for complete electrolyses of 200 mL aliquots of selected compounds.

Organic Reactant (Conc.)	Initial mass (mmol)	Expected CO_2 (mmol)	Actual CO_2 (mmol)	Yield CO_2 (%)	Initial COD (mg O_2 L^{-1})	Final COD (mg O_2 L^{-1})	Decrease in COD (%)
Phenol (5 mM)[a]	1.0	6.0	4.05±0.19	67.5±3.2	1184±35	154±27	87±4
Formic Acid (15 mM)[b]	3.0	3.0	0.89	29.7	303±9	38±9	87±4
Acetic Acid (15 mM)[c]	3.0	6.0	0.21±0.02	3.5±0.3	946±5	905±6	4.3±0.8

[a] Multiple electrolyses (N=5) with multiple determination of COD (N=4) for each sample.
[b] Single electrolysis (N=1) with multiple determination of COD (N=4) for each sample.
[c] Double electrolyses (N=2) multiple determination of COD (N=4) for each sample.

decreased by ca. 93% during a 2.6-h electrolysis. It is apparent that formic acid is readily degraded under these conditions. However, as yet unexplained is the observation that CO_2 production during electrolysis of formic acid corresponded to only ca. 30% of the theoretical yield for the reaction given by Equation [4].

$$HCOOH \rightarrow CO_2 + 2\,H^+ + 2\,e^- \qquad [4]$$

For the 2.6-h electrolysis period for acetic acid, the yield of CO_2 was only 3.8% of the theoretical amount predicted by Equation [5], and the COD was decreased by only 4.3%. Therefore, it is

$$CH_3\text{-}COOH + H_2O \rightarrow 2\,CO_2 + 6\,H^+ + 6\,e^- \qquad [5]$$

apparent that acetic acid is inert at the Fe/Mn-PbO_2 electrode under these conditions. This conclusion is consistent with previous findings for electrolysis of acetic acid at a Pt electrode.[10]

The value 330±4 mg O_2 L^{-1} (N = 3) was obtained for the COD of a 5.0 mM acetic acid solution. This value is in good agreement with the predicted value of 320 mg O_2 L^{-1} for this solution. Based on this result, the final COD of 154±27 mg O_2 L^{-1} for the product solution from electrolysis of 5.0 mM phenol shown in Table 1 is estimated to correspond to ca. 2.5 mM acetic acid. However, based on the predicted reaction described by Equation [2], this value corresponds to only 50% of expected concentration of 5.0 mM for acetic acid. This discrepancy between the predicted and determined COD values is not yet explained.

Several unsuccessful attempts were made to obtain conclusive identification of acetic acid in the final product solution for electrolytic degradation of phenol at the Fe/Mn-PbO_2 electrode. Procedures tested included the extraction of an acidified aliquot into diethylether

with subsequent analysis of the extract by GC-MS using a DB-5 column. No chromatographic peaks could be discerned even when using selected ion monitoring.

The composition of an Fe/Mn-PbO_2 film was determined using EDS immediately after deposition onto a polished Au substrate and following a 3-h electrolysis period (0.22 A cm^{-2}) in 0.10 M $NaNO_3$ (pH 3.5). The bulk surface composition was determined to contain 1.18±0.17 % (at/at) Fe and 0.79±0.07% (at/at) Mn before electrolysis. After electrolysis, the bulk composition corresponded to 1.17±0.32% (at/at) Fe and 0.66±0.14% (at/at) Mn. Electrolysis appears to have resulted in a slight leaching of Mn from the film.

Conclusion

It has been demonstrated that production of CO_2 is terminated prior to complete degradation of phenol at a Fe/Mn-PbO_2 electrode in slightly acidic 0.10 M $NaNO_3$ (pH 3.5). We speculate that this termination corresponds to production of acetic acid which was demonstrated to be inert to further degradation under these conditions. A possible mechanism for production of acetic acid is consistent with that discussed for anodic degradation of 4-chlorophenol.[12] Accordingly, phenol is converted to benzoquinone, followed by ring opening to form the corresponding dicarboxylic acids, with subsequent stepwise decarboxylation to produce CO_2. Ultimately, decarboxylation is terminated at production of acetic acid. It is important that future work is focused on conclusive identification of the final stable product of this anodic reaction.

Acknowledgements

The authors thank Warren Strazheim for surface analysis of the metal oxide films. The authors also thank Ames Laboratory for funding this project. Ames Laboratory is a division of the U.S. Department of Energy and operated under Contract W-7405-Eng-82.

References

1. EPA Health Effects Notebook for Hazardous Air Pollutants. EPA-452/D-95-00. PB95-503579. December 1994.
2. D. W. Kirk. H. Sharifian and F. R. Foulkes. *J. App. Electrochem.*. **15**. 285 (1985).
3. H. Sharifan and D. W. Kirk. *J. Electrochem. Soc.*. **133**. 921 (1986).
4. C. Comninellis and C. Pulgarin. *J. Appl. Electrochem.*. **23(2)**. 108. (1993).
5. C. Comninellis and A. Nerini. *J. Appl. Electrochem.*. **25(1)**. 23. (1995).
6. D. Gandini. C. Comninellis. N. B. Tahar and A. Savall. *Actual. Chim.*. **10**. 68. (1998).
7. X. Li. J. W. Cubbage. T. A. Tetzlaff and W. S. Jenks. *J. Org. Chem.*. **64**. 8509 (1999).
8. X. Li. J. W. Cubbage and W. S. Jenks. *J. Org. Chem.*. **64**. 8525 (1999).
9. S. E. Treimer. J. Feng and D. C. Johnson. *J. Electrochem. Soc.*. in press.
10. *Water Analysis Handbook*. G. A. Walters. Editor. p. 468. Hach Company. Loveland. CO (1989).
11. D. C. Johnson. J. Feng and L. L. Houk. *Electrochim. Acta*. **46**. 323 (2000).
12. S. K. Johnson. L. L. Houk. J. Feng. R. S. Houk and D. C. Johnson. *Environ. Sci Technol.*. **33**. 2638 (1999).

VIII. GENERAL CONCLUSIONS

Throughout this thesis, oxygen-transfer reactions have been studied in detail. Several conclusions can be drawn from this work.

In Chapter II we surveyed various literature citations in an attempt to show the many instances where Koutecky-Levich plots can be linear. It can be deduced that negative curvature in Levich plots (plots of I vs. $\omega^{1/2}$) can be indicative of slow charge-transfer kinetics, as indicated by Equation 10 on page 14. Of course, this is the mechanism presumed in the derivation of the Koutecky-Levich equation and, therefore, the plot of $1/I$ vs. $1/\omega^{1/2}$ is recommended. Accordingly, we recommend estimation of n values from both the linear segment of the Levich plot at low ω values (< ca. 100 rad s^{-1}) and from the linear segment of the Koutecky-Levich plot at large ω values (> ca. 100 rad s^{-1}). Equality of these two n values can be interpreted as confirmation of the diagnosis of a one-step mechanism involving the transfer of n electrons with a moderately slow heterogeneous rate constant (k_h). Furthermore, k_h can be evaluated from the non-zero intercept of the Koutecky-Levich plot, as indicated by Equation 15 on page 15.

Should one observe that the value of n calculated from the Levich plot for low ω values is larger than that estimated from the Koutecky-Levich plot for large ω values can be interpreted as indicative of two or more consecutive charge transfer steps, e.g., E_rE_i and E_rCE_i mechanisms, wherein the second charge-transfer step occurs with a k_h value much smaller than that for the first charge-transfer step. It can be helpful in such cases to

determine an overall n value from coulometric results for an exhaustive electrolysis, or employing other techniques of electrochemistry and/or electrode geometries.

In the development of a mathematical model for O-transfer reactions in Chapter III, it was surprising, upon first inspection, to find that Equation 26 on page 41 did not contain the term k_{WDR}. Of course, this term was eliminated when we made the assumption $k_{WDR} > k_{OTR}C_R^*$, which resulted in Equation 22 (page 41). Hence, it is assumed that the OH flux is sufficiently large to support the convective-diffusion limited flux of the reactant, R.

For an oxygen-transfer mechanism with no adsorption of the reactant species, Case I produces a plot of $1/I_{tot}$ vs. $1/\omega^{1/2}$ with a zero slope and an intercept that is independent of C_R^b. Case II produces a plot of $1/I_{tot}$ vs. $1/\omega^{1/2}$ with a zero slope and an intercept that decreases with increasing C_R^b. Case III produces a plot of $1/I_{tot}$ vs. $1/\omega^{1/2}$ with a non-zero slope with a zero intercept. Only Case IV produces a plot of $1/I_{tot}$ vs. $1/\omega^{1/2}$ with a non-zero slope that decreases with increasing C_R^b and a non-zero intercept that decreases with increasing C^b.

Equation 47 in Chapter III describes I_{tot} as a function of C_R^b for the case of weakly adsorbed reactant:

$$I_{tot} = \frac{2FA(D/\delta)k_{OTR}\Gamma_0\Gamma_s K_{ads}C_R^b}{(D/\delta) + k_{OTR}\Gamma_0\Gamma_s K_{ads}}$$

This is to be compared to Equation 23 for the case of no adsorption under the condition $(D/\delta)k_{WDR} + k_{WDR}k_{OTR} > (D/\delta)k_{OTR}C_R^b$ as is given by:

$$I_{tot} = \left\{\frac{2FA(D/\delta)k_{OTR}C_R^b}{(D/\delta) + k_{OTR}}\right\}$$

Equation 23 is consistent with Equation 47 using the definition:

$$k_{OTR} = k_{OTR}\Gamma_0\Gamma_S \cdot K_{ads}$$

In Chapter IV, the three film electrodes: undoped β-PbO_2, Bi-doped β-PbO_2, and Fe-doped β-PbO_2 exhibited voltammetric waves for oxidation of toluene. However, k_{app} for this anodic reaction was found to be larger at the Fe-PbO_2 electrode than at the Bi-PbO_2 and pure β-PbO_2 electrodes. This is especially noteworthy because of the small amount of Fe(III) in the Fe-PbO_2 film (ca. 1%) as compared to the large amount of Bi(V) in the Bi-PbO_2 film (ca. 33%). Apparently, the high catalytic activity of Fe(III) sites as compared to Bi(V) and Pb(IV) sites is the beneficial consequence of stronger adsorption of aromatic molecules at the Fe(III) sites. This adsorption is expected to occur via interaction of π-electrons in the aromatic compound with partially filled d-orbitals at the Fe(III) sites.

Experimental results for toluene and *m*-xylene are consistent with a step-wise reaction sequence leading to carboxylic acids as final products.

Chapter V demonstrated that electrocatalytic films can be employed for practical applications. With the further development of an inline electrochemical cell using MnO_2 as an anode, benchtop electrochemical incineration of chromatographic waste can become a reality with low cost and complexity to the user.

In Chapter VI we find that the illumination of anode surfaces with low intensity UV light resulted in faster $CO_2(g)$ production during electrochemical incineration of selected organic compounds. We conclude that the use of photo-assisted electrochemical incineration can be important for oxidative degradations of toxic organic wastes, especially at the site of origin.

Based on observations of this photo effect for both aromatic (phenol and aniline) and non-aromatic (*n*-propanol and acetic acid) compounds, we speculate that the photo mechanism results from absorption of UV photons in the surface of the electrode rather than absorption by reactant molecules.

Finally, the Fe,Mn-doped β-PbO_2 film discussed in Chapter VII appears to be the most active anode film yet studied by this group for the anodic electrochemical incineration of the organic compounds phenol and aniline. It is curious and perhaps useful that this electrode selectively stops at the formation of acetate and might offer an interesting study as to the intermediates formed during the early stages of the incineration process. Future work should focus on the conclusive proof of the presence of acetate in the product mixture either by normal phase HPLC using conductivity or GC/MS using a column optimized for the detection of acetic acid in a matrix other than ether.

Future Research

An early revision of Chapter IV brought up the concept that a highly polarized electrode has a lower dielectric constant within the diffusion layer [1-2]. A hypothesis was proposed that organic compounds diffuse into these lower dielectric regions from the bulk and have increased residence time within the diffusion layer to allow oxidation at the electrode. This hypothesis was refuted by at least one individual, but it would be fundamentally instructive to probe this idea further and provide a fundamental reasoning of why we can exhibit the electrochemical incineration of compounds such as benzene and naphthalene in aqueous electrolyte.

After observing the catalytic effect of ultraviolet light on the on the doped lead dioxide films in Chapter VI, I believe it would be very beneficial to revisit Chapter 5 and compare the performance of a single pass electrochemical incineration of a series of chromatographic solvents while illuminating the electrode with UV light. The enhanced activity of the illuminated Fe-doped MnO_2 electrode might enable the electrochemical incineration of more practical concentrations of organic modifiers.

Finally, introductory experiments of the nonpolar species naphthalene, trifluralin, and atrazine showed significantly enhanced electrochemical incineration when sulfated cyclodextrins were added to the aqueous mixture of insoluble organic compounds [3]. One hypothesis is that the hydrophobic cavity of α-, β-, and γ- cyclodextrins have similar size and shape to a variety of nonpolar organic compounds. The sulfated hydrophilic headgroups of these molecules may adsorb to the activated electrode surface allowing increased residence time for electrochemical incineration. Certainly β-cylcodextrin can be obtained in reasonably cheap quantities to make the bulk electrochemical incineration of toxic organic containing waste feasible. One problem that has arisen is that the highly active Fe, Mn-doped PbO_2 electrode actually incinerates the cyclodextrin molecule as well as the added organic compounds, but certainly it would be of much greater benefit to use less active noble metal electrodes if they would prove useful.

References

[1] E. Gileadi, E. Kirowa-Eisner, J. Penciner, *Interfacial Electrochemistry*, p. 15, Addison-Wesley Publishing, London, (1975).

[2] J.O'M. Bockris, A.K.N. Reddy, *Modern Electrochemistry*, p. 756, Plenum Press (1970).

[3] James F. Rusling, *Acc. Chem. Res.*, **1991**, *24*, 75.

ACKNOWLEDGEMENTS

This work was performed at Ames Laboratory under Contract No. W-7405-Eng-82 with the U.S. Department of Energy. The United States government has assigned the DOE Report number IS-T 1955 to this thesis.

I thank my wife, Tammi, for giving me the wonderful family that I look forward to coming home to every night. She supported me throughout these four years with dreams that someday we'll all have the life of happiness that we've earned. She put up with my love of John Deere tractors and the moodiness that always comes with graduate school. Most of all, I know that though she had her doubts and frustrations at times, never once did her love for me waiver.

Like Tammi, I thank my parents, Kenneth and Beverly, for supporting me, believing in me and giving me unconditional love throughout my life. I certainly could not have come this far in life without all the things they did for me. Now as a parent myself, I try to use my father's image as a model, but it's hard to live up to someone who's perfect in your mind.

And that leads me to my final acknowledgement, Dr. Dennis C. Johnson. Words cannot describe the amount of respect and appreciation I have for the tools he has given me to find success in life; we both know this has little to do with earning a wage. Though I was no model graduate student, Doc brought me the courage and confidence to reach this point. Doc gave me responsibility and opportunities, but never pushed. He offered suggestions and questions, but didn't force his view. He did this by treating me like a son, listening like a father when I couldn't talk to mine, reliving his own experiences – even those on John Deere tractors. If ever God were to define patience with a picture, it would be that of "Doc".